Advanced Modelling of Flooding in Urban Areas Integrated 1D/1D and 1D/2D Models

Submitted by

Jorge Eduardo Teixeira Leandro

to the
University of Exeter
as a thesis for the degree of

Doctor of Philosophy in Engineering

October 2008

I certify that all material in this thesis which is not my own work has been identified and that no material has previously been submitted and approved for the award of a degree by this or any other University.

.....

To my family:

Marlene Maria Teixeira Vieira Leandro

Eduardo Manuel Vieira Leandro

Robert Edward Teixeira Leandro

To my girlfriend:

Maike Remmel

Abstract

The research presented in this Thesis aims at defining the strengths and weaknesses of an Improved 1D/1D model when compared with a more accurate 1D/2D model. Although both coupled-models (sewer/surface) solve the St. Venant equations in both layers, the latter uses a higher approximation (2D two-dimensional) on the surface layer. Consequently, the 1D/1D model is computationally more efficient when compared to the 1D/2D model, however there is some compromise with the overall accuracy.

The hypothesis is that "The inundation extent of urban flooding can be reproduced by 1D/1D models in good agreement with the 1D/2D models if the results are kept within certain limits of resolution and under certain conditions".

The Thesis starts by investigating ways of improving an existing 1D/1D model to rival the more accurate 1D/2D model. Parts of the 1D/1D model code are changed and new algorithms and routines implemented. An innovative GIS tool translates the 1D output-results into 2D flood-inundation-maps enabling a thorough comparison between the two models. The methodology assures the set-up of two equivalent models, which includes a novel algorithm for calibrating the 1D/1D model vs. the 1D/2D model results.

Developments are tested in two distinctly different case studies of areas prone to flooding. The conclusion is that the 1D/1D model is able to simulate flooding in good agreement with the 1D/2D model; however, it is found that features such as topography, density of the urbanised areas and rainfall distribution may affect the agreement between both models.

The work presented herein is a step forward in understanding the modelling capabilities of the analysed coupled-models, and to some extent may be extrapolated to other models. Research is growing in urban flooding and this work may well prove to be a strong foundation basis for future research.

Acknowledgements

I wish to thank my supervisors Dr Slobodan Djordjevic and Professor Dragan Savic for their support and guidance throughout my research carried out at the University of Exeter during the past three years.

I also wish to thank Albert Chen for the lively discussions on flooding and for producing all the results of the 1D/2D model used in this Thesis.

The research presented in this Thesis was funded through the Flood Risk Management Research Consortium (FRMRC) Research Priority Area 6 Urban Flood Management, which was led by Professor Adrian Saul. The Consortium was funded by the UK Engineering and Physical Sciences Research Council under grant GR/S76304/01, jointly with the UK Natural Environment Research Council, the Department of the Environment, Food and Rural Affairs, the Environment Agency of England and Wales, the Scottish Executive, the Rivers Agency (Northern Ireland) and the UK Water Industry Research.

I would like to state that I am particularly pleased for having had Professor Garry Pender and Dr Gavin Tabor as my examiners; I truly believed that their expertise have proved the high standard of the work presented herein.

A special note of appreciation goes to Mrs Alex Slater for helping me during my final revision, and to two other good friends Susan Shilsdon and Ian MacBride at different stages of my PhD.

Contents

List of Figures

List of Tables

Nomenclature

(X, Y, Z) Spatial coordinates, page 38

$1D1D\nabla_t^{\alpha_k^j}$ Cumulative volume of the discharge given by the 1D/1D at run time t in a link j, page 95

$1D2D\nabla_t^{\alpha_k^j}$ Cumulative volume of the discharge given by the 1D/2D at run time t in a link j, page 95

α_k^j Control variable j during the k^{th} iteration, page 92

Δhmx Maximum linearization gradient, page 71

$\Delta x; \Delta y$ Regular 2D grid spacing, page 68

λ_k Step size, page 91

ω Weight function, page 91

ψ Non dimensional parameter, page 33

ρ Fluid density, page 33

ε Acceptable error, page 73

A Cross-sectional area of the flow, page 29

a Celerity of the surface waves, page 40

A_0 Area of the orifice, page 48

A_c, n Empirical coefficients for the submerged weir, page 48

a_i, b Constrain constants, page 51

a_i, b_1 Polynomial parameters, page 66

A_{manh} Manhole horizontal area, page 71

Ap Area of the pipe connection, page 77

B Cross-sectional surface width, page 40

b Channel width, page 47

$B1, B2, B3$ Boussinesq terms, page 32

B_k Width of each channel k, page 67

C Set of channel IDs, page 67

c Celerity of the pressure waves, page 33

Cd_1 Discharge coefficient of the sharp crested weir, page 47

Cd_2 Discharge coefficient of the orifice, page 48

Cd_3 Discharge coefficient of submerged weir (Villemont 1947), page 48

Cd_4 Discharge coefficient of submerged weir (Abou-Seida and Quaraishi 1976), page 48

Cd_5 Discharge coefficient of submerged orifice (Abou-Seida and Quaraishi 1976), page 48

Cdf Drowned flow reduction factor, page 48

Ch Sub-set of channels coordinate-points, page 67

CK_w Discharge coefficient of submerged weir (Cunge et. all 1980), page 48

$cVol_p$ Calculated volume, page 68

D Diameter of the pipe, page 33

d_0 Significant height, page 32

d_k Search direction, page 91

D_p Diameter of the pipe connection, page 77

E Young's modulus of elasticity, page 33

e Wall thickness, page 33

F Measure of fit, page 100

$f(x)$ Objective function, page 91

f_i^h Horizontal line, page 63

$f^p(x)$ Piecewise linear function, page 63

f_i Objective function i, page 91

Fr Froude number, page 86

G Set of grid coordinate-points, page 67

g Acceleration due to gravity, page 29

g_k Cost function, page 52

H Piezometric head, page 33

h Flow depth, page 29

H_1 Specific energy at the upstream cross-section, page 47

H_1 Surface water depth, page 76

H_2 Manhole water depth, page 77

H_2 Specific energy at the downstream cross-section, page 48

H_i Water level at node i, page 70

h_i^t Temporal output results of water depth for all channels k, page 67

H_s Height of the vertical shaft, page 77

H_w Weir level, page 70

H_{inl} Height of the inlet box, page 77

h_{min} Minimum water depth, page 100

Hh Set of water heights, page 63

hp^t Temporal output results of water depth for all ponds pk, page 67

Hr Hydraulic radius, page 63

J Friction slope on the x direction, page 29

J_N Cost, page 52

J_x Friction slope on the x direction, page 30

J_y Friction slope on the y direction, page 30

K Bulk modulus of elasticity, page 33

K Roughness coefficient, page 78

k Total number of channels, page 67

k^{th} Iteration, page 92

kM, km Auxiliary variables, page 63

L Cell level, page 68

L_i Perimeter of the inlet box, page 76

L_k Length of each channel k, page 67

lb Interval lower limit, page 91

Lp Connection pipe length, page 78

M Maximum number of iterations, page 92

Ms Threshold on the calculation of $\omega_k^{i,j}$, page 94

n Polynomial degree, page 66

n_{cells} Number of cells in the 2D grid, page 100

Neq Number of equivalent inlets, page 81

np_k Total number of points for each channel k, page 67

P Set of points, page 63

Po Set of ponds coordinate-points, page 67

Q Flow, page 29

Q_i^{pipe} Pipe flow to manhole i, page 80

Q_i^{runoff} Surface run-off to manhole i, page 80

Q_i^{street} Street flow to manhole i, page 80

Q_{aux} Flow from auxiliary equation, page 82

Qc Critical flow, page 63

$Qtop$ Top-discharge, page 71

RCd Instability reduction coefficient, page 82

S Bed slope on the x direction, page 29

S_0 Significant bed slope, page 32

S_x Bed slope on the x direction, page 30

S_y Bed slope on the y direction, page 30

Smh Number of smoothing points above each drop, page 63

T Wave period, page 32

t Time, page 29

t_1, t_2 Two consecutive computational times, page 71

t_f Total computational time, page 73

Ts Threshold on the cross-correlation, page 94

U Velocity component on the x direction, page 30

u_k Control variables, page 52

ub Interval upper limit, page 91

V Velocity component on the y direction, page 30

v_0 Significant velocity, page 32

$Volp^t$ Temporal output results of volume for all ponds pk, page 67

$W(f_i)$ Aggregated function, page 91

w_k Random disturbance, page 52

W_x Length of the inlet box, page 76

W_y Width of the inlet box, page 76

$W_{1D/1D}$ Matrix of water depths with 1's and 0's in the 1D/1D model, page 100

$W_{1D/2D}$ Matrix of water depths with 1's and 0's in the 1D/2D model, page 100

Wp Wet perimeter, page 63

WT Water table, page 63

x Longitudinal direction, page 29

x_i Decision variables, page 51

x_k Point inside the interval of uncertainty, page 91

Z Set of grid elevations, page 67

Z_{dwst} Downstream elevation of each channel k, page 67

Z_{upst} Upstream elevation of each channel k, page 67

Acronyms

1D/1D Integrated model sewer(1D)/surface(1D)

1D/2D Integrated model sewer(1D)/surface(2D)

1D one-dimensional

2D two-dimensional

3D three-dimensional

AD Alternating Direction

ADI Alternating Direction Implicit

Ccm cross-correlation matrix

CFD computational fluid dynamics

Cr control rule

CS control sections

DEM Digital Elevation Model

DOF Dynamic Objective Function algorithm

DP dynamic programming

DTM Digital Terrain Model

E Explicit

FDM Finite Difference Methods

FEM Finite Element Methods

FRMRC Flood Risk Management Research Consortium

GE governing equations

Hr hydraulic radius

I Implicit

IPCCC Intergovernmental Panel on Climate Change

IRG Irregular-Cross-section

LP Linear programming

LS Linear search algorithm

LSB Linear Search Based algorithm

MLE Multiple-Linking-Element

MOC Method of Characteristics

NLP non-linear programming

PPS25 Planning Policy Statement 25

RFM Rapid Flood Models

SIPSON Simulation of Interaction between Pipe flow and Overland flow in Networks

SLE Single-Linking-Element

S-Sub surface-subsurface

Sub-S subsurface-surface

TVD Total Variation Diminishing

UFM Urban Flood Models

UIM Urban Inundation Model

UKCIP UK Climate Impacts program

UN United Nationse

UNFCCC United Nations Framework Convention on Climate Change

Chapter 1

Introduction

1.1 Background

Urban flooding is a phenomenon that affects populations across the globe. The UK flooding in the summer 2007 was a wake up call to challenge scientists and experts to face this problem. The need for investment in developing flood modelling predictive tools became an essential task in order to define the areas of high risk; namely the flood prone areas. The three major questions arising about flooding are: Where, when, and to what extent will it flood? There is no absolute answer. Nevertheless, to reduce the uncertainty of the answer to these questions one can use a multidisciplinary approach, drawing on the expertise of different specialisations. Currently there are several modelling tools believed to be capable of simulating such a phenomenon; however, the level of detail and complexity that limits their range of application is still not clearly defined.

When deciding on which model to use, two extremes need to be considered. One extreme is the need for accurate-flood-models. In this case they should not be over-simplified because they are then neither representative nor effective. The opposite is the need for fast-flood-models. It is imperative to run as many scenarios as possible, despite reducing the quality of the results. These two extremes can be translated into a symbolic mathematical balance of two forces: F_1 (Accuracy) vs. F_2 (Computational Efficiency). Increasing or decreasing F_1 will accordingly decrease or increase F_2. This balance is more difficult to achieve between models than within a specific model. Nevertheless, the model choice and resolution level should be dictated by, amongst others, factors such as aim, importance/consequences, uncertainty, available data and the project deadline.

In this Thesis, two hydraulic models will be tested side by side, 1D/1D and 1D/2D. The 1D/1D models assume that the water flow in the sewers and on the surface is one-dimensional. The 1D/2D models assume that the surface water flow is two-dimensional. The comparison of these models will support the hypothesis and the answer to the research

question. The hypothesis of this Thesis is:

> The inundation extent of urban flooding can be reproduced by 1D/1D models in good agreement with the 1D/2D models if the results are kept within certain limits of resolution and under certain conditions.

Inevitably, the question of whether it is possible to obtain accurate urban-flooding inundation maps with 1D/1D models is answered in the affirmative, but not without constraints. Throughout this Thesis these requirements and limits will be explained in detail, and their relative importance to the main goal highlighted when necessary.

1.2 Context

The first quotation below is taken from the book of Genesis as describing "The Great Deluge" in the time of Noah. The other four quotations are definitions of the word "Flood".

> "A flood sent by God that covered the whole earth as a punishment." (Cambridge Dictionary, 2008)

> "A rising and overflowing of a body of water especially onto normally dry land; also: a condition of overflowing 'rivers in flood'" (Merriam Webster Dictionary, 2008)

> "A large amount of water covering an area that is usually dry." (Cambridge Dictionary, 2008)

> "An overflowing or irruption of a great body of water over land not usually submerged; an inundation, a deluge. In flood, on a flood: (of a river, etc.) overflowing its banks; (of land) in an inundated condition." (Oxford English Dictionary, 2008)

> "Means the temporary covering by water of land not normally covered by water. This shall include floods from rivers, mountain torrents, Mediterranean ephemeral water courses, and floods from the sea in coastal areas, and may exclude floods from sewerage systems" (European Parliament and Council of The European Union, 2007)

Since early times flooding has played a challenging role in the lives of the first settled communities, which were forced to adapt and learn how to mitigate the effects of floods.

Examples of such communities are: the Egyptians (3150-31 BC) by the river Nile, the Mesopotamians (5900-400 BC)) by the Tigris and Euphrates and the Nabataeans (300 BC-AD 300) in south-western Jordan. The people from Mesopotamian had in the use of those rivers across the so called Fertile Crescent, one of the main reasons for the rise and development of their civilization. The rivers were fundamental for water supply, transport of people and goods, recreational purposes, irrigation and land fertilisation. In Egypt, the flooding was seen as a gift from the Pharaoh and the God Hapi who were considered responsible for the Nile's annual inundation. The flooding provided the floodplains with fertilizing nutrients necessary to grow wheat and other crops, essential to establish self-sufficient farming methods and allow for their subsistence. However, these communities also had to face the devastating effects of flooding. The Nabataean civilization centred in the ancient city of Petra, suffered the effects of flash flooding from intense rainfall. In response, a complex system of dams, cisterns and channels was put in place to control the water flows and erosion, thereby preventing flood damage to the city (Ortloff, 2005).

Nowadays, as a result of the creation of extensive conurbations and the globalized demographic boom, there has been pressure on the floodplains for development. When this development is primarily driven by a profit motive, and/or happens without effective planning, such areas can become over developed and vulnerable to flooding. These actions together with extreme climatic events can result in heavy repair costs and in some cases irreversible environmental and ecological damage. Insurance companies in the United Kingdom, put the total cost of the widespread flooding that occurred between June and July 2007, at around GBP 3bn, the largest single claims event in the UK history (ABI, 2007). As an immediate consequence, insurance companies raised insurance premiums on buildings by 3%, and on vehicles, to try to cover the cost of claims (BBC, 2007a). Other countries have suffered similarly; the heavy rain that occurred in the southern Mexican state of Tabasco in November 2007 caused the river banks to burst. According to another bulletin on BBC (BBC, 2007b), the largely low-lying state was said to have lost 100% of its crops and 70% of the state was under water.

Initial awareness of global climate change led to the Kyoto Treaty in 1997. The Treaty was established by the United Nations Framework Convention on Climate Change (UNFCCC) and ratified by 174 countries (the United States of America being a major absentee). The aim was to decide and quantify what could be done to reduce global warming, especially the reduction of emissions of greenhouse gases. The Stern Review on the Economics of Climate Change, released in October 2006, discussed the effects of climate change on the world economy and specified the investment needed to mitigate these effects, and the costs of failing to do so. In November 2007, ten years after the Kyoto Treaty, the In-

tergovernmental Panel on Climate Change (IPCC), a scientific body of the United Nations (UN), issued a report in which the man-made effects on climate change were quantified, and laid down the foundations for the measures needed to counteract such changes.[1] The UN Climate Change conference in Bali, Indonesia December 2007, set the parameters and aims for the further negotiations to be finalised at the UN climate conference to be held in Denmark in 2009. Besides being seen as a platform to launch the negotiations for the period post 2012, the year in which the Kyoto Protocol expires, it also managed to bring the US and China to the climate change negotiating table.

One threat posed by climate change is the increased frequency of extreme events which are responsible for causing severe flooding (as acknowledged in the Planning Policy Statement 25 - PPS25 - based on the UK Climate Impacts program - UKCIP - scenarios (UK Government, 2006)). PPS25 is the document that sets out the UK Government's national policies on land use and development to ensure flood risk is taken into account at all stages of the planning process. Five typical extreme events are: Storm surges, flash flooding, intense rainfall (e.g. monsoonal rainfall), Sewerage blockage and Groundwater. Storm surges are the main driving force for breaching and overtopping flood defences. These events can be triggered by earthquakes, generating powerful Tsunamis, such as the one in the Indian Ocean that hit Thailand, Bangladesh, Sri Lanka and India in December 2004, or by hurricanes such as the Hurricane Katrina that hit New Orleans in August 2005 or Gustav that hit Cuba in August 2008. Flash flooding, can come without warning, and be caused by snow-melting, high tides or torrential rains (i.e. intense rainfall). In Bradford, UK, the Stockbridge area was affected by serious flooding in October 2000 and later on in August 2003. The local drainage systems were reportedly overwhelmed during the heavy rainfall (BBC, 2004). Monsoonal rainfall occurs in regions where the majority of the rain falls during a particular season. In Bangladesh and India it accounts for up to 80% of the total annual rainfall, and can cause floods which claim many lives, losses of property and severe economic damage. The 1998 Bangladesh flood was caused by a mix of high monsoon rainfall and snow-melting from the Himalayas. Sewerage blockage or sewer with insufficient capacity can cause severe flooding. Flooding in Jakarta, Indonesia, is often attributed to a combination of drainage systems being full with stagnant sewage, the flow being blocked by solid waste and the lack of maintenance. Groundwater flow, occurs when water levels in the ground rise above the ground surface level. Due to its nature, this type of flooding may take weeks or months to dissipate as water levels may

[1] Both the IPCC and the former vice-president of the US, Albert Arnold (Al) Gore Jr., were awarded the Nobel Peace Prize because of the joint effort for promoting a campaign on climate change effects and actions to prevent them.

take a long time to fall.

Depending on the type and scale, the effects of flooding can be categorized as direct and indirect damage and social consequences (Konig et al., 2002). Direct damage, refers to the short term or immediate effects; these are the physical damage to property and land, disruption of transport and infrastructure, and loss of human life and livestock. Indirect damage refers to the medium-term effects, which include water supply shortage, the spread of diseases, especially water-borne ones, and the loss of crops and food stockpiles. Social consequences refer to the long term effects such as the economical and psychological damage. Insurance companies and governments can face sizeable compensation payments and rebuilding costs. The damaging loss of homes and loved ones can have strong implications on family structures.

The prediction and quantification of the effects of flooding is a multi-disciplinary task that requires bringing together experts from many different fields. Work has been done by consortiums such as the Flood Risk Management Research Consortium (FRMRC) which tackles the hydrological, hydraulic and health aspects of flooding (Pender, 2006), and the National Flood Forum, which aims to manage the social effects of flooding, to promote self-help and to campaign for flood alleviation. The FRMRC was set up as part of a UK Government action plan to tackle the risk of flooding. The consortium started in 2005 and was successfully concluded in 2008. Recently it has been upgraded to a second funding stage with FRMRC2. Several reports have been produced highlighting the effects of climate change. The IPCC report estimates the man-made effects on climate change, while the Stern Review estimates the economic impacts of climate change (Stern, 2007). The FORESIGHT report acknowledges the direct relation of increased flooding events (the latter predicts that the annual damage from flooding may rise from around 100 million GBP to between 460 and 2500 million GBP). The recent report published by Sir Michael Pitt discusses the need to strengthen the provisions within the PPS25 and Building Regulations to define responsibility-roles on flood-risk-management and recognises that there is room for improving inter-agency cooperation (Pitt, 2008).

1.3 Motivation

The concerns underlying flood management are: the prediction, prevention and mitigation of flooding. The prediction of surface water flow paths is an open research question that looks at whether it is possible to predict the flood routes during an extreme event i.e. the likelihood and extent of flooding and under what circumstances. The answer would

enable the production of flood-inundation-maps and suggest future prevention strategies. The ultimate goal is to mitigate the effects of flooding.

This Thesis aims to enable the enhanced 1D/1D model to produce urban flood inundation maps to assist a supported improvement of current flood management. The enhancements of the existing model will serve as a platform test for future assimilation by commercial software developers. The developed tools/products consist of GIS (Geographic information system) routines, mathematical modelling and calibration methods, so that, after being tested on case studies, they can be used by engineering practitioners. Due to the lack of high-quality real data, the model results (1D/1D) and tools are validated against a more demanding state-of-the-art hydraulic model (1D/2D). It should be acknowledged that the results of the 1D/2D modelling are treated as real data; therefore, the improvements and methodologies developed herein would still be valid had that real data been available.

1.4 Objectives

The main objectives of this Thesis are to develop and test:

1. A methodology for setting up two equivalent 1D/1D and 1D/2D models and two methods for comparison;
2. GIS technique for generating flood-inundation-maps from the results of the 1D/1D model;
3. A theoretical linkage-model of the interaction between the sewer system and the surface system, the Multiple-linking-element;
4. A novel algorithm to calibrate the 1D/1D model with the 1D/2D model results, the Dynamic-Objective-Function algorithm;
5. An improved 1D/1D model, in terms of increased model stability and range of applications.

Finally, to achieve the aims of this Thesis, it is of crucial importance that this work is published and presented in international conferences and recognized scientific journals.

1.5 Organisation

This Thesis is organised in six chapters:

Chapter 1: Introduces the topic of urban flooding. Briefly summarises the research question and the Thesis hypothesis. Describes the thesis contents. Contextualises the topic. Presents the motivation.

Chapter 2: Presents a comprehensive and up to date review over the five topics that constitute the expertise of an urban flood modeller: the governing equations, the numerical schemes, the existing urban flood models, the link between surface and subsurface networks, the calibration methods.

Chapter 3: Restates the research question. Clearly sets out the problem definition, the justification and drivers of the Thesis. Provides examples of practical engineering applications.

Chapter 4: Describes and explains the contributions to knowledge, and the developments made in tackling the problem: The enhancements of the original SIPSON model, the development of the Multiple-Linking-Element approach, the design of the calibration algorithm for 1D/1D models, two methods developed for comparison of the results between the 1D/1D and the 1D/2D model, and the methodology for assuring a valid comparison.

Chapter 5: Demonstrates the suitability of the 1D/1D model to retrieve flood inundation maps in two distinctly differing case studies.

Chapter 6: Discusses the results and draws conclusions about the value of the work presented in the Thesis.

Chapter 2

Literature Review

2.1 Governing Equations

When modelling floods, it is of upmost importance to understand both the hydraulics behind the flow dynamics during a flooding event and the equations used within the hydraulic models. This enables the modeller to control and minimize the errors incurred when modelling these events, and, therefore, discern the failures and the successes of the simulation results on real case studies. During a flood event three main types of flow can occur: The first is free-surface flow, in which the water flow is mainly driven by gravity with the surface kept at atmospheric pressure; the second is pressurized flow, in which the water is confined within a closed cross-section, hence the liquid inside is pressurized; the third is a hybrid version of the two previous types, the free-surface-pressurized flow. Overland flow is mainly free-surface flow; however, exceptions can occur, for instance when the flow water level exceeds the bridge crown level it becomes pressurized. In sewer flows the three types can co-exist. Each flow type is characterized by its own set of governing equations, whereby their underlying assumptions define their applicability. Furthermore, depending on those assumptions it is possible to have the same flow type with different levels of simplifications which then affect the model stability and computational efficiency. This section presents the general forms of the governing equations, simplifications, underlying assumptions, their applicability and some examples of where they have been used.

The free-surface flow. The set of governing equations most frequently used in free-surface flow are the St. Venant equations. These equations were named in honour of St. Venant a French mathematician who first derived them in 1871. These form a system of coupled non-linear hyperbolic partial differential equations, namely continuity and momentum equations. These equations have two dependent variables, either depth and velocity (h, v) or area and flow (A, Q), and two independent variables, longitudinal direction and

time (x, t). Depending on the characteristics of the modelled flow, often these equations are simplified to reduce the computational cost and to increase the model stability (Lal, 1998). Yet by doing so, the model applicability is reduced.

The St. Venant equations are the set of equations that define gradually-varied unsteady flow whereby the pressure distribution is considered hydrostatic. These can be derived by using the system-control-volume transformation (the Reynolds transport theorem) (Potter and Wiggert, 2001). A more general set of equations can be derived by considering a non hydrostatic pressure distribution, known as the Boussinesq equations. These can be obtained by integrating the full three-dimensional Navier-Stokes equations (named after Louis Navier, a French physicist, and George Stokes, a British physicist) in the vertical direction, and by making use of the Boussinesq assumption. In this assumption, the flow velocity in the vertical direction is considered to vary from a minimum zero at the bottom to a maximum at the flow surface (Chaudhry, 1993). Although this last set of equations has been used in flood simulation (ex: DIVAST model) (Lin et al., 2006) it is certainly the exception and not the rule. Moreover, based on the various existing models, other authors disagree on the need to include the earth's rotation or wind shear stress in flood modelling.

The applicability of the St. Venant equations for free-surface flow can be expressed by the following assumptions:

- The pressure distribution is hydrostatic (the flow streamlines do not have sharp curvatures)
- The lateral inflow is nil.
- The longitudinal channel bottom slope is small.
- The flow velocity is uniform across the channel cross section (1D).
- The flow velocity distribution in the vertical direction is uniform (1D and 2D).
- The flow is gradually varied.
- The head loss is approximated by the uniform flow.
- The liquid is incompressible and homogeneous.
- The coriolis and wind forces are negleted.

These equations can be written in the conservative form (equations (2.1) and (2.2)), function of (A, Q), as opposed to the non-conservative form, function of (h, v). The conservative form has the advantage of being superior in conserving the flow variables

(Ramos, 1986). The conservative form of the 1D St. Vennant equations can be written as:

Continuity equation (1D):

$$\frac{\partial A}{\partial t} + \frac{\partial Q}{\partial x} = 0 \tag{2.1}$$

Where A and Q are the dependent variables, namely the cross-sectional area of the fluid and the flow. x and t are the independent variables, longitudinal direction and time. Equation (2.1) states that the variation of mass along time must equal the balance of water entering and leaving the system. In order to include source or sink terms, a positive or a negative value is given instead of the zero on the right hand side of the equation.

Momentum equation (1D):

$$\underbrace{\underbrace{\underbrace{\frac{1}{A}\frac{\partial Q}{\partial t}}_{2^{\cdot 5}} + \underbrace{\frac{1}{A}\frac{\partial}{\partial x}\left(\frac{Q^2}{A}\right) + \underbrace{g\frac{\partial h}{\partial x} = \underbrace{g(S-J)}_{4}}_{3/2^{\cdot 5}}}_{2}}_{1} \tag{2.2}$$

Where h is the flow depth, S is the bed slope on the x direction, J is the friction slope on the x direction and g is acceleration due to gravity. In equation (2.2) , from left to right, the first two terms are the local and convective acceleration, the third is the pressure term and the last are gravity and friction terms. The friction term is usually approximated by the empirical Manning's equation valid for rough turbulent flow, accordingly to the Moody diagram (Butler and Davies, 2000).

The conservative form of the 2D St. Vennant equations, also known as the Shallow Water equations, can be written as:

Continuity equation (2D):

$$\frac{\partial h}{\partial t} + \frac{\partial hU}{\partial x} + \frac{\partial hV}{\partial y} = 0 \tag{2.3}$$

Momentum equations (2D):

$$\underbrace{\underbrace{\underbrace{\frac{\partial hU}{\partial t}}_{2^{\cdot 5}} + \underbrace{\frac{\partial}{\partial x}(hU^2 + \underbrace{0.5gh^2}_{3/2^{\cdot 5}}) + \frac{\partial}{\partial y}(hUV) = \underbrace{gh(S_x - J_x)}_{4}}_{3/2^{\cdot 5}}}_{2}}_{1} \tag{2.4}$$

$$\underbrace{\underbrace{\underbrace{\frac{\partial hV}{\partial t}}_{2^{\cdot 5}} + \underbrace{\frac{\partial}{\partial y}(hV^2 + \underbrace{0.5gh^2}_{3/2^{\cdot 5}}) + \frac{\partial}{\partial x}(hUV) = \underbrace{gh(S_y - J_y)}_{4}}_{3/2^{\cdot 5}}}_{2}}_{1} \tag{2.5}$$

Where U and V are the velocity components on the x and y directions, S_x and S_y are the bed slopes on the x and y directions, $J_x = n^2 U\sqrt{U^2+V^2}/h^{4/3}$ and $J_y = n^2 V\sqrt{U^2+V^2}/h^{4/3}$ are the friction slopes on the x and y directions, and n is the Manning friction coefficient.

Depending on the flow type, accuracy and computational time, some of the terms on the St. Venant equations can be dropped. Looking at equations (2.2), (2.4) and (2.5), an index ranging from one to four is added to help illustrate the various possible levels of simplification[1]. For further details on these models the reader is referred to the work of Tsai and Yen (2001).

- **Full dynamic model.** In the first model (1) all the terms are considered. It allows for modelling of a full transient phenomenon. The horizontal coordinate and time are the independent variables. The equations are of hyperbolic type, hence the equations have two sets of characteristics. Propagations can travel both upstream and downstream depending on the Froude number. 1D models are often based on the full dynamic equations, e.g. HEC-RAS (Hicks and Peacock, 2005) or SWMM (Huber and Dickinson, 1988). On the contrary, only few 2D models apply these equations, e.g. TELEMAC-2D (Horritt and Bates, 2002) or DIVAST model (Lin et al., 2006), the reason being that: some results show that neglecting the advection terms does not have a significant impact on model predictions. However Lin et al. (2006) showed that if both advective and local accelerations are neglected a slowdown on the wave propagation will become visible.

- **Diffusive model with inertia.** In the second model (2), the local acceleration is no longer considered. This approximation is preferable for flows where inertia terms are dominant. As in the previous model, these are hyperbolic equations. These equations where successfully applied in a 2D depth-averaged free surface flow model (Klonidis and Soulis, 2002).

- **Gravity wave model.** An intermediate simplification between the second and third case is the gravity wave approach ($2^{\cdot 5}$). In this model, the convection acceleration is neglected and the local acceleration is kept. The neglected inertial term is responsible for the oscillatory behaviour of the equations' solution (Aronica and Lanza, 2005). These equations, therefore, benefit from an increase of stability while keeping the ability to propagate along two characteristic directions.

[1]It is common in literature about Governing Equations referring to the word "model" as the different levels of approximation of the St. Venant equations, hence the same definition is applied within this section.

- **Diffusive model without inertia.** In the third model (3), the local and convective accelerations are neglected. The equations are of parabolic type. Unlike the previous models, these equations only have one set of characteristics with the same direction as the fluid flow. Therefore, one of the advantages of this model is that the set of two equations can be reduced to a single equation, the convection-diffusion equation. Nonetheless, this model still produces wave diffusion as well as wave translation. The effect of diffusion is the mechanism that enables it to reproduce backwater effects (Ramos and Almeida, 1987). In both models (2) and (3) propagations can travel in both directions, however the propagation in model (3) is infinite since all the acceleration terms are neglected. This type of equations is often used in 2D overland flow models, although some authors have also developed 1D models (Nasello and Tucciarelli, 2005). In 2D models these are commonly described as urban inundation models (Hsu et al., 2000). Other applications include the study of non-homogenous fluids (ex: multi-layers flow) and transport of pollutants (Abbott, 1979).

- **Kinematic wave model.** In the fourth and last model (4), only the gravity and friction terms are considered. The flow is based on a friction law, and, therefore, the relationship between the depth and flow becomes unique. As in the previous model, it is possible to reduce the set of equations to a single equation resulting in only one set of characteristics. Since waves can only travel downstream, this model is inadequate for cases where backwater effects need to be considered: such as large flat areas or ponds. In this model waves translate at a constant speed (celerity) but do not suffer any attenuation (damping). Despite it, this model can exhibit an "artificial-diffusion" dependent on the numerical diffusion of the scheme, function of both the space and time step used. This model is often used for calculating runoff (Klawitter and Ostrowski, 2006) or initial conditions (e.g. SIPSON runoff model) rather than as a hydraulic engine. However, rapid flow models (see section 2.3) have used kinematic wave models as hydraulic engine (Hsu et al., 1999).

Ponce et al. (1978) investigated thoroughly the range of applicability of kinematic and diffusion models. By calculating the propagation celerity and logarithmic decrement corresponding to both models, they were able to define the models' applicability (see equations (2.6) and (2.7)). The bed slope and wave period are the two main driving factors. For large bed slopes, typical of overland flow and long wave periods with slow rising flood waves, the kinematic wave model is appropriate. The diffusion model, on the contrary, is appropriate for a wider range of slopes and periods than the kinematic model. At catchments-scale, the diffusion and the full dynamic model give practically the same

results (Ponce and Pikin, 1987). Later Ponce (1991) added a dynamic component to the kinematic and diffusion models to extend their capabilities to the dynamic model. The use of this dynamic component was shown to increase the applicability of both kinematic and diffusion models. The applicability of the kinematic and diffusion equations is defined by:

$$TS_0\frac{v_0}{d_0} > 171 \tag{2.6}$$

$$TS_0\sqrt{gd_0} > 30 \tag{2.7}$$

Where T is the wave period, S_0 is the significant bed slope, v_0 is the significant velocity and d_0 is the significant depth.

The Boussinesq equations. The St. Venant equations are the most used set of equations in the majority of the existing numerical models. Looking at their assumptions, it is readily seen that they are not valid when modelling steep wave fronts. If the flow streamlines have sharp curvatures, the pressure distribution is no longer hydrostatic. In this case the Boussinesq assumption (Chaudhry, 1993) should be used. The St. Venant equations can be altered to include the Boussinesq terms. However, there is some debate about whether additional terms should be used. Equation (2.8) illustrates the momentum equation with the corresponding Boussinesq terms added in the case of rectangular channels:

$$\frac{\partial vh}{\partial t} + \frac{\partial}{\partial x}\left(v^2h + g\frac{h^2}{2} + B1 + B2 + B3\right) = g(S - J) \tag{2.8}$$

where:

$$B1 = -\frac{h^3}{3}\frac{\partial^2 v}{\partial x \partial t} \tag{2.9}$$

$$B2 = -\frac{h^3}{3}v\frac{\partial^2 v}{\partial x^2} \tag{2.10}$$

$$B3 = \frac{h^3}{3}\left(\frac{\partial v}{\partial x}\right)^2 \tag{2.11}$$

Mohapatra and Chaudhry (2004) showed that the St. Venant equations alone are a good approximation for modelling the complex dam-break problem. They conclude that there is no need to incorporate in the governing equations any additional terms such as the Boussinesq terms shown in equations (2.9), (2.10) and (2.11)[2].

[2]In urban flood modelling a typical wave front will be smaller and less steeper than the one generated by a dam-break, hence the same conclusions must hold.

The Pressurized flow. Unlike the St. Venant equations, the two dependent variables are the piezometric head and flow (H, Q), while the two independent variables are kept the same, (x, t). As in free-surface flow, these equations can be further simplified (Almeida, 1983).

In this case the following assumptions are taken into account:

- The pressure distribution is hydrostatic (the flow streamlines do not have sharp curvatures)
- The lateral inflow is nil.
- The pipe has a linear elastic behaviour.
- The flow velocity is uniform across the pipe cross section.
- The flow is gradually varied.
- The head loss is approximated by the steady-state resistance laws.
- The liquid is incompressible and homogeneous.

Continuity and momentum equations can be written in the conservative form (equations (2.12) and (2.13)) as:

Continuity equation

$$\frac{\partial H}{\partial t} + \frac{c^2}{gA}\frac{\partial Q}{\partial x} = 0 \tag{2.12}$$

Momentum equation

$$\frac{1}{A}\frac{\partial Q}{\partial t} + \frac{1}{A}\frac{\partial}{\partial x}\left(\frac{Q^2}{A}\right) + g\frac{\partial H}{\partial x} = g(S - J) \tag{2.13}$$

Where H is the piezometric head. Besides the change in dependent variables, it is readily seen that the second term of equation (2.12) is different from that in (2.1). c is the celerity of the pressure waves ((2.14)) and is defined by (Chaudhry, 1987):

$$c = \sqrt{\frac{K}{\rho\left(1 + \frac{K}{E}\psi\right)}} \tag{2.14}$$

Where ρ is the fluid density, K is the bulk modulus of elasticity, E is the Young's modulus of elasticity of the conduit walls and ψ is a non-dimensional parameter. Equation (2.14) shows that the celerity calculation is dependent upon the elastic properties of the conduit. Except for thick-walled elastic conduits, celerity is assumed as constant for each pipe. For example, in the case of rigid conduits, ψ equals 0, and in case of thin-walled

elastic conduits with frequent expansion joints, it equals $\psi = D/e$, where D = diameter of the pipe and e = wall thickness.

The equation (2.13) differs from the equation (2.2) in the friction term. This term is replaced by the Colebrook-White equation, valid for the transition zone from laminar to fully turbulent flow on the Moody diagram. Alternatively it can be approximated less accurately by the Hazen-Williams or the Chezy-Manning equation (Potter and Wiggert, 2001).

The above equations, for free-surface and pressurized flow, show that: Firstly, although similar they do not provide a unified system of equations for the mixed type of flow (free-surface-pressurized flow). Therefore, the task of accurately simulating the transition state between free and pressurized flow becomes a complex task. In section 2.3, some simplified ways to overcome this issue will be presented. Secondly, analytical solutions of the full dynamic equations only exist for very simplified cases. Hence, numerical techniques are essential in order to solve them. The next section presents and discusses some of the available numerical schemes.

2.2 Numerical Schemes

Unsteady gradually varied flow is better described by the full dynamic equations, for both free-surface and pressurized flow. Because of the presence of non-linear terms, an analytical solution of these equations does not exist except for simplified cases, therefore, the equations are solved by numerical methods. Each numerical method has its own advantages and disadvantages that depending on the problem specifications influence the quality of the results. Problems such as numerical diffusion, oscillations and instabilities can be explained by an inadequate choice of parameters or/and numerical scheme. Having a good understanding of the numerical schemes used in the different models is of prime importance for analysing and cross-comparing the models' results. In the literature, these numerical schemes are often tested on simplified cases for which analytical solutions are available, such as the classic instantaneous dam-break problem in a rectangular channel. In this way, it is possible to assess their agreement.

The following describes some of the numerical schemes often used in the literature, and discusses their strong and week points. These classical methods are well established in the science community and can be found applied within existing urban flood models.

The Classical Methods. There is a wide choice of available numerical methods in the literature starting from the method of the characteristics developed by Monge (1789) to the more advanced TVD schemes introduced by Harten (1983). Although the St. Venant equations had been presented already in 1871 (de Saint-Venant, 1871), only with the advances in computer engineering was it made possible to test thoroughly and develop the various numerical methods. Among the classical methods, it is possible to further divide them into three sub-groups:

- Method of Characteristics (MOC)
- Finite-difference methods (FDM)
- Finite-element methods (FEM)

In MOC, the governing equations are converted into characteristic equations. This method is not used as much in free-surface flow as it is in pressurized flow. In free-surface flow the MOC fails because of the convergence of characteristic curves whenever a bore or shock forms (Chaudhry, 1987). However it is commonly used in association with FDM for prescribing the boundary conditions (Ramos, 1995). Recently, Mohammadian et al. (2007) presented a conservative extension of the MOC which allowed for simulation of 1D shallow flows by using a uniform non-oscillatory scheme and a conservative interpolation function.

In FDM the governing equations are approximated with finite difference quotients. These methods can be further divided into explicit schemes and implicit schemes. Explicit schemes are conditionally stable under the Courant-Friedrichs-Lewy condition which sets a limit on the maximum allowable time step (Courant et al., 1967). In explicit schemes the solution is calculated directly in terms of known quantities (usually easy to implement, but computationally expensive). On the contrary, implicit schemes are unconditionally stable; hence, they do not have any stability restriction on the size of the time step. In implicit schemes, the solution is calculated in terms of unknown quantities. They tend to be more robust in execution, but more difficult to program. Explicit schemes are preferred for unsteady flow problems since the linearization introduced in implicit schemes to make them efficient (by the use of the Thomas algorithm (Thomas, 1949)), requires the governing equations to be written in a non-conservative form. The Thomas algorithm is easily implemented if the system can be cast into a three diagonal system of equations. It consists of a double sweep; the first is a forward sweep where a matrix is obtained with two diagonals. The second is a backward sweep that allows the matrix obtained in the previous step to be solved (Djordjevic, 2001). Taylor-series expansion or polynomial

fitting is used to obtain approximations to the first, second, or higher order derivatives of the variables with respect to the coordinates (Ferziger and Peric, 2002).

In FDM, a variety of numerical methods for simulating mixed flows with shocks have been introduced. Fennema and Chaudhry (1987) reviewed and compared the MacCormack, Gaubutti, and Preissmann schemes. Harten (1983) was the first to introduce the notion of total variation diminishing (TVD) to solve hyperbolic equations. Later authors that had used the original MacCormack's scheme (Franco, 1988), adapted it to become TVD (Garcia-Navarro et al., 1992; Franco, 1996). Tseng and Chu (2000) then investigated the accuracy of the combined approach using four different versions of predictor-corrector schemes. Ferreira (2005) found that the MacCormack/TVD scheme produced a step-discontinuity in the flow variable. This was found in the transition from sub-critical to supercritical flow in a channel where the slope changed and where Froude number equalled unity. The author concluded that the bed slope acted as a source term and was responsible for this behaviour. As a solution, the author suggested the use of artificial viscosity instead of TVD to smooth this transition. Artificial viscosity has the advantage of substantially reducing the oscillations ahead of a shock, at the cost of spreading the shock over several grid points (Fletcher, 1991).

Preissmann's scheme is one of the most widely used methods in free-surface 1D numerical modelling. It is an implicit scheme, which means that the unknown variables appear in the algebraic equations; therefore, the set of equations must be solved simultaneously. Meselhe and Holly (1997) showed that it cannot be used to simulate transcritical flow. Later Djordjevic et al. (2004) presented some measures to reduce this limitation. Although implicit models do not have to respect Courant's stability criteria (Chaudhry, 1987), they suffer from instability derived from oscillations whenever the changes of flow or depth are too rapid within a time step. This is more likely to occur in the presence of small water depths; in that case depth oscillations can be sufficient to cause the simulation to fail.

In 2D numerical modelling, implicit schemes have been introduced by Leendertse (1967) with the Alternating Direction Implicit (ADI). Later it has been subsequently improved by others such as Stelling et al. (1986) and Falconer (1980). The ADI method splits the procedures for solving the 2D finite difference equations into two steps: one where the x derivative is taken implicitly and a second where the y derivative is taken implicitly; by doing so the two systems of equations can then be solved separately. As in 1D numerical modelling, here the main concern is the ability of the scheme to model flows with discontinuities (Liang et al., 2007).

Venutelli (2006) extended the use of polynomials to FDM, by presenting a third-order explicit time-stepping model. The results were compared with analytical and experimental

results, but no comparison was made against existing numerical methods. Jha et al. (1995) investigated the applicability of a first-order flux difference splitting scheme and its second-order extensions. The objective was to demonstrate that although higher-order schemes provide better shock resolution, Roe's first-order scheme (Roe, 1981) may be preferred for practical applications whenever computational time and applicability are the main concerns.

The FEM method is particularly useful when a robust approximation is sought to solve partial differential equations on a non-homogeneous mesh. In FEM the domain is broken into a set of discrete elements that are generally unstructured. The distinguishing feature of FEM is that the equations are multiplied by a weighting function before being integrated over the entire domain. The solution is approximated by a shape function, within each element, in a way to assure continuity across each element's boundaries. This approximation is then substituted into the weighted-integral of the conservation-law and the equations to be solved are derived by imposing the derivative of the integral to be zero in respect to each nodal value. The method's main advantage is its ability to deal with unstructured grids, and its main disadvantage is that the matrices are not well structured, which imposes difficulties on solving methods (Ferziger and Peric, 2002). Venutelli (2004) obtained the spatial discretization by the standard Petrov-Galerkin finite element method, with two parameters cubic weight functions.

The next section reviews the urban flood models concepts, terminology and definitions, and presents an overview of the existing hydraulic models along with the case studies where they have been successfully applied.

2.3 Urban Flood Models

Pluvial flooding in urban areas is a phenomenon caused by an extreme rainfall event whereby the surface flooding is augmented by the sewer surcharge. When the rainfall runoff exceeds the conveyance capacity of the sewer system, the surface flow cannot enter the sewer and surcharge water from the manholes may occur contributing to the exceedance flow on the surface. At this point a consistent urban flood model should be able to consider the linkage between the two systems. The dual drainage concept, as introduced by Djordjevic et al. (2005), acknowledge the need to consider the interactions between a minor system and a major system. The major system includes all above ground flood pathways (natural and man-made), including both open and culverted watercourses. The minor system is the drainage sewer network, including the manholes and the inlet connections.

When these two systems are modelled together, they form the integrated hydraulic models.

The major system is often modelled by either one-dimensional (1D) or two-dimensional (2D) models. Looking at the man-made pathways of an urban mesh, as long as the flow on the surface remains within the street profile, the 1D models can be considered a good approximation (Mark et al., 2004). However, if the flow overtops the curb levels, the 2D models are a better choice. Mostly because open channels in rural areas have not been subject to a proper design to convey flow (natural channels), therefore, their paths tend to be irregular with many exit points. Moreover, new surface flood pathways, highly dependent on the rainfall intensity, are generated by the exceedance flow, which are hard to predict making difficult the task of identifying them, and, therefore, including them in the 1D model. One way to discretise the surface network (in 1D models) is to consider the domain as a set of nodes connected by links (Nasello and Tucciarelli, 2005). Here the nodes represent the channel junctions, ponds or crossings, connected by links, mainly the open channels. In 2D models the domain is discretised as a coordinate system of nodes (i.e. grid of points or mesh), where each point on the grid is represented by spatial coordinates (X, Y, Z). Both models share two unknown variables, namely flow and water level, with the difference that in the 1D approach the velocity has only one component, and in the 2D approach it can be decomposed into two orthogonal components (X, Y).

The minor system in urban flooding has exclusively been modelled by 1D models; this is easily explained with the preferential direction of the flow along the longitudinal pipe axis (1D assumption). If the water level remains lower than the pipe crown, then the water flow inside the pipe remains with free-surface. However, if the water level reaches the pipe crown, the water flow will become pressurized, and it is then possible to have both types of flows occurring at the same time, in a single pipe. Free-surface flows that are expected to partially pressurize are called free-surface-pressurized flows (section 2.1). In order to account for this type of flow shift, most models adopt the Preissmann slot concept (Preissmann, 1961). When modelling with 1D models in the major system, the domain is discretised as a network constituted of nodes and links. In this case the nodes represent the manholes and the links correspond to the pipes or culverts. The two unknown variables are the flow and the water level.

The need to predict correctly the extent of the flood led to the development of the dual drainage concept. Early attempts to accomplish that were unsatisfactory as the two systems were modelled separately neglecting the interaction between them (Ellis et al., 1982). This issue was highlighted with the arising need of assessing damage cost due to the water surcharged from the manholes (Schmitt et al., 2004). Furthermore, the determination of the correct flood-extents had become a challenging issue (Dey and Kamioka,

2006). With SWMM came the first attempt to model the surcharged flow:

> "The surcharged flow is kept atop of the manholes and only allowed to be drained back to the sewer once the sewer capacity is made available" (Rossman, 2005)

This procedure would only be correct if the manholes were located in a depression. Otherwise, it would be unrealistic because the water was prevented from naturally propagating (on the surface) downstream once the manholes surcharged. Three questions arose these early attempts on applying the dual drainage concept:

1. How to implement effectively the dual drainage concept?
2. How to define the linking element to determine the flow exchange? (section 4.2)
3. How to define the time synchronization between the two models (minor/major)?

Whenever a model links a major to a minor system by elements which enable the flow transfer between both systems in a synchronized manner, it is called an integrated model. This type of models can be further classified into partially and fully integrated. Fully integrated models couple the two systems using the same time step, generally driven by applying a time step limiter for stability, such as the Courant condition. In the partially integrated approach, both models are run separately and the flow exchange is only done at specific time steps (synchronization) (Schmitt et al., 2004; Chen et al., 2007). Three types of models can be derived: 1D/1D, 1D/2D and 1D/3D. The first two differ on applying a 1D or a 2D model to the major system, the last one incorporates the possibility of using a full three-dimensional model (3D), but this is rarely the case in urban flood modelling, hence it will not be further discussed. These models can be coupled by conserving either of three quantities: Energy, continuity or momentum. The last is rarely applied due to the difficulty in transferring momentum from a vertical direction to a horizontal and vice-versa. Most models tend to use conservation of energy and continuity. Energy conservation is achieved by matching both water levels in both systems subtracted from any local losses and kinetic energy, whereas the continuity conservation is obtained by transferring the same volume of water per unit time between the two systems (Verwey, 2007).

The concept that enabled transferring from theory to practice the dual drainage concept is the open slot concept. This simple concept, introduced by Preissmann, allows for the modelling of free-surface-pressurized flows. This technique shows that the St. Venant equations (valid for free surface flow) can still be applied to pressurized flow (see section 2.1) provided that the two following conditions are satisfied (Chaudhry, 1987):

1. The depth of flow (h), in free surface, must be identical to the piezometric head (H) in pressurized flow.
2. The celerity ($a = \sqrt{g\frac{A}{B}}$), in free surface, must equal the celerity of the pressure waves (c) in pressurized flow (B = cross-sectional surface width).

In the original technique, a narrow slot is set at the top of the crown level. The width is selected in order to satisfy the second condition, $a = c$, whilst it is expected that the increase of area and changes in the hydraulic radius are not significant. Most commercial models use this technique (MOUSE, XPSWMM, PCSWMM and InfoWorks). Others modified this technique either by applying a smooth transition (Djordjevic et al., 2004), or considering a fixed width of 0.1% of the maximum width, and disregarding the extra area added and wetted perimeter introduced by the slot (Zhong, 1998). The simplistic approach is to take a fixed value for the celerity (c), such as 10m/s (Inoue et al., 1999).

As an alternative Vasconcelos et al. (2006) developed the Two-Component Pressure Approach, and later compared it with the Preissmann slot concept (Vasconcelos et al., 2005). In this approach, the hydrostatic pressure term is decoupled from the pressure terms that appear in the pressurized flow regime. Similarly as in the Preissmann slot, the celerity is assumed constant throughout the pressurized flow regime. The improvement lies in the possibility of modelling negative pressures, hence enabling simulation of negative pressure waves.

The Existing Flood Models. The existing urban flood models can be classified into two main categories, research based applications and commercial software packages. These two main model categories generally do not share the same strengths and weaknesses. The first tend to be more heterogeneous, where governing equations, numerical schemes and links between overland flow and sewer flow may differ across applications. In addition, some of these models are developed for research purposes, which outcomes need to be tested/validated. Consequently, these rather recent hydraulic models can generate great interest within the scientific community, however often they are also less robust. On the contrary, the second category is characterized by the use of similar, well established governing equations, and comprehensively tested numerical schemes. Therefore, in this category the models tend to be more robust and well tested. This standardization led the developers to focus on the development of user-friendly graphical interfaces, which make them appealing to the end user. Some of the studies based on both these categories will now be discussed.

Chen et al. (2007) linked two research based applications, SIPSON with UIM. SIPSON solves simultaneously the continuity equations for network nodes, the complete St. Venant

equations for the 1D networks and the links equations (Djordjevic et al., 2005). The UIM is a 2D diffusive overland-flow model that solves the non-inertia flow equations. Chen et al. (2005) used a two-step alternating direction (AD) explicit numerical scheme for solving the governing equations. Since both models have different time steps, a synchronization procedure was developed to ensure a proper transfer of discharges. The proposed model, SIPSON/UIM, was said to simulate the complex flow process on overland-surface of pluvial flooding cases, more effectively than the 1D model.

Carr and Smith (2006) presented a 1D/2D model which linked the 1D sewer network model MIKE STORM (DHI, 2007b), with the overland 2D flow model MIKE 21 (DHI, 2007a). In this study, the performance of the 1D/2D model was compared to the 1D/1D MIKE STORM. The comparison was done based on a time series downstream-discharge on two catchments, Auckland (New Zealand) and the Upper Middle Harbour catchments of Sydney in Australia. The authors concluded that the 1D/2D model provided better fit to the time series, and it had the advantage of not having to delineate the flow paths, as compared with the 1D/1D model. MIKE STORM shares the hydraulic engine with MOUSE, the first hydraulic model developed by DHI in 1983. This model is based on an implicit FDM.

O'Loughlin et al. (2006) analysed the DRAINS model. The author stated that for complex cases of overland flow, the Drains model was not realistic and that the surface model should be run separately either by using HEC-RAS or 2D models. As for setting up the model, the author found it difficult to define accurately surface pathways in two particular situations: when a subsurface path is encountered and in cases where the flow overtops the pathways. The study concluded with the need for developing and integrated sewer an overland flow model.

Philips et al. (2005) used XP-SWMM2D to simulate Cumberland highway sub-catchments, Cabramatta (Australia). XP-SWMM2D is an integrated model that links 1D XP-SWMM, to model the minor system, with the 2D TUFLOW, to model the major system. The increased availability of aerial laser scanning (ALS) is said to provide enough detail to support the 2D modelling. A flood extent comparison was done using TUFLOW alone, and integrated with XP-SWWM. Strong differences were highlighted in this comparison, encouraging the use of integrated linking. In this same study, a coupled model was used to perform a review of flood levels in Prospect Creek floodplain. In this case the 2D model was compared with the 1D/2D model, where the river was modelled as a 1D channel. The 1D/2D was said to outperform the 2D based on loss of definition of channel sections (using a 10 m grid). Having a 1D channel avoided the need for a finer grid to be used on the river bed. SWWM is the EPA Storm Water

Management tool, which was first developed in 1971, and it has undergone several upgrades, until its latest version, EPA-SWWM5. This last version is freely downloadable at ":http://www.epa.gov/athens/wwqtsc/html/swmm.html" TUFLOW was first released in 1990 as a joint project from WBM Pty Ltd and The University of Queensland. The 2D solution is based on the Stelling finite difference, alternating direction implicit (ADI) method. The 1D solution is based on a two-stage explicit method. XP-SWWM is a software package copyright of XP Software Inc. which uses SWWM as the hydraulic engine.

Bolle et al. (2006) studied the bi-directional interaction between the sewer network of Erpe-network in Belgium and the Molenbeeek River using the SOBEK model. Although SOBEK can also accommodate 2D simulations, both sewer and river were modelled using 1D models. This study indicates that whether the simulation objectives are upon the sewer or the river results, the bi-directional interaction becomes respectively more or less relevant. This is to say that bi-directionality is required whenever the interests in sewer behaviour becomes gradually more important. Spatially the sewer water level differences become largely higher at the downstream ends, and decrease towards the upstream ends. The authors however concluded that this last statement is strongly system dependent. SOBEK is copyright of Delft Hydraulics, Netherlands. It is based on the 1D full dynamic equations and the 2D shallow water equations, using an implicit scheme known as the Delft Scheme.

Spry and Zhang (2006) used the 1D/1D models XP-SWMM and DRAINS to model two distinct case studies. The surface network was delineated based on digital-terrain-model (DTM), and fine-tuned based on cadastre, site reconnaissance and aerial photography. It was assumed that generally the surface pathways would follow kerb lines along driveways, roads and property boundaries. The study concluded that it was necessary to use integrated models, and that 1D/1D models can be an economic and robust alternative for 1D/2D models in case of lack of data or non existence of flat areas.

Lhomme et al. (2006) compared a 1D GIS based model (kinematic) with the 2D model RUBAR 20 (shallow water Equations). The authors concluded that the former model accurately models the steepest streets but is less suitable for flatter streets. Moreover the distribution of flows at crossroads and disregarding of backwater effects were expected to be a major source of errors in the 1D model.

Mark et al. (2004) studied the potential and limitations of 1D/1D modelling. The study was divided into three parts. The first part defined the modelling approach, and where pipes and surface paths were set to be modelled as 1D elements. The second part discussed the data required for validation. The last part focused on the outline of a simple cost function for assessing damage cost. In the authors' opinion it was necessary to use

the full dynamic equation to model urban flooding to fully capture backwater effects and rapid changes of water level (section 2.1, discussion on equation (2.2)). With regard to the surface network, it was found necessary to compute accurately storage level curves, and determine the flood pathways based on a GIS procedure using a Digital-Elevation-Model (DEM). The study concluded that during heavy flooding the 1D approach may be insufficient, and indicated the need to use a full 2D dynamic model to describe the surface flow.

Vaes et al. (2004) used the 1D/1D model INFOWORKS CS. The author applied the concept of dual drainage, and used this commercial software to link a 1D sewer network with a 1D surface pathways network. Several interesting issues were brought up in this study. Firstly, the rainfall input: instead of inputting the rainfall into the sewer nodes, it distinguished between areas draining to the surface pathways and roofs, and other areas draining directly to the sewer network. Secondly, slope limiter: the need to include a limit to the pipe slopes, as that was recognized as a potential cause of numerical problems. Thirdly, Preissmann scheme weighting factor: instabilities may force the modeller to increase this value closer to 1, with the counter effect of increasing the numerical diffusion. Fourthly, small water depths: Loss of accuracy in the surface network for small water depths when the inertia terms of St. Venant equations are phased out for high Froude numbers. The surface pathways were represented by a wide cross-section. In INFOWORKS CS it is possible to pre-specify which pipes will be pressurized and, therefore, use the correct set of equations (equations (2.12) and (2.13)). However in this case the conduit is not allowed to have free-surface flow (Wallingford-Software, 2006). Recently it was enhanced to an integrated 1D/2D model with the release of INFOWORKS CS2D. INFOWORKS CS was released in 1998 and is copyright of Wallingford Software Ltd.

Paquier et al. (2003) compared the 1D model REM U with the 2D model RUBAR 20 in an urban study. It was concluded that the 1D model is a privileged tool for modelling highly urbanized areas because those areas penalise 2D models. The study suggested the need to develop coupled 1D-2D models, where 1D models would replace the streets and 2D models would be used in singular points such as street-crossings, parking areas and other wider areas.

The Rapid Flood Models (RFM). Calibration techniques may be the future bridge that will enable fast storage cell models to compete with the well established flood models, reviewed in the previous section. Hankin et al. (2008) stated that fast storage cells can be used at national level for highlighting areas at greatest risk and identify areas that need greater modelling detail. In the literature, integrated and coupled models are often used

with the same meaning. However, in this Thesis they are defined as follows. An integrated model is defined as: simultaneously linking and simulating two or more systems (e.g. minor, major and underground systems). A coupled model is defined as: simultaneously linking and simulating two systems (e.g. minor and major systems). With the above definitions, it is clear that all coupled models are necessarily integrated; however, the reverse may not be true. According to Hunter et al. (2005b), one of the earliest coupled models was developed between 1975-1976, by coupling a 1D full dynamic sewer-model with an inertia-less storage cell algorithm. At that time the computational cost enabled kinematic wave models to be deemed acceptable. Generally, they worked by using either a weir type equation or a friction law to drive the flow between cells. Some of the unacceptable drawbacks of the kinematic wave model can be reduced by using a suitable calibration technique, by taking advantage of the very low computation time of a full simulation. Krupka et al. (2007) reported simulation times of up to a second. The final paragraph of this section presents the pros and cons of some of the existing RFM.

Storage cell models tend to have the propagation speed of wave fronts highly dependent on the model grid scale and insensitivity to the floodplain friction. Hunter et al. (2005a) introduced a technique, in an existing storage cell model LISFLOOD-FP, based on adaptive time step, and tested it in a case study with real data. In this study, the original flow limiter used to prevent the over or under shoot of the solution, is replaced by a variable optimal-time-step calculated at each computational time that enables the solution to remain stable. It was found, however, that below a given threshold, defined by the water level difference between two cells, the momentum equations needed to be linearised to ensure stability. One of the main drawbacks reported was the increase in computational time of up to 6 times.

Villanueva and Wright (2006) compared LISFLOOD with TRENT. TRENT is a research based 2D model based on a Godunov, splitting approach and an approximate Riemman solver by Roe (Roe, 1981). It is an explicit FDM, first order in time and in space, that discretises the full dynamic equations. The authors reported that the LISFLOOD model needed to be calibrated when the grid resolution was changed to higher resolutions. On the contrary, the TRENT model showed convergence to a single solution when the grid was refined. With an optimum-grid-size determined to be 18 m and 12000 cells, the storage cell model took 2h30 against the 7h30 taken by the TRENT model to simulate a 300h event. The study concluded that the storage cell model was applicable whenever studying relatively slow-varying inundation-events (in agreement with Ponce et al. (1978) see section 2.1).

Hsu et al. (1999) developed a flood inundation model based on the concept of storage

cells. Instead of using a friction law, the authors used weirs, orifices and channel-links to drive the flow across cells. Each cell was modelled with individual parameters, which in turn transformed the task of modelling into a cumbersome task of calibration. Each cell parameter had to be calibrated against a 2D FDM model. Pa-chang Creek basin, in Taiwan, was the site used to test the model. With a total area of 20500 hectares, the model comprised 159 cells with an average area of 136 ha. The author concluded that it was suitable to be used as an inundation model of the Pa-chang Creek basin to produce inundation-maps.

Nevertheless, RFM models rely on the modeller's expertise to define the number of cells. As the velocity of propagation is highly dependent on the number of cells, during a calibration run the parameters may move away from their physical value. Furthermore, these models are more efficient with coarser grids (Hunter et al. (2005a) suggested grid sizes greater than 50m). This could prevent the model capturing important topographic features like ponds, buildings or roads. Maksimovic and Prodanovic (2001) presented a discussion of ongoing research into dealing with data within urban flood modelling. The resolution required for a computer to distinguish between a street and a house, namely the horizontal resolution, has to be in the order of 1 to 2 meters. Moreover, they concluded that in order to capture the water flow realistically, the vertical resolution has to be of less than a kerb height. The CIRIA report recognized that features such as kerb heights and property threshold can significantly affect flood risk (Lancaster et al., 2004). Because RFM are said to be efficient with large grid sizes, their application can become compromised depending on the accuracy required for modelling surface floods.

Table 2.1, summarizes existing urban flood models. The table is divided into two parts: the first part lists the commercial software and the second part the research based applications. Unfortunately not all information was available to complete the table. Where this information was not available, the symbol "(?)" appears instead. For further reading on this topic the reader is referred to the works of Zoppou (2001) where a description of several storm-water models can be found; Hunter et al. (2008) where six two-dimensional (2D) hydraulic-models (DIVAST, DIVAST-TVD, TUFLOW, JFLOW, TRENT and LISFLOOD-FP7) were compared in a benchmark study; and Elliot and Trowsdale (2007) where a review of models for low-impact urban storm-water drainage on water quality and flow effects is presented, as well as a description of future research for improving the existing models.

Next section describes the various elements used to link the minor to the major system in the models discussed so far, and presents the general governing equations that are the backbone of such elements.

UFM	Linking	Model type	Num. Sch.	G.E.
HEC	no	1D	(I)	(1)
MOUSE	no	1D	(I)	(1)
REM U	no	1D	(E)	(1)
MIKE21	no	2D	(I)	(1)
DIVAST	no	2D	(I)	(1)
DIVAST-TVD	no	2D	(E)	(1)
JFLOW	no	2D	(E)	(3)
RUBAR 20	no	2D	(E)	(1)
SWMM	yes	1D/1D	(E) and (I)	(1),(4)
MIKESTORM	yes	1D/1D	(I)	(1))
XP-SWMM	yes	1D/1D	(E) and (I)	(1)
INFOWORKS CS	yes	1D/1D	(I)	(1)
DRAINS	yes	1D/1D	(?)	(1)
TUFLOW	yes	1D/2D	(E)/(I)	(1)
XP-SWMM2D	yes	1D/2D	(E)	(1)
SOBEK	yes	1D/1D or 1D/2D	(I)	(1)
LISFLOOD-FP	no	storage cell	(E)	(4)
SIPSON	yes	1D/1D	(I)	(1)
SIPSON/UIM	yes	1D/2D	(I)/(E)	(1)/(3)
TRENT	yes	1D/2D	(E)	(1)

Table 2.1: List of existing Urban Flood Models (UFM) and their linking and model types, numerical schemes (Num.Sch.) E-explicit, I-implicit, and governing equations (G.E.) with the indexes used in equation (2.2).

2.4 Linking Surface with Subsurface Networks

As discussed in the previous section only the integrated models fully consider the link between the surface (major system) and the sub-surface (minor system). It is this feature that distinguishes integrated models, and enables the modelling of urban flooding. The linking element defines how appropriate a model is to address urban flooding. The exceedance flow is controlled by the discharges allowed by these elements to transfer flow from the sub-surface to the surface and vice-versa. While being the main feature responsible for regulating the volume discharged onto the surface, these elements end up

defining and constraining the extent of the flood inundation. Surprisingly there is a lack of research on this topic. It is imperative to have a good understanding of the physics, governing equations and geometric characteristics of these elements, to obtain a better agreement between our modelling and the reality.

General references in this subject disregard the interaction between these two systems. They assume the inlet capacity to be controlled solely by the inlet type and the flow on the surface (Akan and Houghtalen, 2003) or, alternatively, by defining a gully efficiency (Balmforth et al., 2006). The geometry of the inlet below ground is considered irrelevant. The most common way in which this element has been modelled is through the use of either a weir equation or an orifice equation, or a combination of both. However, none of these elements are representative of the real flow conditions. Moreover, the real linking elements include not only the surface inlet, but also the pipe inlet and its connections, the manhole and the buried sewer pipe connections.

The Fundamental Equations. Four different weir/orifice types of equations can be found in the literature. Broad-Crested weir, sharp-crested, orifice and submerged weir. All can be derived using the Bernoulli and continuity equations. The four types will now be reviewed.

In the broad-crested weir the streamlines become parallel, resulting in an hydrostatic pressure distribution. The equation is obtained by applying the Bernoulli equation in a rectangular channel between two points (the first upstream the broad weir and the second on the crest), and by neglecting the kinetic energy upstream from the broad weir (Potter and Wiggert, 2001). Since there is no contraction of the flow over the crest, there is no need to use a discharge coefficient. The following equation is obtained:

$$Q = \frac{2}{3}\sqrt{\frac{2}{3}g}bH_1^{3/2} \tag{2.15}$$

Where H_1 is the specific energy, Q is the discharge flow and b is the channel width.

For the sharp crested weir, the flow is first assumed idealized: no contraction, atmospheric pressure in the nappe and uniform flow with negligible kinetic energy before the weir. In this case there is a need to add a discharge coefficient (Cd_1) in order to approximate the theoretical to the experimental results. Butler and Davies (2000) suggest values between 0.6 and 0.7. The equation obtained is:

$$Q = Cd_1\frac{2}{3}\sqrt{2g}bH_1^{3/2} \tag{2.16}$$

Where Cd_1 is the discharge coefficient of the sharp crested weir.

The orifice type of equations can be derived by applying the Bernoulli and continuity equations between two points, before and after the orifice, along the centre streamline, in a horizontal duct with area A, which has an orifice plate with area A_0. In this case the discharge coefficient (Cd_2) is given as a function of: the reduction of area by the orifice plate, A_1 to A_0, the contraction coefficient (Cc) due to the "vena contracta" downstream of the orifice, A_c, and another discharge coefficient (Cd_k) to account for the unknown exact values at the section area of the "vena contracta" (for further information on experimental discharge coefficients the reader is referred to the work of Chanson (1999)). The flow rate equation is given by the relation:

$$Q = Cd_2 A_0 \sqrt{2g\left(H_1 - H_2\right)} \tag{2.17}$$

Where H_2 is the specific energy at the downstream point, A_0 is the area of the orifice and Cd_2 is the discharge coefficient of the orifice given by:

$$Cd_2 = \frac{Cd_k}{\sqrt{1 - 4Cc\sqrt{A_0/A_1}}} \tag{2.18}$$

As for the submerged weir three different ways are presented in the literature. Villemont in 1947 proposed the use of a drowned flow reduction factor (Cdf) into equation (2.16), to take into account the specific energy downstream of the weir. In this case the third discharge coefficient equals $Cd_3 = Cd_1.Cdf$ where Cdf is given by:

$$Cdf = A_c \left[1 - \left(\frac{H_2}{H_1}\right)^{1.5}\right]^n \tag{2.19}$$

Where A_c and n are empirical coefficients. Later in 1952, Gibson assumed that the discharge could be broken into two parts. The upper part of depth $H_2 - H_1$, is defined as a weir equation, and the lower part of depth H_2, is defined as a submerged orifice. Values for the discharge coefficients Cd_4 and Cd_5 can be found in the work of Abou-Seida and Quaraishi (1976).

$$Q = Cd_4 \frac{2}{3}\sqrt{2g} b \left(H_1 - H_2\right)^{3/2} + Cd_5 \sqrt{2g} b H2 \left(H_1 - H_2\right)^{1/2} \tag{2.20}$$

Where Cd_4 and Cd_5 are the discharge coefficients of the weir and the orifice part. Cunge et al. (1980) suggested using equation 2.21 instead, where in equation 2.16 the term $Cd_1\frac{2}{3}$ is replaced by CK_w, and the hydraulic gradient is replaced by the difference in both heads.

$$Q = CK_w H2\sqrt{2g} b \left(H_1 - H_2\right)^{1/2} \tag{2.21}$$

The next paragraph presents some of the studies that attempted to model the linkage of the surface sub-surface by using the above expressions or a combination of those.

The Existing Equivalent Elements. In the report by Mark (2005) the 1D MOUSE was linked with the 2D MIKE21. Four options were considered: An energy formulation, an orifice, a weir and a maximum discharge. The user could then choose which one to use. The energy formulation is similar to equation (2.17), obtained by replacing the Area by the minimum of the manhole area and the inlet area, and without neglecting the kinetic energy from the upstream section of the orifice. The orifice equation is similar to equation (2.17), where the Area is replaced by the minimum of the manhole area and the inlet area. Both of these formulations were said to be most suitable only when the manhole is submerged. The weir equation was allowed to have two configurations submerged and free, with the choice between them made automatically during the calculation. The weir crest length was set equal to the perimeter of the manhole. The maximum discharge is set to overrule any of the previous formulations in case this value is exceeded.

Nasello and Tucciarelli (2005) considered two equations, namely a weir and orifice. The weir equation was switched to the orifice when the water level on the manhole was above ground level. Furthermore the weir equation was split into one for small depths, where an equation similar to (2.15) was used, and another for larger values of depth, where an equation similar to (2.17) was applied with $H_2 = 0$. Discharge coefficients were suggested for each formulation.

In both studies from Mark et al. (2004) and Djordjevic et al. (2005) two situations were distinguished, namely before and after surcharging. It was the authors' opinion that the link between the surface and subsurface network is better modelled as a weir equation if the flow is from the street to the pipe. In this case it handles both free and submerged flows. The weir crest length is defined as the manhole perimeter and the crest level as the street bottom level. The head is defined by the manhole water level. If submerged, a reduction coefficient is applied to the discharge, depending on the street water level. If fully surcharged the weir equation is switched to an orifice equation, where the driving head changes to the difference between the pressurized manhole and the water in the street.

The study by Vaes et al. (2004) clearly showed the limitations of the current models. Despite the geniality of modelling the filling up of a garage using a storage node, a pipe and a flap valve, in order to avoid the initial condition of flooded water depth, the linkage between the surface and sewer networks was simply simulated as a weir equation. Other studies often simulated that linkage similarly (Dey and Kamioka, 2006).

Hosoda et al. (2002) developed a refined 1D model, using a weir equation for linking the surface and the underground flow. The model refinement was done through considering air pressure changes in the momentum equation of open channels. The results were validated against an experimental set-up. However in the experimental set-up the manhole connections were simplified to a single vertical shaft connecting the sewer to the surface.

2.5 Calibration Methods

Coupling an urban flood model with an automatic calibration procedure generates a powerful tool for urban flood managers. The use of a model validated with real data enables decision makers to have confidence in the outcomes of strategic policies. The side effects of deficient urban plan developments can be easily checked against model outputs such as flood risk maps. It is therefore of paramount importance to have a well calibrated urban flood model able to predict accurately scenarios of the most probable extent of flooding.

"Model calibration is thus defined as the procedure which assesses that a model is properly setup and that it simulates well the selected system" to quote Jean-Philippe et al. (2005) in "Towards a reasoned 1D river model calibration". During a calibration process the model responses are fitted to real observed data by adjusting a set of parameters (decision variables). The parameters can be tuned, either manually or by an automatic procedure, i.e. an algorithm. An algorithms' efficiency is dependent on the type of model to be calibrated and the selected parameters. Even the relatively fast implicit 1D/1D integrated urban flood model can be computationally inefficient for calibration. In effect it discards the use of any automatic calibration where the use of large numbers of repeated simulations is required to achieve a good solution (i.e. Monte Carlo or Genetic Algorithms). To date the calibration process of urban flood models remains a weakly explored topic. This Thesis aims to pioneer the research on efficient algorithms for 1D/1D flood models.

Optimisation refers to the study of problems in which one seeks an optimum solution for a fitting function by systematically choosing the values of parameters from within a set of constraints. The fitting of a model to the observed data is measured by an objective function. Depending on whether the goal is to minimize or maximize the objective function, the optimum solution becomes the minimum or the maximum value obtained on the defined objective function. The constraints define intervals with upper and lower limits which define the allowable values of the parameters. Some techniques ensure that the global optimum solution is found, others only ensure that a local optimum can be

found.

Optimisation techniques can be classified based on the type of decision variables, of constrains and objective functions. The decision variables can be treated either as a discrete or as a continuous domain, depending on whether they can take integer or real values. If the domain is unbounded the constraints are said to be without restrictions (unconstrained), otherwise the constraints can be either linearly or non-linearly restricted (constrained). If the goal of the optimisation is to find the "best" solution, then a single objective function is used, normally by lumping together all objectives and it is called a "single objective problem". If the different objectives cannot be lumped together such that it is not possible to determine the best solution, the optimisation is called a "multiple objective problem". In the latter case, the objectives can be mutually inclusive or exclusive depending on whether by improving one the other(s) are not penalised. Also, in this case, the solution is no longer represented by a single optimum, rather instead by a set of compromised solutions called non-dominated or Pareto-front (Savic, 2002). A multiple objective problem can always be transformed into a single objective problem simply by aggregating all the objectives into one.

Optimisation techniques can be broadly classified into three types: Linear programming (LP)), dynamic programming (DP) and non-linear programming (NLP).

1. **Linear programming.** LP is more suitable for problems where the objective function (2.22) and the constraints (2.23) and (2.24) are a linear function of the decision variables. Even for NLP problems these are often approximated by linear functions and solved by LP methods such as the simplex method or the gradient method. Optimisation techniques are popular in business applications, water resources (Simonovic and Nirupama, 2005) and in water distribution networks, where their use is widespread (Samani and Mottaghi, 2006; Dorini et al., 2006; Farmani et al., 2006). An objective function can be defined mathematically as:

$$f(x_i) = \sum_i a_i x_i \tag{2.22}$$

subject to:

$$\sum_i a_i x_i \leq b \tag{2.23}$$

and:

$$x_i \leq 0 \tag{2.24}$$

Where x_i are the decision variables, and a_i and b are constants. The two inequalities are examples of possible constraints. Inequality (2.23) is a problem physical constraint and inequality (2.24) is the non-negativity constraint.

2. **Dynamic programming.** In order to be effective DP requires the problem to possess an optimal-structure and overlapping sub-problems. In this case computational efficiency can be obtained using memorization techniques Bellman and Dreyfus (1962). In a system with N stages, a cost function $g_k = (x_k, u_k, w_k)$ as a function of state variables (x_k), control variables (u_k) and random disturbance (w_k), the optimal cost $J^*(x_0)$ is equal to $J_0(x_0)$, given by the last step of the following algorithm:

$$\begin{gathered} J_N(x_N) = g_N(x_N), \\ J_k(x_k) = \min E\left\{g_N(x_N, u_N, w_N) + J_{k+1}\right\}, \\ k = 0, 1, ..., N-1 \end{gathered} \tag{2.25}$$

Where the expectation (E), depends on g_k. Furthermore if u^* minimises equation (2.25) for each x_k and k, the policy (solution of the DP problem) $\pi^* = \left\{u_0^*, ..., u_{N-1}^*\right\}$ is optimal (Bertsekas, 2000).

In order to speed up the process, the cost is often calculated using recursive equations. These however are more difficult to programme and depending on the number of stages it may require the increase of the computer memory. It has been used mostly in transport problems such as finding the shortest path or the travelling salesman problem.

3. **Non-linear programming.** NLP is required when either the objective function or at least one of the constraints is a non-linear function of the decision variables. These types of methods can be classified as search methods hence they do not guarantee that the global optimum solution is found, but rather a local optimum. However if more than one search path is used, it is possible to reduce the risk of being entrapped in a local optimum. Examples of NLP are the line search or the conjugate gradient Bazaraa and Shetty (1993). In many of these methods, the search direction is determined by the gradient of the objective function. The choice between selecting the descending or the ascending direction depends on the optimisation problem (i.e. minimization or maximization). Nonetheless, it is possible in some cases to transform a non-linear problem into a linear problem and solve it iteratively with a LP technique. Yet, despite using this simpler approach, the computational time may increase if the non-linear effects become dominant.

The reader is referred to Murty (1976) for further information on LP. Bellman and Dreyfus (1962) give an extensive overview of diverse DP methods, while Bazaraa and Shetty (1993) provide for further reading on NLP. Most studies so far failed to provide a comprehensive methodology for calibration of flood models, due to the computational cost of 2D models. Broadly speaking, a sensitivity analysis is often preferred for calibration of those models. It provides a good insight of the decision variables to use in a calibration procedure. There are however some exceptions despite the limited range of applicability. These studies are discussed in the following paragraph.

Flood applications. Horritt (2006) developed a methodology for comparing uncertain maps of inundation extent with a single observed event. The GLUE procedure (Beven and Binley, 1992) was applied. It includes a Monte Carlo sampling of simulations of a deterministic model used to assign a weighting of how well each simulation fits the observed data (Aronica et al., 2002). A weighted sum of the predictions for each simulation, based on wet (account for) or dry (discard), resulted in an uncertain inundation model prediction. The validation of the uncertain model predictions was based on precision, measured by entropy like parameter, and accuracy, measured by a Reliability diagram. These quantities were calculated per simulation run based on the weighted average fit of the cells in the model for each simulation run. This methodology has the advantage of only needing one recorded event to perform the calibration, on the other hand it was also verified that when the methodology was repeated in a second event the model parameters diverged substantially from the previous calibration.

Carr and Smith (2006) developed an iterative three-step calibration methodology to two urbanized catchments in Australia and New Zealand. The three steps were organized as follows: First, an adjustment on the losses of the surface-runoff model is made to match the expected flow; secondly, the modelled peak water levels are compared with the historical ones; and thirdly, and adjustment to the pipe's surface roughness and inlet parameters is made to improve the estimates obtained in the previous step. The model calibration considered as parameters, the surface roughness, the pipe roughness and the pit inlet coefficients. This study introduces the inlet discharge as a parameter for the first time, however due to the model limitations, when significant flooding occurred and the sewer network surcharged the only effective parameter for calibration was the surface roughness.

A study from Mark et al. (2004) (although without providing an automatic calibration procedure) suggested which parameters and objectives to use for calibrating a 1D/1D model. The authors defined the flood extent and flood depth as the main objectives

of calibration. For a start, the surface runoff model was calibrated before the drainage system, where the calibration was done by adjusting hydrological parameters, such as the concentration time. This validation should be done on collected data of surface runoff. The next step was to calibrate the drainage system by varying the Manning's number. For this the modeller would have to use the data of observed water levels in the pipe system. It also emphasized the need to have an accurate and well defined surface network, i.e. flow paths, cross-sections and capacity.

Horritt and Bates (2002) compared a 1D to a 2D model on a 60km reach of the River Severn. They used the floodplain and channel friction as parameters for calibration. The validation was done against an observed inundated area and records of downstream discharge. An interesting conclusion is copied here:

> "It would therefore make sense to define a 'good' model, as one which can be calibrated against discharge measurements and then provides the most accurate predictions of flood extent."

Besides the emphasized need to perform a calibration on real measurements, the importance in calibrating the discharge variable was for the first time recognized .

An important issue was the available data for calibration. Whilst in river flooding the levels reached can (usually) be visually inspected after the event, when dealing with the sewer systems this can become an arduous task. Beffa et al. (2001) surveyed all the overtopping lengths and levee breaches after the flood events in 1986 and 1994 on the Waihao River rural flood plain in New Zealand. The overtopping hydrographs from the levees could be reconstructed, and used as parameter to calibrate the flood depths on both floods. The procedure taken was to increase the parameter gradually to fit the flooded area. Regarding the sewer data O'Loughlin et al. (2006) pointed out the little data available, especially in large sewer systems, to validate calibration results. The author also stressed the lack of quality of some of the available data.

2.6 Conclusions

Chapter 2 reviewed the theoretical background of five subjects that constitute the backbone of an expert in urban flood modelling: Governing equations, Numerical Schemes, Existing Urban Flood Models, Linking Surface with Sub-Surface and Calibration. Since this is a specialized area of knowledge within Civil Engineering these subjects had to be exhaustively investigated. An extensive part of that research is therefore presented here to

give the reader a thorough understanding of Urban Flood Modelling, helping to identify the contributions of this Thesis (see also section 3) as well as its driving motivations.

Chapter 3

Research Question and Justification

3.1 Question

Whilst the last couple of years have seen an increased popularity in the use of 1D/2D models and a decline in the use of 1D/1D models, this Thesis takes a fresh look at the latter in response to the question:

> **How can 1D/1D models be constructed to reproduce maps of the inundation extent of urban flooding in good agreement with 1D/2D models?**

Finding the answer to the above question would enable the use of a faster model with a similar level of numerical accuracy when compared to its equivalent 1D/2D model.

3.2 Justification

The justification for the research presented in this Thesis is supported by the literature review presented in the previous chapter. In total there are seven areas/points where the author believes that there is a need for further understanding. Hence, this will be the focus of this thesis. In some cases, the model type in the seven points has been deliberately omitted. The reason for this is that some of them are actually a common requirement of all types of coupled models, and not only of the 1D/1D model. In order of importance these are:

1-The need for effective 1D/1D vs. 1D/2D model comparison. Although in river modelling there are some studies comparing 1D and 2D models, in urban flooding this

is scarce. Spry and Zhang (2006) used the 1D/1D models XP-SWMM and DRAINS to model two distinct case studies. The study conclusions indicated the need to use integrated models, however, there is no reference to 2D modelling or integrated 1D/2D modelling being done to compare and support such remarks. Chen et al. (2007) presented a 1D/2D coupled model. The proposed model was said to simulate the complex flow process on the overland-surface of pluvial flooding cases, better than the 1D model. However, in that study, no effective comparison was done to support this statement. The comparison will allow urban flood managers to decide when to use one or the other model.

2-The need for better visualization of 1D/1D results. When comparing results between 1D/1D and 1D/2D models, it is hard not to be impressed by the inundation maps drawn based on the 2D results, and neglect the 1D/1D results on the grounds of the latter being an inferior approach. Often the results' output, common from similar software (i.e. 1D/1D models), is limited to traditional plots such as the (x, t) graphs, or animations of the network with colours which vary according to the values of the selected dependent variable (depth or velocity). Inundation maps, broadly speaking, are simply not available or are a result of a linear extrapolation between surface nodes, producing a very unrealistic image (see, for example Figure B.3).

3-The need for a better linking element. This point concerns both 1D/1D and 1D/2D models. It can be posed as a question (section 2.3), How can the flow exchange of the linking element be defined? The question has no easy answer. As discussed in section 2.4 the general references disregard the interaction between these two systems (Akan and Houghtalen, 2003; Balmforth et al., 2006). None of the existing expressions presented in section 2.3 are directly valid for modelling the link between the surface and sub-surface flow. Due to the lack of research on this topic, currently there is no general formulation that can be universally applied, based either on experimental tests or on theoretical results. Despite this, various models try to fit these expressions into an equivalent element to model the linkage. These are either justified in changing and/or adapting the above equations; however, they are based upon questionable assumptions.

In the report by Mark (2005) the 1D MOUSE was linked with the 2D MIKE21. There are four main criticisms of the way linking is achieved that need to be addressed in this work: (1) The need to select previously the correct linking formulation in the model when that may change during the simulation; (2) The use of the manhole perimeter as the weir crest, which would only be correct in the case of complete removal of the manhole-cover; (3) The need to set a maximum discharge highlights the fact that the link formulations

are exceeding the real discharge capacity and generating instability in the model; (4) The disregard of the existence of discharge coefficients, even if in this case they are unknown due to the lack of experimental studies.

Most commonly the existing models consider either a weir or an orifice that can switch from one to the other depending on the water levels (Mark et al., 2004; Djordjevic et al., 2005), or a weir equation (Vaes et al., 2004; Dey and Kamioka, 2006). These models failed in prescribing the parameters for the above formulations. This is mainly because there is no effective visualization or correspondence from the parameters of the equations to the real connection between surface and sub-surface.

4-The need for calibration (fast and accurate models). As previously mentioned (section 2.5), until now the development of calibration procedures for urban flood models has not been fully explored. This is mostly because of the heavy burden they bear, i.e. the large computational effort required by flood models. Nonetheless, as seen in section 2.5, there are some exceptions.

Horritt (2006) developed a methodology for comparing the uncertainty of flood-inundation extents with a single observed event. This methodology owes its success to the use of a RFM (see discussion in section 2.3), which limits its application to this specific type of model. In this case, although a LIDAR data with a 1 metre resolution was used, it is clear that, in order to perform the 500 simulations required by the Monte Carlo technique, the cells needed to be averaged over 250 meter lengths, therefore, inevitably smearing topographic features (Hunter et al., 2005a).

Whenever starting a calibration, modellers need to ask two important questions: (1) Which parameters to calibrate? (2) Which variables to optimise? Manning's roughness is often selected as parameter for calibration (Beffa et al., 2001; Horritt and Bates, 2002), despite reported ineffectiveness in the output results (Carr and Smith, 2006), and warnings on the misuse of that parameter, with the purpose of accounting for errors within models (Wallingford-Software, 2004). Carr and Smith (2006) is the first study that mentions the inlet parameters being used in calibration, however, due to the model limitations it seemed to lack great effect once the surface was heavily flooded.

5-The need for stability improvement. Instability is one of the common unavoidable problems of numerical models. When Vaes et al. (2004) used the 1D/1D model INFOWORKS CS, the author concluded that instabilities may force the modeller to increase the Preissmann scheme weighting factor value to be closer to 1. However it had the counter-effect of increasing the numerical diffusion. In order to retain a one-point boundary

condition throughout the simulations (subcritical-like characteristic structures), the inertia terms of the St. Venant equations are phased out for high Froude numbers (Wallingford-Software, 2000). However, without the inertia terms the model's range of application is reduced (section 2.1). Cunge et al. (1980) studied instabilities related to weir oscillations. They reported that when the hydraulic gradient approaches "0" the discharge derivative approaches infinity, hence, for a given time step discretization the calculated discharge magnitude can become larger than the volume available on the node, and cause the model to fail or give erroneous results.

6-The need for an algorithm to deal with irregular cross-sections in 1D model. Algorithms dealing with irregular cross-sections need to account for the possibility of an unrealistic drop in the flow capacity curve (section 4.1.2). All commercial urban flood models include some sort of algorithm to deal with irregular cross-sections. However, the information on how this is done within the models is scarce. The users' level of confidence is, therefore, low. When Vaes et al. (2004) used the 1D/1D model INFOWORKS CS, instead of using irregular cross-sections the author represented the surface pathways using wide cross-sections. This unrealistic approach indicates that there is still a need for investigating such algorithms.

7-The need for full dynamic models. This need concerns both 1D/1D and 1D/2D models. As discussed in section 2.1 1D models often use the full dynamic equations, but the same is not the case with 2D models. 2D models commonly use the diffusive model without inertia. In this case they are described as urban inundation models (Hsu et al., 2000). These models still keep the ability to reproduce backwater effects (Ramos and Almeida, 1987). However, Lin et al. (2006) found a visible slowdown of the wave propagation. This represents one of the main disadvantages on some of the coupled 1D/2D models.

3.3 Discussion

The complex 1D/2D models based on the St. Venant equations are an accurate and powerful tool to model urban flooding. Without any other considerations/requirements, these tools represent the best modelling option. However, the heavy computational burden associated with them makes their application impractical when the available time restricts the total number of runs. For example, calibration runs or Monte Carlo analysis often require a large number of simulations to be performed. Another constraining situation may occur whenever the maximum memory allocation in the computer is exceeded. For example, simulation of large areas with small grid sizes requires a large amount of memory.

In both cases, lower-order models must be applied.

Practical engineering applications include (amongst others): (1) the definition of flood risk maps; (2) the definition of criticality of an asset; and (3) real time modelling. The first is done in the context of urban flood management. In this case, the definition of flood inundation-maps multiplied by damage, for several return periods, enables urban flood managers to define flood risk maps and support sustainable investments. The second fits within asset management routines. Here, the concept of criticality of assets enables prioritisation of investments, and thereby the development of asset management plans, which will allow for the allocation of resources. The last, refers to the need to perform calibration on real data. In this case, the calibration process in real-time-modelling problems needs to be done continuously in order to ensure that the models closely follow the event being simulated. All these applications benefit from fast and accurate models. In conclusion, addressing the question of this thesis not only provides very relevant and topical subject matter, but also answers present and future practitioners' questions on when to use each model.

Chapter 4

Urban Flood Modelling

4.1 Improved SIPSON

4.1.1 Introduction

SIPSON is a 1D/1D integrated hydraulic model developed by Djordjevic (1999) at the University of Belgrade. The acronym SIPSON stands for "Simulation of Interaction between Pipe flow and Overland flow in Networks". SIPSON, besides being a hydraulic model, also incorporates a hydrologic model (rainfall run-off), called BEMUS, which is used for calculating the surface run-off input to the hydraulic model. A GIS interface, named 3DNet, works as the platform for management and editing of data and visualization of the SIPSON results. Djordjevic was one of the first authors to develop a fully 1D/1D integrated model applying the dual drainage concept (Djordjevic et al., 1999). During the modelling stage of the case studies for the FRMRC project, some limitations of the 1D/1D were spotted and improvements in SIPSON were sought. This section discusses the Improved SIPSON. Because most of the existing 1D/1D models share the same weaknesses, these improvements can easily be extended and applied to other 1D/1D models and, to some extent, also to more complex models such as 1D/2D.

A total of six improvements were outlined:

1. **Multiple-Linking-Element (MLE).** An element to connect both networks (section 4.2). Although the 1D/1D model already applies the dual drainage concept, some limitations were found in the connection between sewer and surface systems. For example, an inherent insensitivity to the water level in the sewer, when these were exceeded by the water levels at the surface. The lack of sensitivity was identified to be in the equation chosen to control the flow rate from the surface to the sewer. As a consequence, if the shift between the direction of flow (sewer-surface and vice-versa) was sudden, it could cause the simulation to halt.

2. **Irregular-Cross-section (IRG).** An algorithm for handling with the non-uniqueness of geometric characteristics of irregular cross-sections (subsection 4.1.2). This is motivated by the discussion in section 2.3. When the flow overtops the kerb level it may spill to natural or alternative channels, which may possess irregular cross-sections. Depending on the relationship between the area and the wetted perimeter the hydraulic radius may become a one-to-many function.

3. **Visualisation of Results.** A GIS tool to transform the 1D/1D model results into a 2D grid (subsection 4.1.3). As the author will show, the introduction of DTM into urban flood modelling not only made possible the widespread use of 2D models, but also brought new strength to the 1D surface modelling.

4. **Internal Boundary Conditions.** Three types of internal boundary conditions (subsection 4.1.4). The following are implemented: orifices to model submerged linkages (e.g. exits from underground tanks), partially submerged weirs, and flap valves.

5. **Volume Control.** A volume control limiter to improve the model stability (subsection 4.1.5).

6. **Hot Start.** A technique to calculate the initial conditions (subsection 4.1.6).

4.1.2 Algorithm for Handling Non-uniqueness of Geometric Characteristics of Irregular Cross-sections

The current section presents the Irregular-Cross-Section algorithm. The algorithm is designed to assess the Area, Perimeter, Width and Hydraulic Radius, for both man-made and natural irregular cross-sections (section 3.2). The IRG outputs a table where the cross-section characteristics can be retrieved according to the water depth, and the critical flow can be obtained according to the critical depth.

However, as the water height (h) increases, if the increase in water table (WT) is disproportionably large when compared with the increase in cross-sectional area (e.g. in the floodplains) the hydraulic radius (Hr) (equation (4.5)) can decrease, and an unrealistic drop in the flow capacity is obtained. At this point the hydraulic radius becomes a one-to-many function.

A classic solution to this problem is to work with composite cross-sections (Quintela, 1996). Although this solution has the advantage of eliminating the unrealistic drop in the flow capacity, it produces different values for the kinetic energy for each sub-section which then have to be lumped together (USACE, 2002). Furthermore (when in the presence of

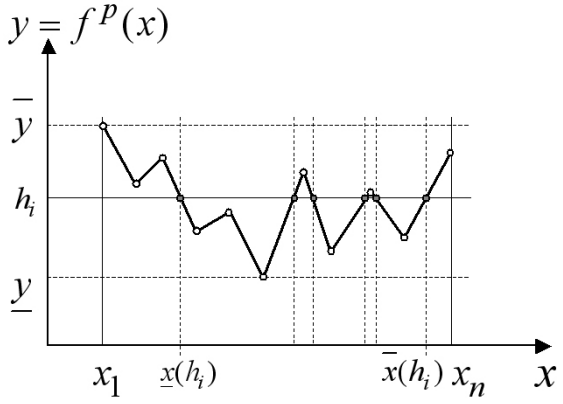

Figure 4.1: The piecewise linear function $y = f^p(x)$ and the horizontal line $y = f_i^h$ for a typical irregular cross-section.

the unrealistic drop) the cross section will have multiple minimums in the total energy curve, and this approach can lead to incorrect estimates of critical depth. In HEC it is up to the user to decide if this may happen in order to switch from two available methods to calculate the critical depth[1].

In this Thesis a correction procedure based on a third order polynomial is developed to handle the non-uniqueness of the hydraulic radius. The correction procedure introduces a smooth transition by fitting a third degree polynomial curve in the hydraulic radius curve and, therefore, avoiding the unwanted drop. This procedure keeps a single cross-section with an unique value of critical depth. Lastly, it is worth emphasising that this drop is responsible for oscillations on the computed solution that can cause the model to fail. The non-univocal characteristic of the solution, where two different depths share the same flow capacity is the main trigger of the oscillatory behaviour.

Summary of the IRG algorithm

Initialization step.

The irregular cross-section is defined by a piecewise linear function $f^p : [x_1, x_n] \rightarrow \left[\underline{y}, \overline{y}\right]$ obtained by linking a set of points $P = \{(x_1, y_1), (x_2, y_2), ..., (x_n, y_n)\}$ such that $x_1 < x_2 < .... < x_n$ using linear interpolation. $Hh = \{h_1, h_2, ..., h_k\}$ is a set of water heights, such that $\underline{y} < h < \overline{y} \forall h \in Hh$, and Smh is the number of smoothing points above each drop. [2]

[1] Two methods are available: "parabolic" (by default) does not account for local minima, "secant" is limited to a maximum of three local minima

[2] If the set P has less than 3 points, then the algorithm stops. A cross-section needs at least three points to be defined.

Main step.

1. For all values $h_i \in$ set Hh.

   (a) Find the intersection of function $y = f^p(x)$ with the horizontal line $y = f_i^h$ (Figure 4.1). Generally this intersection has several distinct points, whose x-coordinates are $\{x \in [x_1, x_n] \,|f^p(x) = h_i\}$. Let us denote the two extremes with $\underline{x}(h_i)$ and $\overline{x}(h_i)$ and include them into P, $P := P \cup \{(\underline{x}, f(\underline{x})), (\overline{x}, f(\overline{x}))\}$

   Let us extract a new subset $P(h_i) \subseteq P$:

$$\begin{aligned} &P(h_i) := \{(x,y) \in P \,|\underline{x} \leq x \leq \overline{x}\} = \\ &= \{(\underline{x}, f(\underline{x})), (x_{km+1}, y_{km+1}), ..., (x_{kM-1}, y_{kM-1}), (\overline{x}, f(\overline{x}))\} = \\ &= \{(x_{km}, y_{km}), ..., (x_{kM}, y_{kM})\} \end{aligned}$$

   (b) Calculate for h_i, the Area[3] (A_i), the wetted perimeter (Wp_i), the water table (WT_i), the hydraulic Radius (Hr_i) and the critical flow (Qc_i).

   (c) Select Case: $(kM - km) + 1$

      i. Case = 3

$$A_i = 0.5\left(\left(x_{km+1} - x_{km}\right)\left(y_{km+2} - y_{km}\right) - \left(x_{km+2} - x_{km}\right)\left(y_{km+1} - y_{km}\right)\right) \tag{4.1}$$

      ii. Case > 3:

$$\begin{gathered} A_i = \sum_{j=km}^{kM-1} A_j \\ A_{km} = x_{km}\left(y_{km+1} - y_{kM}\right) + x_{kM}\left(y_{km} - y_{kM-1}\right) \\ j \in [km+1, kM-1] \\ A_j = 0.5\left(A_{j-1} + x_j\left(y_{j+1} - y_{j-1}\right)\right) \end{gathered} \tag{4.2}$$

   (d) End Select.

   (e) Calculate:

$$\begin{gathered} Wp_i = \sum_{j=km}^{kM-1} Wp_j \\ Wp_{km} = \sqrt{\left(x_{km} - y_{km+1}\right)^2 + \left(y_{km} - y_{km+1}\right)^2} \\ j \in [km+1, kM-1] \\ Wpj = Wp_{j-1} + \sqrt{\left(x_j - y_{j+1}\right)^2 + \left(yj - y_{j+1}\right)^2} \end{gathered} \tag{4.3}$$

$$WT_i = \sqrt{\left(x_{km} - y_{kM}\right)^2 + \left(y_{km} - y_{kM}\right)^2} \tag{4.4}$$

[3]The cross-sectional area (A) comes from a code originally converted by Alan Miller (2000-07-04) and taken from the Naval Surface Warfare Center Mathematical Library.

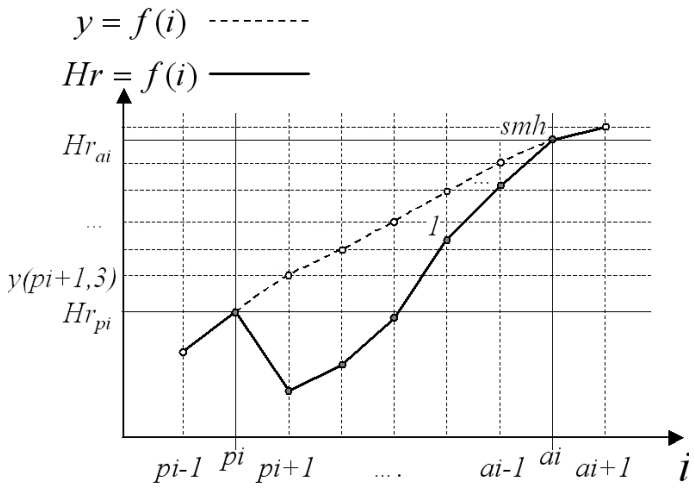

Figure 4.2: The correction procedure on the hydraulic radius $Hr = f(i)$ and the third degree polynomial $y = f(i)$ for a typical curve.

$$Hr_i = \frac{A_i}{Wp_i} \tag{4.5}$$

$$Qc_i = \sqrt{\frac{gA_i^3}{WT_i}} \tag{4.6}$$

2. Loop.

3. If in set $Hr = \{Hr_1, Hr_2, ..., Hr_k\}$ there is at least one inflection $Hr_{i+1} < Hr_i$,Then Go To 4, Else Go To 5.

4. Call the Correction Procedure to all inflection points and update the values of parameters Wp and Qc, using equations (4.5),(4.6) while keeping the area A unchanged.

5. Construct a table to be used as lookup table by SIPSON using as index the set Hh, Stop.

Correction Procedure.

1. Let $pi = i$ be the peak before inflection, and $ai = i$ the end of the correction procedure as a function of the smh considered (Figure 4.2). Initialise $d = 0$, Go to 2.

2. Do $ai = ai + 1$

   (a) If $Hr_{ai} > Hr_{pi}$ Then $d = d + 1$

3. Until $d = smh$. Go to 4. [4]

4. Fit the third degree curve $y(x, 3)$ between points Hr_{pi} and Hr_{ai} (equation (4.7)):

   (a) Define two boundary conditions as the two values of Hr_{pi} and Hr_{ai}.

   (b) Define two boundary conditions as the two derivatives $\frac{dy(x,1)}{dx}$ at those two points determined by first degree curves $y(x, 1)$ (equation (4.8)) using the two outer points Hr_{pi-1} at Hr_{ai+1}

   (c) Solve the system of four equations and four unknowns, replacing the boundary conditions defined earlier in the following equations.

$$y(x, n) = \sum_{i=1}^{n} a_i x^i + b_1 \tag{4.7}$$

$$\frac{dy(x, n)}{dx} = i \sum_{i=1}^{n} a_i x^{i-1} \tag{4.8}$$

   Where in equations (4.7) and (4.8), n is the polynomial degree, y and x are the vertical and horizontal polynomial coordinates, a_i and b_1 are the polynomial parameters.

5. Update the new vertical coordinates, $Hr(i) := y(i, 3) \forall i \in [pi + 1, ai - 1]$.

4.1.3 Algorithm for Visualising 1D Surface Results in a 2D Grid

The importance of visualising the results is closely related to the importance of good communication. The 2D maps, a common feature of 2D models, are a better visualisation tool than the traditional water-depth curves used in 1D models in communicating the flood-inundation extent. The 2D maps give strength and credibility to the results.

3DNet is the visualization tool associated with SIPSON. The results, as in most similar software (i.e. 1D/1D models), are confined to traditional plots such as (x, t) graphs and animations where the nodes and channels have their colours varying accordingly to the values of the selected dependent variable. Inundation maps, broadly speaking, are simply not available or are a result of a linear extrapolation between surface nodes, producing

[4] If d never reaches smh the algorithm stops. This case was never found in any of the cross-sections analysed so far hence it is disregarded. Moreover in practical terms it would take two flat plains connected by a small step where normally the vertical step in cross-sections is of order 0.01m and Smh takes values between 3 and 10.

an unpredictable/unrealistic image (Figure (B.3)). The introduction of DTM into urban flood modelling, brought reliable data and consistency to the 2D models, but also brought new strengths to the 1D surface modelling. The key idea in visualisation explored and developed in this Thesis makes use of the DTM. In a first stage, a more accurate surface network is produced, and in a second stage, the temporal output results of the 1D/1D model are transformed into a 2D grid. This section presents two visualization algorithms, one for dealing with channels and a second for dealing with ponds. The goal is to obtain a GIS tool capable of translating the 1D/1D model results into a two dimensional grid, hence generating flood inundation maps for any given time during a flood (second item in the list of needs, section 3.2).

Summary of the Visualisation algorithm

Initialization step.

Given the temporal output results, for any $t \in [0, t\,\max]$, of depth h_i^t for all channels k, where $i \in [1, np_k]$ and np_k is the total number of points for each channel k of length L_k and width B_k, the upstream and downstream elevation of each channel k, Z_{upst} and Z_{dwst}. Given the temporal output results, for any $t \in [0, t\,\max]$, of depth hp^t, volume $Volp^t$ for all ponds pk with coordinates defined by a set of points $Po = \{(x_1, y_1), (x_2, y_2), ..., (x_{pk}, y_{pk})\}$. Given a vector file (Boonya-Aroonnet et al., 2007) with the coordinates defined by a set of subsets $C = \{Ch_1, Ch_2, ..., Ch_k\}$, where each subset is defined by a set of points $Ch = \{(x_1, y_1), (x_2, y_2), ..., (x_{nk}, y_{nk})\}$. Given a DTM with a regular grid, $\Delta x = \Delta y$, coordinates defined by a set of points $G = \{(x_1, y_1), (x_2, y_2), ..., (x_m, y_m)\}$ and terrain elevation by a set $Z = \{z_1, z_2, ..., z_m\}$ (Figure 4.3).

Main step.

1. For all channels k and $t \in [0, t\,\max]$, Initialise $i = 1$ and $d = 2$ Call ChannelSub, Go To step 2.

2. For all ponds pk and $t \in [0, t\,\max]$ Call PondSub, Stop.

ChannelSub.

1. If $i\frac{L_k}{nk} < Dist(p_1, p_d)$, Then Go To step 2.

   (a) Else $d = d + 1$, Go to 1.

2. Interpolate linearly $i\frac{L_k}{nk}$ in $[p_d, p_{d-1}] \rightarrow a$. Go to step 3.

3. Calculate $Z_a = Dist(p_1, a)\frac{Z_{upst} - Z_{dwst}}{L_k}$ and $g_{min} = minDist(g_j, a)$, Go To step 4.

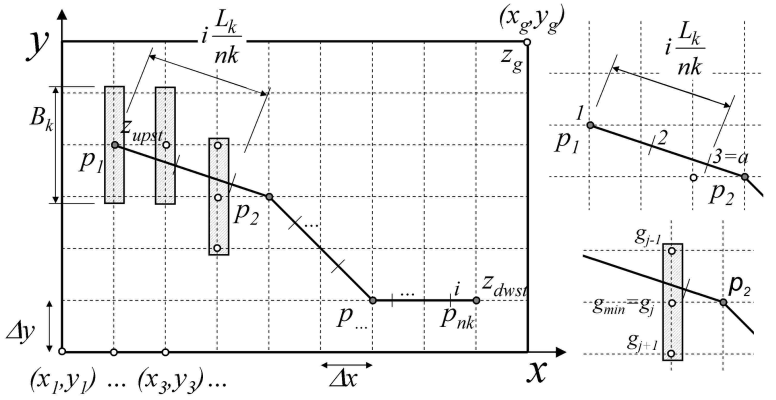

Figure 4.3: Channel k, with length L_k, width B_k, n_k points, upstream and downstream elevation Z_{upst} Z_{dwst}, a regular grid $\Delta x = \Delta y$ with g grid points.

4. Do

   (a) Fill cells with water $\{..., g_{j-1}, g_j, g_{j+1}, ...\}$ above and below point g_{min}

5. Until $h_a + Z_a < z_j \vee Dist(g_j, g_{min}) < \frac{B_k}{2}$, Go To step 6.

6. Write to file $ChInunMap_k^t$ $\{..., g_{j-1}, g_j, g_{j+1}, ...\}$ with water level $h_a + Z_a$, Go To step 7.

7. If $i \leq nk$ Then Increment i Go To step 1, Else Stop.

PondSub.

1. Locate p_{pk} in grid $G \rightarrow g_{pk}$ (Figure 4.4), Initialize $L = 1$[5] Go To step 2.

2. Calculate $wl_{pk} = hp^t + z_{pk}$, Go To step 3.

3. If $wl_{pk} > z_{pk}$ Then

   (a) Calculate $cVol_p = \Delta x.\Delta y.hp^t$

   (b) If $cVol_p < Vol_p$ Then Go To 5, Else Go To 7.

4. Else $wl_i = 0$ Go to 7.

5. Do $L = L + 1$

   (a) For all cells $i \in L$

      i. If exists one neighbouring[6] j cell of i where $wl_j > z_i$ Then

         A. Calculate $wl_i = wl_{pk}$ and $cVol_p = \Delta x.\Delta y.\left(wl_i - z_i\right) + cVol_p$

[5]Cell Level L refers to all cells i that are either $horizDist(g_{pk}) = L.\Delta x$ or $vertDist(g_{pk}) = L.\Delta y$

[6]It is considered that each cell has 8 neighbouring cells.

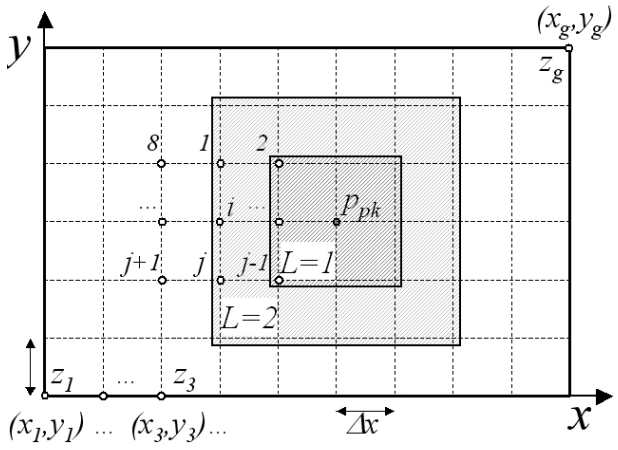

Figure 4.4: Pond pk, cell levels $L = 1$ and $L = 2$, neighbouring j cells of i, regular grid $\Delta x = \Delta y$ with g grid points.

B. If $cVol_p < Vol_p$ Then Go To iii Else Go To 7.

ii. Else $wl_i =$ "$Empty$" Go to step b.

iii. Write to file $PndInunMap^t_{pk}$ g_i with water level wl_i Go To step b.

(b) Loop.

6. Until $wl_i =$ "$Empty$"$\forall i \in L$. Go to 7.

7. Write to file $PndInunMap^t_{pk}$ g_i with water level wl_i Stop.

4.1.4 Addition of Internal Boundary Conditions

This section presents the three internal boundary conditions added to SIPSON. These boundary conditions are suitable to connect two nodes where the assumptions of free/submerged weir or orifice are valid or where a flap valve exists.

Figure 4.5 shows the schematics of the boundary conditions and variables. H_i is defined as the water level at node i, H_w the level of the weir connecting the two nodes, and the hydraulic gradients are defined as $\Delta H = H_2 - H_w$, $\Delta H2 = min(\Delta H3, \Delta H4)$, $\Delta H2' = min(\Delta H, \Delta H4)$, $\Delta H3 = H_1 - H_w$, $\Delta H4 = H_1 - H_2$.

The following equations are based on the discussion presented in section 2.4.

Free/submerged weir. This internal boundary condition is based on the weir equation (2.21), where the hydraulic gradients are replaced by the difference in heads for free and

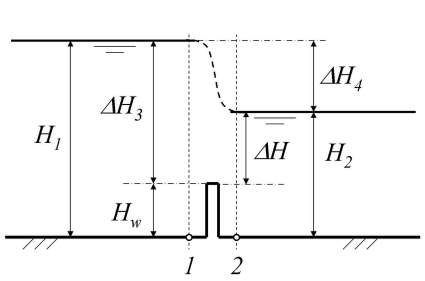

(a) For free and submerged weir cases.

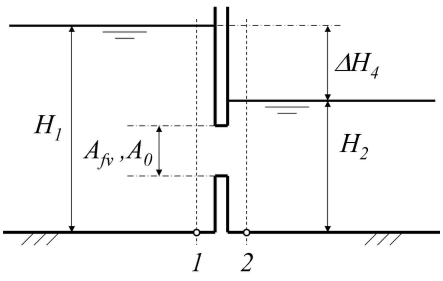

(b) For orifice and flap valve cases.

Figure 4.5: Definition of the hydraulic gradients when connecting two nodes with different water levels.

submerged conditions.

$$\begin{array}{rcl} Q = K_w b \Delta H3 \sqrt{2g\Delta H3} & , & \begin{array}{c}\Delta H < 0 \\ \Delta H3 > 0\end{array} \\ Q = K_w b \Delta H \sqrt{2g\Delta H2} & , & \Delta H3 > \Delta H \\ Q = 0 & , & \Delta H3 < 0 \\ Q = K_w b \Delta H \sqrt{2g\Delta H} & , & \begin{array}{c}\Delta H > 0 \\ \Delta H3 < 0\end{array} \\ Q = K_w b \Delta H3 \sqrt{2g\Delta H2'} & , & \Delta H > \Delta H3 \\ Q = 0 & , & \Delta H < 0 \end{array} \tag{4.9}$$

Orifice. The orifice equation (4.10) is the same as in equation (2.17), where the hydraulic gradient is replaced by the difference in heads of the two connecting nodes. This equation is reversible, meaning that the direction of discharge depends solely on which head of the two connecting nodes is greater.

$$\begin{array}{rcl} Q = C d_2 A_o \sqrt{2g\Delta H4} & , & \Delta H4 > 0 \\ Q = C d_2 A_o \sqrt{2g(-\Delta H4)} & , & \Delta H4 < 0 \end{array} \tag{4.10}$$

Flap valve. The flap valve equation (4.11) also uses the equation (2.17), yet here the discharge coefficient is replaced by the discharge coefficient of the flap valve K_{fv}, and the hydraulic gradient is replaced by the difference in heads of the two connecting nodes.

$$\begin{array}{rcl} Q = K_{fv} A_{fv} \sqrt{2g\Delta H4} & , & \Delta H4 > 0 \\ Q = 0 & , & \Delta H4 < 0 \end{array} \tag{4.11}$$

Linearization procedure. When dealing with small hydraulic gradients, weir oscillations may cause the flow to keep switching direction, and eventually cause the model to fail. As discussed earlier (section 3.2), when the hydraulic gradient approaches "0"

the discharge derivative approaches infinity, hence for a given time-step-discretization, the calculated discharge magnitude can become larger than the volume available on the node (Cunge et al., 1980). Although SIPSON applies an iterative procedure, these types of oscillations and overestimating discharges can still happen and cause the model to fail or give erroneous results. To minimize these oscillations a linearization procedure is applied to the above equations as proposed by Cunge et al. (1980).

For illustration purposes, the procedure will be summarized with its application to the first of the equations in (4.9).

- Set the maximum linearization gradient value (Δhmx).
- Obtain the top-discharge value ($Qtop$) by replacing Δhmx on the desired equation.

$$Qtop = K_w b \Delta hmx \sqrt{2g\Delta hmx} \tag{4.12}$$

- All values above Δhmx use the non-linearized equation, all values below it use the linearized equation (4.13).

$$Q = \frac{Qtop}{\Delta hmx} \Delta H3 \quad , \quad \Delta H3 < \Delta hmx \tag{4.13}$$

4.1.5 The Volume Control Limiter

In SIPSON, time steps are chosen at the beginning of the simulation and set constant throughout. It may happen that within a time step, if the calculated discharge between two nodes exceeds the volume available in the node with outflow, the water level can become negative and the model fails (fifth item in the list of needs, section 3.2). One way to prevent this is to reduce the time step enough to avoid the water level becoming negative. Another way is to limit the magnitude of the discharge to the available volume. The first slows down the computation considerably by reducing the time step, and some difficulties arise in determining the next time step when the water depth becomes close to "0". The second is preferred and applied accordingly with the expression (4.14):

$$\int_{t_1}^{t_2} Q.dt = \int_{0}^{h_1} A_{manh}\,(h)\, h.dh \tag{4.14}$$

Where t_1 and t_2 are consecutive computational times, h_1 is the water depth at time t_1 and $A_{manh}\,(h)$ is the manhole area as a function of h.

4.1.6 HotStart

When analysing unsteady flows, usually a start-up time is defined for the calculations. The flow conditions at the start-up time are called the initial conditions. With the purpose of increasing the computational efficiency and the overall accuracy of the results, a good estimation of the initial condition can provide a stable and free from oscillations start-up. The Hot Start appears as a powerful technique used in a variety of fields (Microsoft, 2006) to enable a faster start-up avoiding the need to compute the initial conditions. In the Hot Start, the dependent variable values obtained at the end of the previous run k, are used as the initial state of the dependent variable of the current run k+1 (Rakha et al., 1997).

Generally an accurate initial condition in a model is the steady state obtained for the boundary conditions at the start up time. SIPSON applies an implicit scheme where the unknown dependent values at t+1 appear implicitly in the system of equations. Implicit schemes are not restricted by a stability criterion hence it is possible to use larger time steps (Chaudhry, 1987). This feature in SIPSON is the central idea used in the algorithm developed in this Thesis to implement the Hot Start.

> Run the model with a constant state equal to the initial conditions, until the variation of the dependent variables becomes negligible, and thus obtaining the corresponding values of the system's true initial conditions.

Note: This argument apparently is in contradiction with what is stated in Chaudhry (1987), pages 404-407, whereby the preferred solution solves a simplified version of the diffusive-with-inertia model (equation (4.18)) in detriment of the St. Venant Equations (section 2.1).

The equation can be retrieved by considering the diffusive-with-inertia model, equation (4.15):

$$\frac{1}{A}\frac{\partial}{\partial x}\left(\frac{Q^2}{A}\right) + g\frac{\partial h}{\partial x} = g(S - J) \tag{4.15}$$

Considering that the channel has continuous side slopes:

$$\frac{\partial A}{\partial x} = \frac{dA}{dh}\frac{\partial h}{\partial x} = B(h)\frac{\partial h}{\partial x} \tag{4.16}$$

With equation (4.15) and (4.16):

$$-\frac{1}{g}\frac{Q^2}{A^3}B\frac{\partial h}{\partial x} + \frac{\partial h}{\partial x} = (S - J) \tag{4.17}$$

This simplifies into:

$$\frac{\partial h}{\partial x} = \frac{(S - J)}{1 - \frac{Q^2 B}{gA^3}} \tag{4.18}$$

The simplification allows solving a first-order differential equation for each channel to compute the water profiles. The procedure carries on from downstream to upstream by adding up the channel flows at the junctions and using the energy equation to close the systems of equations with two unknowns (Q, h). This procedure works well if the network is only branched. If the system has one or more than one loop it is necessary to iterate the solution to obtain the correct flow on the looped network (similarly with the procedure adopted here). In these circumstances it is concluded that this procedure has negligible advantage when compared with the one implemented in this Thesis. Moreover the Hot Start has proven to be more useful in looped networks as shown in section 4.2.2.4.

Summary of the Hot Start algorithm

Initialization step.

Given a type of initial condition equal to 4 (specific to SIPSON), the initial boundary conditions (bcs) for the dependent variables $(Q_i, h_i)_{bcs}$ for all channels i, acceptable error ε and total computational time t_f.

Main step.

1. If initial condition file exists, Then Go To step 2, Else Go To step 5.
2. Read from file, the *bcs* $\left(\overline{Q_i, h_i}\right)_{bcs}$ for all channels i, Go To step 3.
3. If $\left|\left(\overline{Q_i, h_i}\right)_{bcs} - (Q_i, h_i)_{bcs}\right| \leq 0$ for all channels i, Then Go To step 4, Else Go To step 5.
4. Read from file, the initial conditions $\left(\overline{Q_i, h_i}\right)$, Go To step 7.
5. Run SIPSON using the $(Q_i, h_i)_{bcs}$ constant Until $\left|(Q_i, h_i)^{t-1} - (Q_i, h_i)^t\right| \leq \varepsilon$. If $t \leq t_f$, Then Go To 6, Else Go To 8.
6. Write to file $(Q_i, h_i)_{bcs}$ and $(Q_i, h_i)^t$, Go To 7.
7. Run SIPSON using the $\max\left((Q_i, h_i)^t, \left(\overline{Q_i, h_i}\right)\right)$, Stop.
8. Write Message "The model can not converge to a steady state, use other type of initial condition", Stop.

4.1.7 Conclusions

The SIPSON original model has been expanded to an improved version. In total, six additions/improvements have been implemented in the model, namely: the Multiple-

Linking-Element (next section), the ability to deal with irregular cross-sections, new internal boundary conditions, the volume control for stability, the hot start and the technique for visualisation of results. These improvements will enable the modelling of larger networks, with irregular cross-sections, a variety of internal boundary conditions and with an increased stability. All these improvements have been applied in this Thesis. Therefore their success can be directly and/or indirectly measured by the output results presented in the case studies section 5 and section 4.2.

4.2 The Multiple-Linking-Element Theory and Assumptions

4.2.1 Introduction

The main objective in developing integrated models is to increase the overall accuracy of flood modelling. Therefore one of the key issues is how to improve the link between the surface and the subsurface networks. Surprisingly, there is a lack of research on this subject. The importance of accurate linking between the surface and subsurface network is such that it ultimately determines and regulates the extent and the damage due to flooding on the surface network caused by sewer surcharge. General references in this subject disregard the interaction between these two systems (discussion on section 2.4), so how can we model the hydraulic behaviour of this link? Previous studies simplify the manhole connections by using a weir or an orifice equation without providing guidance for which parameter values to use in each equation. By doing this they neglect the inlet characteristics, the number of inlets and the discharge pattern of the different inlet components and how these are related to one another. In this section, a new linking element between surface and subsurface networks is developed in response to the third item in the list of needs presented in section 3.2. The Multiple-Linking-Element (MLE) is implemented in the SIPSON model to improve the simulation of subsurface and surface exchange. The theory and underlying assumptions are described in detail and a methodology for setting up real case applications is presented.

4.2.2 MLE methodology

The linking element should be able to cope with the flow exchange between the surface and subsurface networks and adjust the rate exchanged and direction depending on the local time-varying features in both networks. Due to the complexity of the surface-subsurface link, the methodology developed in this section can be described in three conceptual stages. In the first stage the connection components are broken-down and isolated into fundamental elements. In the second stage, these elements are analysed in detail to decide

on how can they be characterized and, when suitable, what fundamental equation can best describe their behaviour (section 2.4). In the third and last stage these elements are reassembled into a unique element, the Multiple-linking-element (MLE) that now gathers all the fundamental elements.

The identified components are as follows:

- **Geometry types (Manholes, inlets, pipes).** Manholes are generally of cylindrical shape defined by a diameter, a bottom and a top level. There are several types of inlets which are defined according to: the location within the street profile, the opening area, the perimeter of the inlet, and the storage volume capacity. The connection from the inlets to the manhole is made through a pipe, defined by the upstream and the downstream level, slope and diameter.

- **Multiple inlet connections.** A manhole can be connected to several inlets. Although there is no prescribed limitation for the number of inlets, physically it is limited to a small number of pipes, depending on the diameter of the manhole and the diameter of the connected pipes. This physical limitation is due to the difficulty in assuring water tightness of the manhole if the number of inlets is too high.

- **Difference in inlets ground levels.** In the case of multiple inlets, sloped streets and local irregularities may cause different inlets connected to the same manhole to have different elevations. For the same water level, not all the inlets will be functioning with the same flow rate. This will affect the way that total capacity is determined.

- **Street geometry (slope, shape, roughness).** Street geometry directly influences the flow depth and therefore the flow exchange between surface and underground networks. The main characteristics are slope, channel shape approximation and roughness.

- **Blockage.** Especially during a flooding event debris and other objects may obstruct the inlet and reduce its capacity. The blockage effect needs to be taken into account through a statistical approach, but the deterministic model has to accommodate this possibility.

- **Delay in time in reaching the full capacity (only relevant in multiple inlet connections).** Although the system capacity will be directly related to the number of inlets connected to a manhole, it is reasonable to assume that this full capacity will only be at work if all the inlets are working. The multiple inlets will start with

only one working inlet, and gradually build up until all the inlets are working. This can be seen as a delay time taken to reach full capacity.

- **Control sections.** To determine which part of the connections between surface and underground networks dominate the flow exchange, the control sections (CS) have to be determined. These would be the inlet, the pipe connector, the manhole and the system of pipes connected to the manhole.

The next group of subsections will see the setting up of the MLE. In subsection 4.2.2.1 an intermediate stage to reach the full MLE, called the Single-Linking-Element (SLE), is assembled with the fundamental components identified earlier. Followed by subsection 4.2.2.2 where the behaviour of the SLE is analysed in detail and the benefits of this intermediate stage are outlined. In subsection 4.2.2.3 blockage of inlets and removal of partial or full manhole cover is included as an extra feature in the SLE. The final subsection 4.2.2.4, presents the validation of the MLE as a combination of several SLE, considering both equal and different inlet levels, and restrictions for tackling stability.

4.2.2.1 SLE Theory and Assumptions

A generic link between surface and subsurface networks is considered defined by : a rectangular gutter, a boxed shape inlet, a pipe connection and a manhole (Figure 4.6) (this geometry can be adapted for other cases). The concept is to define all the control sections in the element and determine which section restricts the flow rate. The result should be a more accurate discharge curve that reflects the actual type of connection between surface-pipe-surface as a whole. A steady-state flow condition is assumed in the analysis.

The derived equations for each control section are described by:

- **CS1.** From the gutter to the inlet, the Bernoulli equation is considered valid. The flow enters the inlet at critical depth. In this way the flow is controlled by a weir type formula. Although the approximation used is the same as for a broad crested weir (equation (2.15)), there is a need to consider a discharge coefficient [7].

$$Q_{cs1} = Cd\tfrac{2}{3}H_1 L_i\sqrt{\tfrac{2}{3}gH_1} \quad , \quad H_1 \geq 0 \tag{4.19}$$

Where in equation (4.19) Cd is the discharge coefficient, H_1 is the surface water depth (m), $L_i = 2(W_x + W_y)$ is the perimeter of the inlet box, W_x is the length and W_y is the width of the inlet box (m).

[7] There are different discharge coefficients assessed experimentally for other applications. A default value of 0.5 is used, but this should be adjusted as the experimental data is made available.

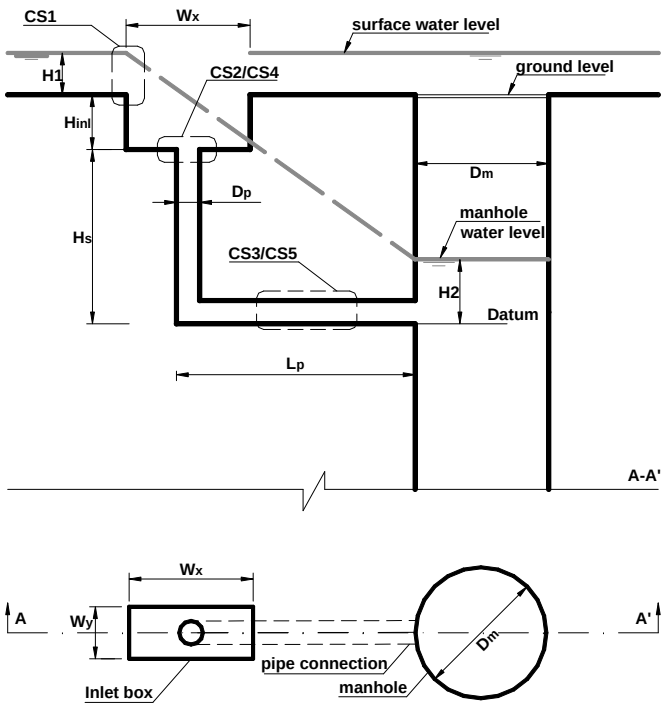

Figure 4.6: Profile and plan view of a link between surface and subsurface network. The SLE geometry schematisation and control sections. Variables definition.

- **CS2 and CS4.** From the inlet to the vertical pipe, the Bernoulli equation is again used. It is assumed that it will only start working when the water level in the inlet box reaches the ground level. This will enable us to plot this control section along with the previous one. This is a realistic assumption because only when the volume of the inlet is filled, can the vertical shaft start to influence the flow discharge from the weir. This will have the appearance of an orifice type formula [8]. CS2 is used for the discharge from surface to subsurface, for the reverse discharge CS2 is switched to CS4.

$$\begin{aligned} Q_{cs2} &= CdAp\sqrt{2g\left(H_1 + H_{inl}\right)} \quad , \quad H_1 + H_{inl} \geq 0 \\ Q_{cs4} &= -CdAp\sqrt{2g\left(H_2 - H_1 - H_{inl} - H_s\right)} \quad , \quad H_2 \geq H_1 + H_{inl} + H_s \end{aligned} \tag{4.20}$$

Where in equation (4.20) $Ap = \pi D_p^2/4$ is the section area of the pipe connection (m2) with D_p diameter (m), the H_{inl} is the height of the inlet box (m), the H_s is the height of the vertical shaft (m), and H_2 is the manhole water depth (m).

[8] Similarly as in the previous control section a default value of 0.5 is used, but this should be adjusted as the experimental data is made available.

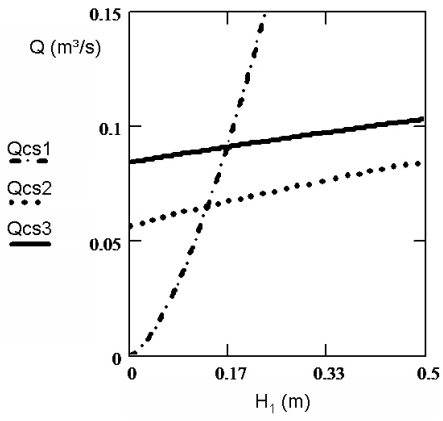

(a) For $H_1 = [0, 0.5]m$ and $H_2 = 0m$.

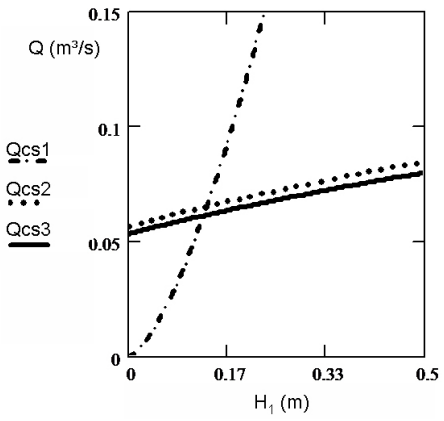

(b) For $H_1 = [0, 0.5]m$ and $H_2 = 0.6m$.

Figure 4.7: Plots of control sections(cs) cs1, cs2 and cs3.

- **CS3 and CS5.** From the orifice to the manhole, a friction energy loss will be used to assess the full discharge capacity of the pipe. As in the previous control, it is considered that it will only start working when the water in the inlet box is at least at the ground level. CS3 is used for the discharge from surface to subsurface, for the reverse discharge, CS5 is used instead.

$$\begin{aligned} Q_{cs3} &= KApR^{2/3}\sqrt{\tfrac{(H_1+H_{inl}+H_s-H_2)}{Lp}} \quad , \quad H_1 + H_{inl} + H_s \geq H_2 \\ Q_{cs5} &= -KApHr^{2/3}\sqrt{\tfrac{(H_2-H_1-H_{inl}-H_s)}{Lp}} \quad , \quad H_2 \geq H_1 + H_{inl} + H_s \end{aligned} \tag{4.21}$$

Where in equation 4.21 K is the roughness coefficient ($m^{1/3}/s$), Hr is the hydraulic radius (m), and Lp is the connection pipe length (m).

4.2.2.2 SLE Behaviour

Figures 4.8(a) and 4.8(b) show the results considering $H_2 = 0$ (no surcharge in the manhole) and $H_2 = 0.6m$, respectively. The following default values are used in the remaining subsections: $L_i = 0.80m$, $H_{inl} = 0.40m$, $H_s = 0,60m$, $Lp = 5.00m$, $Dp = 80mm$ (DN80), $Dm = 1,00m$, $K = 80m^{1/3}/s$.

Figure 4.8(a) shows that CS2 starts to dominate CS1, at approximately H_1 equal to 0.18m. Figure 4.8(b) on the contrary, shows a global change from CS2 to CS3 just by changing the flow depth in the manhole.

It is possible to plot these variations as a function of both depths H_1 and H_2. Figure 4.9(a) is a 3D plot where the flow is restricted to from surface to subsurface network, and Figure 4.9(b) is another 3D plot that considers both directions.

What is interesting to learn from the graph on Figure 4.9(a) is the perception that full pipe flow becomes more restrictive than any other control-section as soon as the manhole

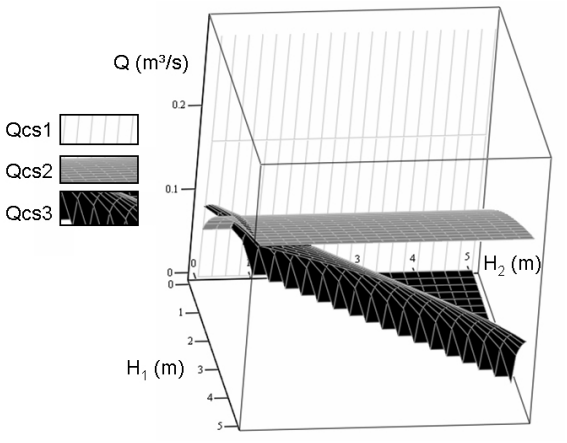

(a) For $H_1 = [0, 5]m$ and $H_2 = [0, 5]m$.

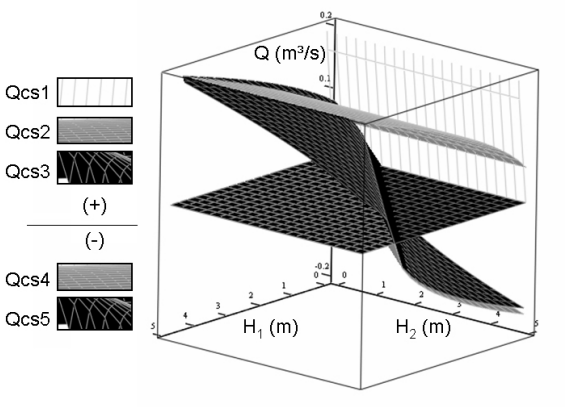

(b) For $H_1 = [0, 5]m$ and $H_2 = [0, 5]m$.

Figure 4.8: Plots of control sections(cs) cs1 to cs5.

starts to surcharge. Both CS1 and CS2 are insensitive to the manhole surcharge. Also the water flow is approaching zero as the water level in the manhole reaches the water level in the surface (as expected).

Now let us suppose that the water level in the manhole increases above the water level at the surface (i.e. pressurises), then the water flow would be in the reversed direction, i.e. flow from the manhole to the surface. In this case the first pair of equations in (4.20) and (4.21) from CS2 and CS3 need to switch to the second pair of equations in (4.20) and (4.21) from CS4 and CS5, and CS1 is no longer valid. Figure 4.9(b) shows that both CS4 and CS5 are very close. This means that the determination of the predominant control section will greatly depend on the specific field's characteristics.

With these two final graphs the SLE analysis is concluded, and a generic formulation has been presented whereby with a rigorous change of the control sections, the SLE can be applied to other types of links (as highlighted in the next subsection). It is also now possible to define the flow exchange (i.e. direction and flow rate) based on the water levels in both the surface and sub subsurface networks.

4.2.2.3 SLE Other applications

In order to demonstrate the versatility of the developed methodology in defining the SLE, the same procedure will now be applied to two other geometries:

1. A manhole without any inlets and the flow entering through the manhole cover considering a small percentage of the cover area as an inlet. This can simulate blockage, a badly sealed cover or some damaged cover. This can be achieved by considering an orifice area of a small percentage of the total manhole area (e.g. 1.0%) in equation 4.20.

2. A manhole without any inlets and the flow entering through the manhole cover considering a big percentage of the cover area as an inlet. This can simulate a non existent or misplaced cover, due to careless maintenance or movement during severe flooding. This can be achieved by considering an orifice area of a large percentage of the total manhole area (e.g. 60.0%) in equation 4.20.

In the above two cases the Ap, in equations 4.20 and 4.21, is replaced by a percentage of the section area of the manhole (Am) and in equations 4.19 the L_i is replaced by a percentage of the perimeter of the manhole. The manhole is considered to have 1.0m internal diameter.

If the effective area becomes too large, care has to be taken to include the sewer network node capacity in order to restrict the three control sections. The network node capacity depends on the heads of other nodes. This could be introduced by coupling several nodes in a network, and using the network node capacity as a function of full pipe flow between nodes. Finally, continuity equation states that the flow balance must always equal 0. Although under certain conditions water flow (Q) is expected to be either sewer-surface or surface-sewer, this cannot ever be greater than the sum of flows at a given node within a time step.

$$\sum Q_i^{pipe} + \sum Q_i^{street} + Q_i^{runoff} = \frac{dZ}{dt} Am \tag{4.22}$$

Where in equation 4.22 Q_i^{pipe} is the pipe flow to manhole i (m^3/s), Q_i^{street} is the street flow to manhole i (m^3/s), Q_i^{runoff} is the surface run off to manhole i (m^3/s), $\frac{dZ}{dt}$ is the gradient of water level in the manhole (m/s).

This highlights that it is possible to keep using the SLE to model a manhole working as an inlet, as long as it is kept within reasonable limits, otherwise the control section switches to a control based on the available volume[9].

[9]This paragraph is intended to show the flexibility of the developed methodology, but this can only be considered after calibration over existing data.

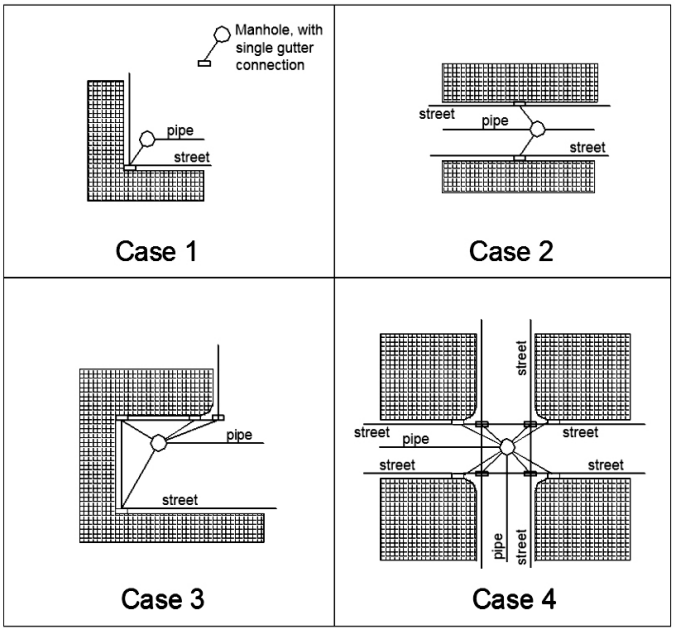

Figure 4.9: Four typical connections to the sewer, single (top left), double (top right), triple (bottom left) and quadruple (bottom right) using the SLE.

4.2.2.4 MLE validation through SLE

In order to validate the results of using the MLE against the SLE, a sensitivity analysis is carried out. Four typical real cases are set-up in the SIPSON model with the number of equivalent inlets (Neq) being the corresponding case number. The objective is to compare the performance of the real number of inlets through the use of the SLE, with the use of a single inlet through the use of the MLE (Figures 4.9 and 4.10).

Stability. The SIPSON model applies an implicit numerical scheme (Preissmann four-point method); although implicit models do not have to respect the Courant's stability criteria, they may suffer from instability as discussed in section 2.2. This is more prone in cases with small water depth (fifth item in the list of needs, section 3.2).

To overcome this instability two actions have to be taken [10]:

1. To apply an instability-reduction-coefficient to an auxiliary equation and to the CS1 in the proposed single linkage element.

   From surface to subsurface the CS1 is dominant for small water depths. If no instability-reduction-coefficient is used to constrain equation 4.19, the initial flow variations have a high initial gradient. An instability-reduction-coefficient is applied (RCd). This equation is useful to control the gradient, due to the fact that it has

[10] This is specific of the model used for testing the MLE other models may have other requirements.

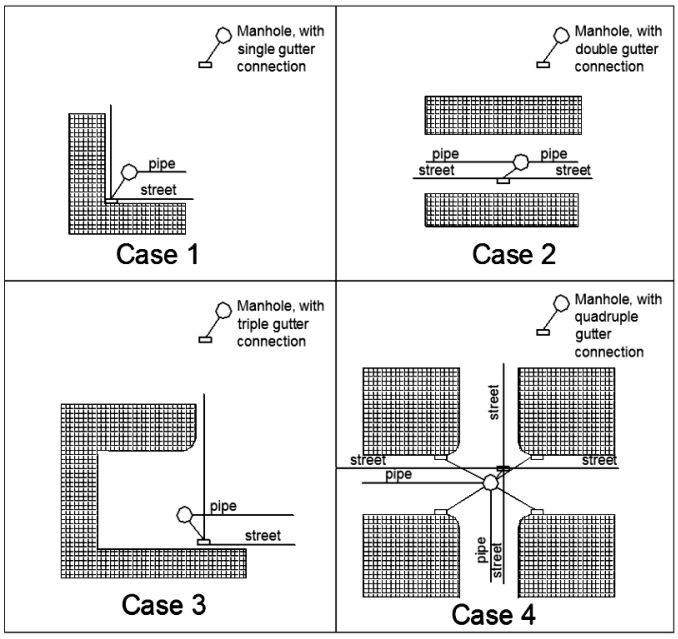

Figure 4.10: Four typical connections to the sewer, single (top left), double (top right), triple (bottom left) and quadruple (bottom right) using the MLE.

one horizontal asymptote equal to 0 when the height tends to 0.

$$Q_{cs1} = RCd\frac{2}{3}CdH_1L_i\sqrt{\frac{2}{3}gH_1} \quad , \quad H_1 \geq 0 \tag{4.23}$$

None of the first equations in both 4.20 and 4.21, used in CS2 and CS3, need to be reduced. The SLE method is sensitive to both water levels at the surface and in the manhole therefore an auxiliary equation (weir type) is added to ensure a gradual transition to zero flow (Q_{aux}) when the manhole water level reaches the surface water level. An instability-reduction-coefficient is again used.

$$Q_{aux} = -RCd\frac{2}{3}Cd(H_2 - H_1 - H_i - H_s)L_i\sqrt{\frac{2}{3}g(H_2 - H_1 - H_inl - H_s)} \quad , \quad H_2 \geq H_1 + H_inl + H_s \tag{4.24}$$

To illustrate, Figure 4.12(a) shows the flow from subsurface to surface, and Figure 4.12(b) shows the reverse flow, both with an RCd of 0.15.

For each case only one instability-reduction-coefficient was used. However it was found that in the four cases, the RCd was not the same. The procedure used to determine the correct RCd was by test and trial until the full simulation was achieved without unwanted oscillations.

2. To limit the number of equations used per time step.

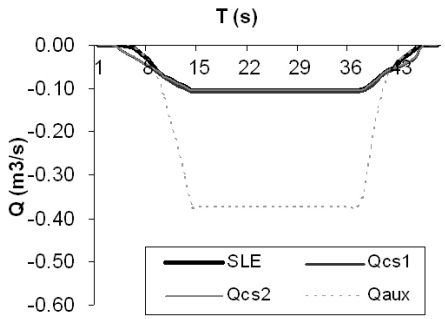

(a) Flow from subsurface to surface network (positive discharge).

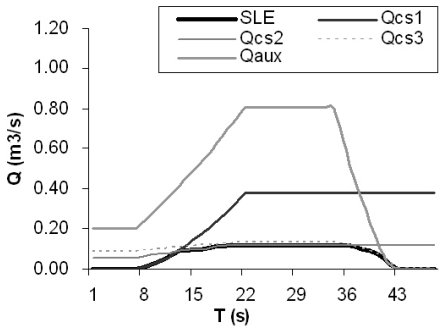

(b) Flow from surface to subsurface network (negative discharge).

Figure 4.11: The effect of the instability-reduction-coefficient applied to the auxiliary equation and control section 1 in the single linkage element. RCd=0.15.

During the simulation, when the flow was near the interception of two different equations, the solution tended to oscillate between them. This could lead to unwanted oscillations of the solutions, but not necessarily lead to a crash in the simulation.

MLE With same inlet elevations. For each case, two simulations are conducted in order to assess the overall performance of the MLE methodology: the first simulation, where the direction of flow is predominantly from subsurface to surface networks (pipe-street), and the second where it is predominantly from surface to subsurface networks (street-pipe). This is achieved by using a trapezoidal hydrograph with elevated inflow in the network where flow is required to be predominant combined with a constant hydrograph with lower inflow in the other network.

In the MLE methodology, an irregular cross section is used to join the two side channels used in the SLE methodology. It is interesting to notice that, the MLE methodology not only reduces the number of inlets used but also reduces the number of channels in the street network, thereby decreasing the number of loops in a network (Figure 4.12).

Figures 4.13 to 4.16 show the flow discharge curves of the four case studies. The thin solid lines are the results obtained by using SLE. The thicker solid lines are the MLE results.

Test case 1 has identical results in both SLE and MLE (Figure 4.13). This case is used to verify and validate the MLE implementation in SIPSON.

Figure 4.14 shows a good agreement between SLE and MLE results, for test case 2. The slight increase in flow surface-subsurface (S-Sub) by using the MLE methodology can be explained by the change in the channel downstream boundary conditions due to the change in channel geometry. Although the channel area remains the same, the IRG algorithm to

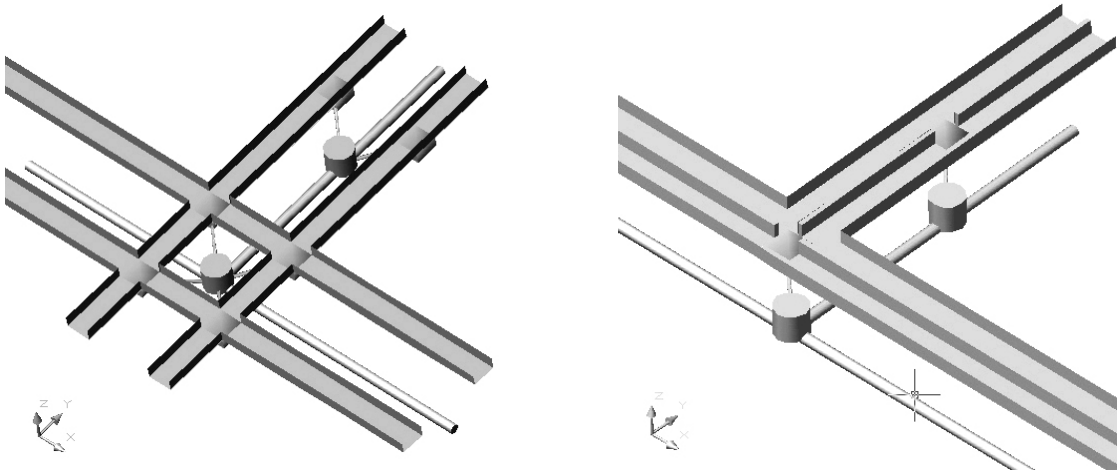

(a) MLE single inlet connection.

(b) SLE four inlet connections.

Figure 4.12: SLE and MLE concept with illustration of one manhole connecting surface and subsurface networks.

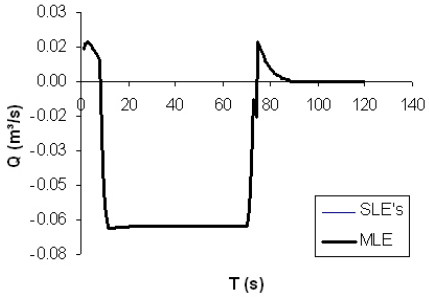

(a) Flow from subsurface to surface network (positive discharge). RCd=0.15, MLE=1xSLE.

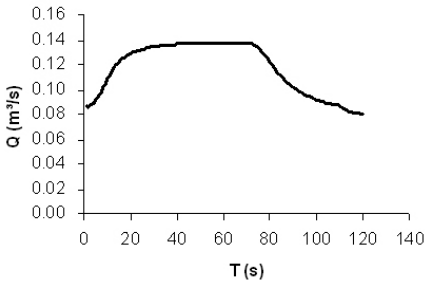

(b) Flow from surface to subsurface network (negative discharge). RCd=0.15, MLE=1xSLE.

Figure 4.13: SLE and MLE discharge results for cases 1.

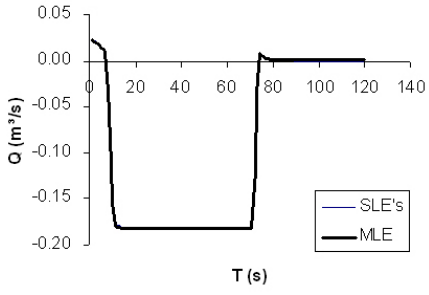

(a) Flow from subsurface to surface network (positive discharge). RCd=0.08, MLE=2xSLE.

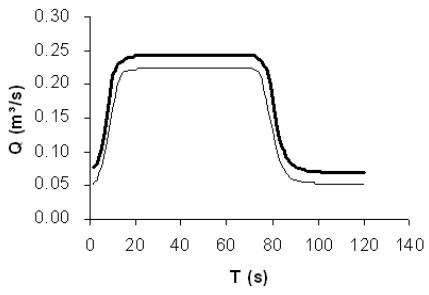

(b) Flow from surface to subsurface network (negative discharge). RCd=0.08, MLE=2xSLE.

Figure 4.14: SLE and MLE discharge results for cases 2.

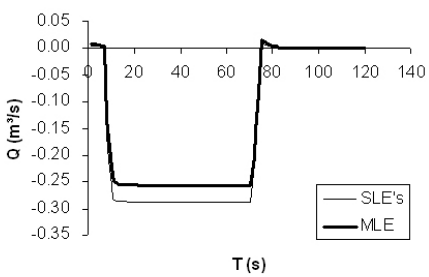

(a) Flow from subsurface to surface network (positive discharge). RCd=0.03, MLE=2.3xSLE.

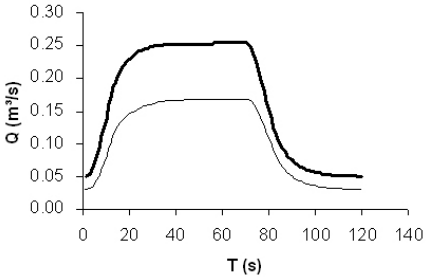

(b) Flow from surface to subsurface network (negative discharge). RCd=0.03, MLE=2.3xSLE.

Figure 4.15: SLE and MLE discharge results for cases 3.

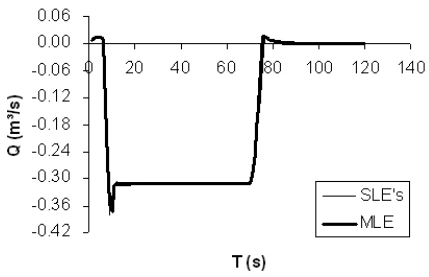

(a) Flow from subsurface to surface network (positive discharge). RCd=0.04, MLE=4xSLE.

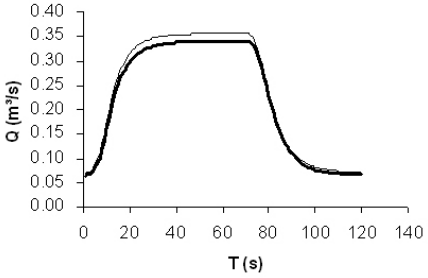

(b) Flow from surface to subsurface network (negative discharge). RCd=0.04, MLE=4xSLE.

Figure 4.16: SLE and MLE discharge results for cases 4.

compute the new cross-section (double rectangular channel) uses the same formulation to calculate the Froude number as in the single independent rectangular channel. Since the Froude number is given by $Fr = v/\sqrt{g \times A/B}$ and the downstream boundary condition is critical depth then Fr=1. The increase in the width of the channel reduces the Fr number; hence it has to be balanced by increasing the water depth. This rise in water depth may explain the rise in flow seen on the graph.

Test case 3 turns out to be the most difficult case to model through the use of this methodology, without any further change (Figure 4.15). The non symmetry of the test case produces a different behaviour in subsurface-surface (Sub-S) and S-Sub. If in Sub-S this is not so visible since no major simplification is introduced in the pipe network (responsible for the flow input in this situation) in the S-Sub the difference is enhanced once the street network is simplified. The non symmetry of the inlet distribution makes inlets work in different flow ranges, hence the equivalent element is not able to achieve the same results, considering only one element (delay in time of full capacity reach). The best fitting results were obtained using a Neq of 2.3 rather than 3.

Figure 4.16 shows a good agreement in both Sub-S and S-Sub, for test case 4. This case is the more complex to simulate in SIPSON, since it involves a looped surface network. In order to get accurate results and to prevent an unrealistic start, a special treatment to the initial condition was required. For this the Hot Start method is used (section 4.1.6).

MLE with different inlet elevations. To study the influence of variable ground levels at gutter inlets, cases 2 and 4 are chosen (Figures 4.17 and 4.18).

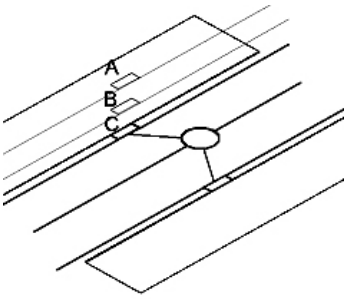

Figure 4.17: MLE with different inlet elevations (case 2). One inlet raised of height A (+30cm), B (+15cm) and C (+0cm).

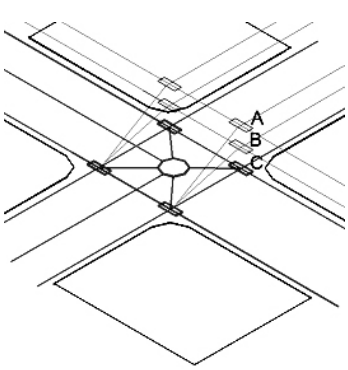

(a) Two inlets raised of heights A (+30cm), B (+15cm) and C (+0cm).

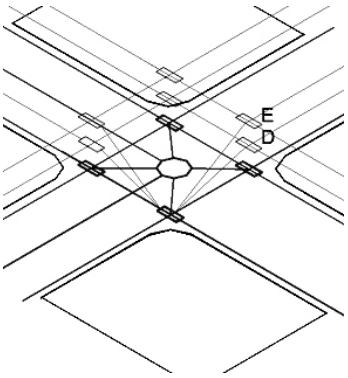

(b) Three inlets raised of heights A (+30cm), B (+15cm) and C (+0cm).

Figure 4.18: MLE with different inlet elevations (case 4).

For the SLE method, the studied cases are referred to as the SLE-sets, and these are:

- For case 2 three different heights are studied. The difference between them is 15 cm. Set C corresponds to the previous Case 2. Set B the inlet is 15 cm higher, and set A is 30 cm higher than C[11].
- For case 4 five different heights are studied. Set C corresponds to the previous Case

[11] Only the ground levels of the inlets are changed.

4. The heights in Sets A and B are raised 30 and 15 cm, respectively. Sets E and D have three inlet heights raised 15 and 30 cm, respectively.

For the MLE method, the studied case is referred to as the MLE-sets, and these are:

- For case 2, the same as in the previous SLE method but considering only one inlet.
- For case 4, three sets are used for the comparison. Namely A, B and C. Case A uses 30 cm as inlet height, case B uses 15 cm as inlet height and Case C 0 cm as inlet height.

Figures 4.19 and 4.20 show the comparison of the MLE-sets with the corresponding SLE results, for the flow curves of cases 2 and 4.

To compare the performances of MLE vs. the SLE, an error analysis of the results is made. First the error is normalized to the value expected in the SLE method (equation (4.25)) and then a coefficient is applied in order to reduce the weight of small flows and enhance the ones near the maximum values (equation (4.26)). The MLE error average (equation (4.27)) is calculated by taking the simulation time outputs as the sampled population. Where N is the total number of simulations taken for computing the error average (this depends on considering Sub-S, S-Sub or global), and $i = \{A, B, C, D*, E*\}, j = \{A, B, C\}, t = [1, ..., tf]$ (note that D^*, E^* are only used in case 4).

$$Error_{i,j}^{t} = \left| Coef_{i}^{t} \times \frac{SLE_{i}^{t} - MLE_{j}^{t}}{SLE_{i}^{t}} \right| \tag{4.25}$$

$$Coef_{i}^{t} = 1 - \frac{Max(\left|SLE_{i}^{t}\right|) - \left|SLE_{i}^{t}\right|}{Max(|SLE_{i}^{t}|)} \tag{4.26}$$

$$ErrorAverage_{j} = \sum_{i} \sum_{t=1}^{tf} Error_{i,j}^{t} \Big/ N \tag{4.27}$$

Figure 4.21 shows that using a mean value as the inlet height leads to the best global optimum performance. However if the flow is expected to have a predominant direction either Sub-S or S-Sub, it is possible to reduce the error by using a different value for the adopted inlet height.

4.2.3 Surface/Sub-surface Links in 1D/2D Modelling

Although 1D/2D models are one order higher dimensionally, when modelling the surface, they also need to model the link between surface and sub-surface. Despite this, the 1D/2D coupled hydraulic model that will be used to retrieve the data for comparison in section 4.4, is still coupled using a weir and/or orifice equation. The drawbacks of this approach

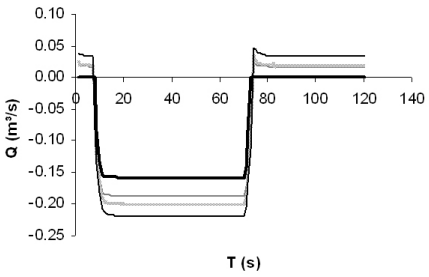

(a) Flow from subsurface to surface network (positive discharge). SLE RCd=0.18, MLE RCd=0.06.

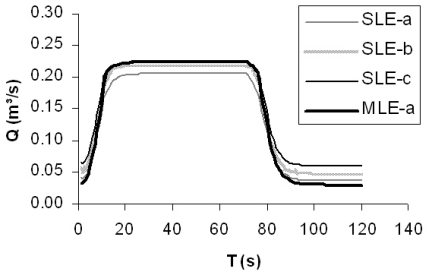

(b) Flow from surface to subsurface network (negative discharge). RCd=0.08.

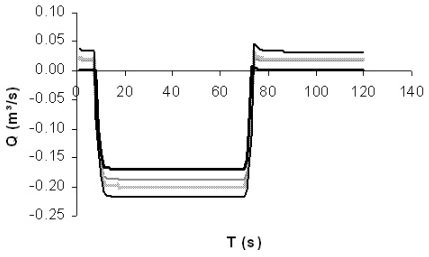

(c) Flow from subsurface to surface network (positive discharge). SLE RCd=0.18, MLE RCd=0.06.

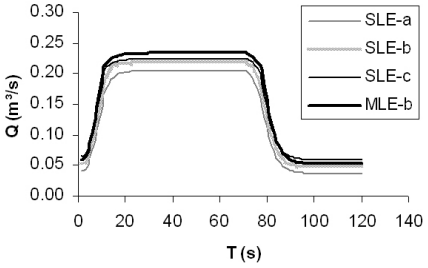

(d) Flow from surface to subsurface network (negative discharge). RCd=0.08.

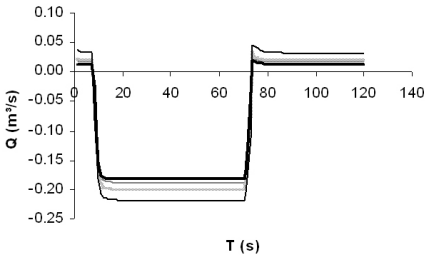

(e) Flow from subsurface to surface network (positive discharge). SLE RCd=0.18, MLE RCd=0.06.

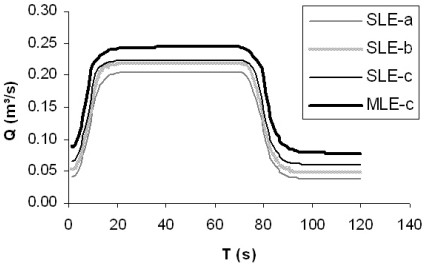

(f) Flow from surface to subsurface network (negative discharge). RCd=0.08.

Figure 4.19: Results of MLE with different inlet elevations (case 2).

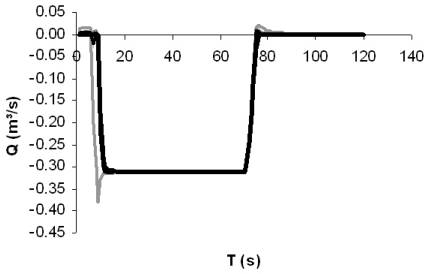

(a) Flow from subsurface to surface network (positive discharge). RCd=0.04.

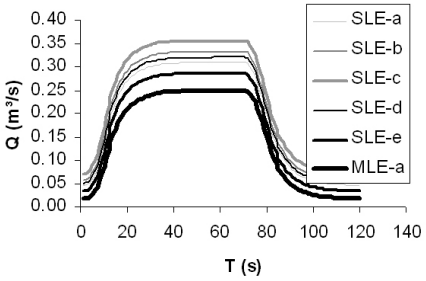

(b) Flow from surface to subsurface network (negative discharge). RCd=0.04.

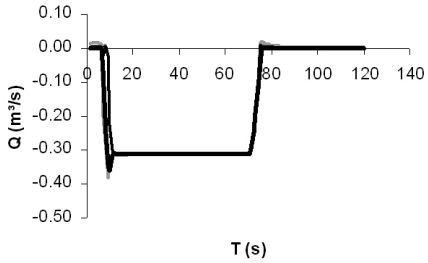

(c) Flow from subsurface to surface network (positive discharge). RCd=0.04.

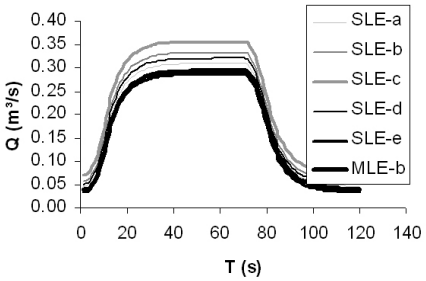

(d) Flow from surface to subsurface network (negative discharge). RCd=0.04.

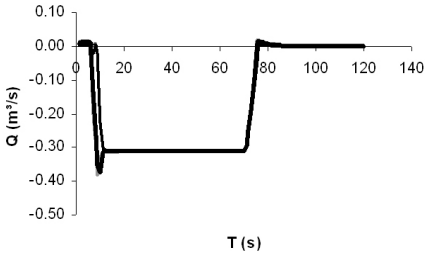

(e) Flow from subsurface to surface network (positive discharge). RCd=0.04.

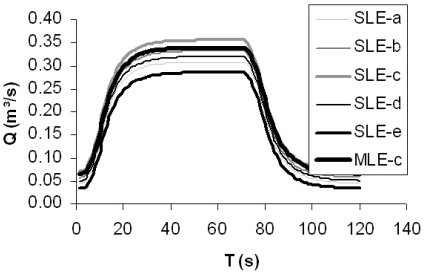

(f) Flow from surface to subsurface network (negative discharge). RCd=0.04.

Figure 4.20: Results of MLE with different inlet elevations (case 4).

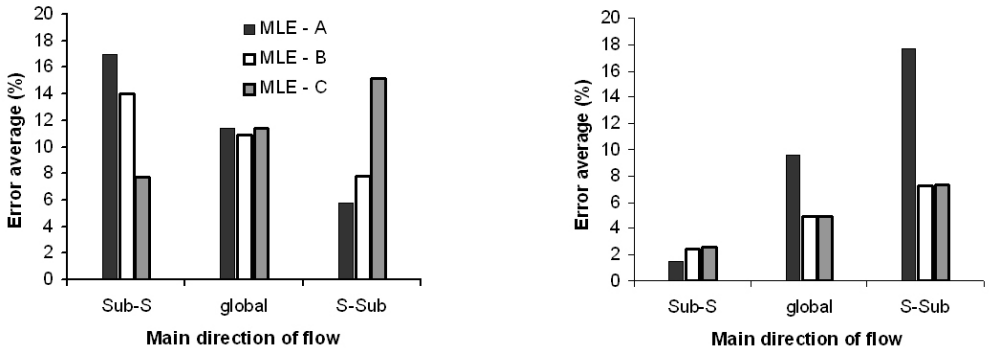

(a) Case 2.

(b) Case 4.

Figure 4.21: Error average graph showing the performance of adopting different levels as the MLE inlet level.

will be clearly shown when the discharge on the manholes between surface and sub-surface are compared in the case study section 5.

4.2.4 Conclusions

The MLE methodology developed for linking Surface/Sub-surface in the 1D/1D model promises to be a step forward in improving the validation of coupled models, and can be extended to 1D/2D models. The consideration of a more complex overview of the hydraulic behaviour of an inlet is successfully implemented in the SIPSON model and can be extended to other models. However the increase in complexity may lead to some unwanted stability problems in the model. Two possible ways to overcome this were shown. The simplification of the manhole inlets by a single inlet provides good results. In real cases, where manhole inlet information is not available this may be sufficient as an initial guess, but care has to be taken in order to judge the correctness of the results obtained. If this information is available, a similar study should be performed in order to determine the correct number of inlets (Neq) and what values of instability reduction coefficients (RCd) to apply.

4.3 Flood Model Calibration

4.3.1 Introduction

Complex 1D/2D models based on the St. Venant equations are a solid tool to model urban flooding. Where there are no prior constraints, these models are the best option. However, the heavy computational burden makes their application impractical when the time available restricts the total number of runs. Consequently, 1D/1D models are a

feasible solution provided that their accuracy is assured by calibration using high-quality data. Recalling the two questions posed earlier in section 3.2, when referring to the need for calibration: (1) Which parameters to calibrate? (decision variables) (2) Which variables to optimise? (objective functions) This section presents two algorithms for the calibration of 1D/1D flood models, and discusses a possible answer for these two questions.

4.3.2 Linear Search Algorithm

Recalling the discussion on section 2.5, here the objective function $f(x)$ is defined as a function of a set of parameters x bounded by an interval with lower and upper limits lb and ub. The problem is set as a minimization hence the goal is to obtain the minimum value of the objective function. Furthermore, multi-objectives are treated as a single-objective by aggregation of several objective functions into an aggregated function $W(f_i)$ as:

$$f(x) = W(f_i) = \sum_{i}^{m} (\omega_i \cdot f_i) \tag{4.28}$$

Where in equation (4.28), W and ω are the aggregated and the weight given to each individual objective function.

Linear search (LS) is the backbone of many optimization/calibration algorithms (Bazaraa and Shetty, 1993). The algorithm is best described by the following three steps:

Summary of the LS Algorithm

Initialization step.

Define the objective function $f(x)$ and the lower and upper limits lb and ub.

Main step.

1. Select a point x_k inside the interval of uncertainty $[lb, ub]$;
2. Find a direction d_k and the step size λ_k;
3. Obtain the next point $x_{k+1} = x_k + \lambda_k \cdot d_k$.

This algorithm cannot be applied directly with SIPSON because the model complexity forces it to behave closer to a "Black box system". Therefore, both the direction d_k and the step size λ_k cannot be calculated explicitly. The next section presents an altered LS algorithm.

4.3.3 Linear Search Based algorithm

The LS algorithm is changed, and renamed as the Linear Search Based (LSB) algorithm. The algorithm is better described by:

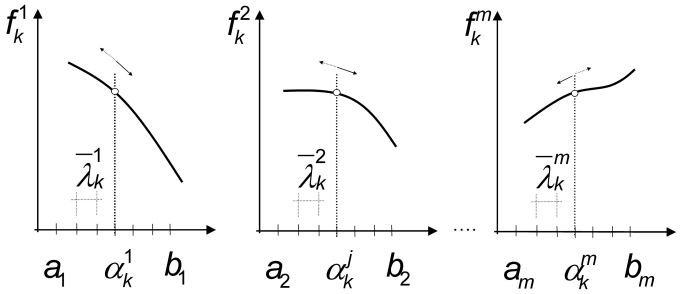

Figure 4.22: The Linear-Search-Based algorithm conceptual scheme, e.g. applied to the j variable with lower a_j and upper bounds b_j and grid lengths $\overline{\lambda}_k^j$ during the k^{th} iteration.

Summary of the LS algorithm

Initialization step.

Define the objective function $f(x)$ and the lower and upper limits lb and ub.

Main step.

1. Select a point x_k inside the interval of uncertainty $[lb, ub]$;
2. Define a grid length $\overline{\lambda}_k$;
   (a) use the following control rule:
   (b) $\begin{cases} \overline{\lambda}_k = \overline{\lambda}_{k-1} : f_k \leq f_{k-1} \\ \overline{\lambda}_k = -\overline{\lambda}_{k-1} : f_k > f_{k-1} \end{cases}$;
3. Obtain the next point $x_{k+1} = x_k + \overline{\lambda}_k \cdot d_k$.

The LSB is repeated until the maximum number of iterations M is reached. The algorithm can be readily applied to a generic problem with m independent objective functions, f_k^j, and an equal number of control variables, α_k^j, where the subscript k refers to the iteration number, and the superscript j refers to the variable index. Figure 4.22 illustrates the LSB during the k^{th} iteration.

4.3.4 Dynamic Objective Function Algorithm

The Dynamic Objective Function (DOF) algorithm assumes that there is a linear dependency between objective functions and that it can be captured by a time varying weight function ω_j.

$$f_i^{'}(x) = W'(f_1, f_2, ..., f_m) = \sum_{j=1}^{m} (\omega_j (f_1, f_2, ..., f_m) \cdot f_j) \tag{4.29}$$

Equation (4.29) shows ω_j dependent of the values of all the objective functions. The LSB algorithm is changed and renamed as DOF:

Summary of the DOF algorithm

Initialization step.

Define the objective function $f(x)$ and the lower and upper limits lb and ub.

Main step.

1. Select a point x_k inside the interval of uncertainty $[lb, ub]$;
2. Define a grid length $\overline{\lambda}_k$;
   (a) use the following control rule:
   (b) $\omega_k^{i,j} = \frac{Ccm(f^i_{k,\dots,k-\beta}, f^j_{k,\dots,k-\beta})}{\sum_{t=1}^{m} Ccm(f^i_{k,\dots,k-\beta}, f^t_{k,\dots,k-\beta})}$;
      i. Use the two following control rules:
      ii. $\begin{cases} \omega_k^{i,j} = \omega_k^{i,j} : Ccm(f^i_{k,\dots k-\beta}, f^j_{k,\dots k-\beta}) \geq Ts \\ \omega_k^{i,j} = 0 : Ccm(f^i_{k,\dots k-\beta}, f^j_{k,\dots k-\beta}) < Ts \end{cases}$ (Cr.1);
      iii. $\begin{cases} f_k^i = f_k^i : \left| slope(f^i_{k,\dots k-\theta}) \right| \geq Ms \\ f_k^i = 0 : \left| slope(f^i_{k,\dots k-\theta}) \right| < Ms \end{cases}$ (Cr.2);
   (c) $\begin{cases} \overline{\lambda}_k = \overline{\lambda}_{k-1} : f_k \leq f_{k-1} \\ \overline{\lambda}_k = -\overline{\lambda}_{k-1} : f_k > f_{k-1} \end{cases}$ (Cr.3);
3. Obtain the next point $x_{k+1} = x_k + \overline{\lambda}_k \cdot d_k$.

The outer cycle (i.e. from step 1-3) follows the same sequence as in the LSB. The first inner cycle (i.e. from step a-b) changes from the LSB in step b. The DOF calculates the ω_j based on a cross-correlation matrix (Ccm) [12] , and the m sets defined as $f^{1\dots m}_{k,k-1,\dots,k-\beta}$ using equation (4.29). The β parameter defines the number of past iterations used, hence it regulates the amount of information stored. The use of smaller or bigger values of β will result in faster or slower algorithms with few or enough data to accurately calculate the Ccm. The ω_j, in step b, is better visualised as a bi-dimensional matrix of $m \times m$ with its values representing relationships between two indexes. The relative weight of the $\omega_k^{i,j}$ in the Ccm between $f^i_{k,\dots,k-\beta}$ with $f^j_{k,\dots,k-\beta}$ determines the influence of the control variable α^i_k on $f^j_{k,\dots,k-\beta}$ at run time, and a dynamic objective-function is retrieved, hence the name

[12] Cross-correlation is a statistical concept that measures the linear relationship between two signals. The closer the cross-correlation coefficient is to the unity the stronger the relationship. This can be extended to multiple sets by the Ccm.

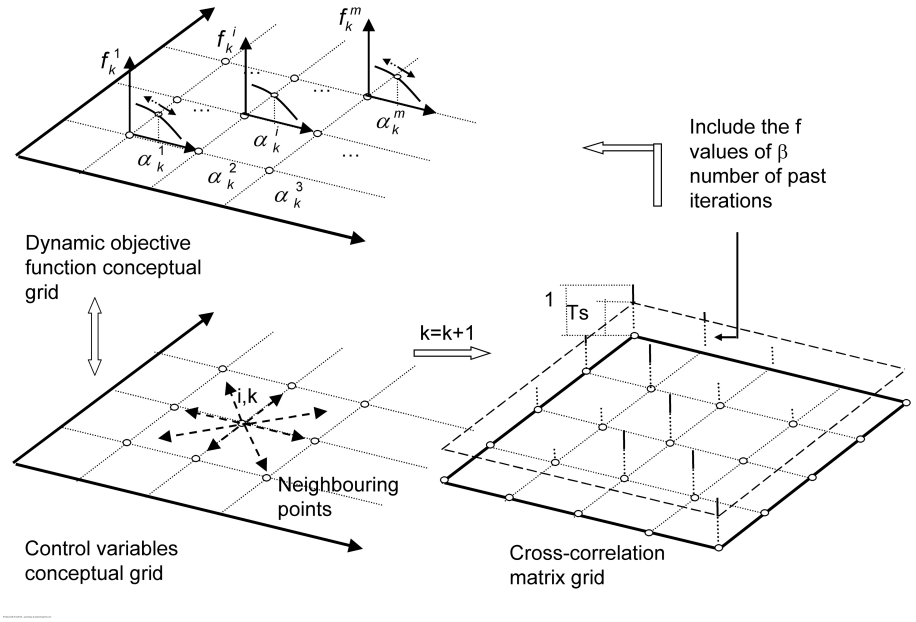

Figure 4.23: The Dynamic-objective-function conceptual scheme, e.g. applied to i variable with lower a_j and upper bounds b_j and grid lengths $\overline{\lambda}_k^j$ during the k^{th} iteration. View of the conceptual grid with similar individual Linear Search Based (Top-left). The neighbouring points of i displayed on the grid (bottom-left). A 3D view of the cross-correlation matrix grid and threshold Ts (bottom-right).

of the algorithm:

$$f_k^j(x) = \sum_{i=1}^{m} \left(\omega_k^{i,j} \cdot f_k^i \right) \tag{4.30}$$

The second inner cycle (i.e. from i.iii) controls the inclusion or exclusion of a neighbouring f_k^j. The first control rule (Cr.1) defines a threshold Ts on the cross-correlation between two sets, whereas the Cr.2 defines a slope threshold Ms on the calculation of $\omega_k^{i,j}$. Cr.1 is justified in order to keep a very high correlation between sets, and Cr.2 is justified by the "noise" added on the DOF f_k^j (slowing the algorithm), when f_k^i is kept for $\omega_k^{i,j}$ calculations after α_k^i achieved a horizontal slope, i.e. "possible convergence". Figure 4.23 illustrates the DOF during the k^{th} iteration.

4.3.5 Discussion on the Selection of Decision Variables and Objective Function

Recalling the two questions asked earlier in the Introduction, the first (1) asks for the parameter to calibrate (i.e. the control/decision variables), and the second (2) the variable to optimize (i.e. to define the objective function). In order to answer these questions, it is necessary to define the problem and the purpose of the calibration. This Thesis

aims to enable 1D/1D models to produce maps of flood inundation in good agreement with the 1D/2D models. Assuming that a proper methodology is applied to assure the equivalence between two models (section 4.4.2), then if we are interested in reproducing the same surface flow behaviour, it is of paramount importance to assure the same boundary conditions on the surface in both models.

The elements connecting the surface with the sewer pipes are responsible for providing the boundary conditions on the surface network of the 1D/1D model and on the surface system of the 1D/2D model. In the 1D/1D models these elements are the MLE's (section 4.2). The MLE sets the rate of the volume of water transferred between the surface and the sewer below. Hence to achieve similar boundary conditions it is imperative to use the volume transferred as the objective function, and the MLE parameters as the control variables.

Equation (4.31) defines the objective function as the difference between the discharges from/to the manholes connecting the surface with the sewer.

$$f_k^j(\alpha_k^j) = \sum_{t=1}^{T} \left| 1D1D\nabla_t^{\alpha_k^j} - 1D2D\nabla_t^{\alpha_k^j} \right| \tag{4.31}$$

The variables $1D1D\nabla_t^{\alpha_k^j}$ and $1D2D\nabla_t^{\alpha_k^j}$ are the cumulative volume of the discharge given by the 1D/1D and 1D/2D models at run time t at link j, T is the total number of time steps in a single run of the 1D/1D model.

The control variables are the Neq_j in the MLE, for a given link j, at a k^{th} iteration of the algorithm.

4.3.6 Conclusion

The previous section presented two methods for calibrating the 1D/1D model, using the volume surcharged from the minor system as the objective to be minimised, and the Neq_j in the MLE as the control variables; the Linear Search Based (LSB) and the Dynamic Objective Function (DOF) algorithms. The LSB is based on the well-known linear search algorithm, and the DOF is an extension of the LSB which assumes that there is a linear dependency between objective functions. Section 5 will compare the two in two different case studies.

4.4 Flood Modelling Comparision 1D/1D Vs 1D/2D

4.4.1 Introduction

The directive 2007/60 of the European Parliament and of the Council on Flood Risk Assessment and Management, aims to reduce the risk of flooding on health, environment and economic activities. The EU three-step procedure consists of some preliminary assessments by 2011, flood mappings by 2013 and flood risk management plans by 2015. Flood inundation maps for different return periods need to be produced in order to determine the areas that are potentially at risk of being flooded. This Thesis focuses on the 1D/1D hydraulic model, and on the driving question of how well can it reproduce 1D/2D flood inundation maps? This section builds on the first item in the list of needs presented in section 3.2. It aims firstly to present the methodology needed to setup two equivalent models, secondly to present two methods to compare the flood results from both 1D/1D and 1D/2D models and thirdly to show how we can improve our confidence in the model by adjusting the resolution level of the results.

4.4.2 Methodology to Set-up the Two Models

In order to enable a meaningful comparison between the 1D/1D and the 1D/2D, the models need to be built following a step by step methodology. Table 4.1 shows the summary of the steps, where the cross indicates the need to use the corresponding modelling element in the corresponding hydraulic model.

Below are the five steps as shown in Table 4.1 in greater detail:

1. The first step deals with acquisition and handling of data. The same sewer network is used in both 1D/1D and 1D/2D models. The manhole cover levels should coincide with the surface elevations of the corresponding grid cells in the DEM obtained from the LiDAR data, however in practice this is not the case for a number of manholes. Averaging the DEM has the benefit of reducing the computational effort of the 2D surface model and increasing the efficiency of the GIS tools used for the 1D surface network. Maksimovic and Prodanovic (2001) suggest values between 1-2m and Mark et al. (2004) suggest values between 1-5m. Coarser grids would lead to inaccuracies due to averaging of these features.

2. The second step runs a set of algorithms included in the GIS tool. This is done only for the 1D/1D model. The GIS tool developed generates the pathways, ponds and their interactions with the sewer network (Boonya-Aroonnet et al., 2007). It uses the DEM obtained in the previous step. The linking elements between sewer and

ID	Steps		1D/1D	1D/2D
(1)	Data acquisition	1D sewer network	x	x
		3D DEM	x	x
(2)	Run modules	GIS tools		
		pathways	x	-
		links	x	-
		ponds	x	-
(3)	Linking elements	MLE	x	-
		Weirs	x	x
		Orifice	-	x
(4)	Rainfall inputs	Sub catchments delineation	x	x
		Rainfall events	x	x
(5)	Calibration	DOF/LSB	x	x

Table 4.1: Summary of the methodology steps for enabling the models comparison

surface are set based on the criteria of proximity of the manhole to the pathway node. These are the same manholes connected to the surface system in the 1D/2D model.

3. The third step defines the linking elements. In this Thesis the sewer is connected to the surface network using the MLE. When setting up the MLE parameters in the 1D/1D model, the number of equivalent elements (Neq_j) should be equal to the number of inlets in each manhole. However, since this data is generally not available, 4 inlets per manhole can be assumed as an initial guess (these values will only influence the time taken by the calibration, in the fifth step, to find the best fit for the 1D/1D model; after calibration the new values obtained will replace the original guess). In the 1D/2D model the weir crests and lengths are assigned by inspecting the DEM.

4. The next step defines the single rainfall event to be applied in the methodology. The rainfall should be selected:

   (a) large enough to overwhelm the manholes such that in the 5th step the parameters of the selected linking elements can be properly calibrated;

   (b) to be greater than or equal to the rainfall event(s) the user would wish to model using the 1D/1D model so that the whole working range of the linking elements

can be calibrated.

The runoff hydrographs calculated by SIPSON are introduced directly to the pipe network nodes, assuming that the capacity of the inlets is sufficient to collect the entire runoff. This assumption may be incorrect for those manholes that surcharge while runoff hydrographs still have significant values. However the assumption is purposely kept in order to enable consistent comparison between the results of two modelling approaches.

5. The fifth and last step runs the DOF/LSB calibration algorithm, using the flow discharges exchanged in the links between sewer and surface networks of the 1D/1D model and the 1D/2D model results to calculate the objective function. The calibration parameters are the number of the equivalent elements in the MLEs. This step aims to calibrate the 1D/1D model to assure similar boundary conditions on the surface in both hydraulic models. Though the calibration is done using the DOF/LSB, in principle other algorithms could be used as long as the selected parameters and objective function remain the same.

In step 2, if the GIS tool is not available the pathways and ponds can be alternatively determined by inspecting the DEM. The pathways can be defined by, firstly, looking at the elevations of neighbouring cells, where water is assumed to flow from the highest to the lowest elevation and, secondly, based on the street network where these should serve as preferential flow-paths. Ponds can be defined by building the water-volume curves from the lowest points identified in the DEM.

In step 3 it should also be noted that in the case that the coupled model does not include the MLE linking element, other types of elements can also be used though they may be less realistic. As discussed in section 2.4, the most commonly used elements are weirs and orifices. In that case, during step 5, the suggested calibration parameter should be changed to a different variable to match of those connecting elements, e.g. the manhole area in the case of orifices or the weir crest width in the case of orifices. Also in step 5, it is possible to replace the DOF with a different calibration algorithm, however, the objective function should be kept unchanged (as discussed in section 4.3.5).

Notes: Two notes have to be added (1) justification of the last step, (2) justification of disregarding ground-truthing:

(1) Although the Neq_j represents the number of inlets in each manhole, this information may not be available; in this case a calibration procedure is needed to ensure that a value closer to reality is found by calibrating the discharges measured at the manholes.

Nevertheless, even if this information is available, it is also necessary to run a calibration, because the inlets may be partially/completely obstructed, the data may contain errors or other unforeseen circumstances, all can affect the inlet capacity (as in section 4.2.2.3). In that case a calibration will help to minimize those errors.

(2) In flood modelling, ground-truthing consists of lowering the DEM ground elevation where it coincides with roads and streets with the aim of reducing the inaccuracies of the DEM. Although the author agrees that some level of ground-truthing should be used on the DEM, to account for errors (Neelz and Pender, 2006), the lack of studies on the effect of such technique on the overall benefit lead to disregarding this. The author believes that the use of a level of ground-truthing (unsupported by research) leads to a biased comparison between the 1D/1D and the 1D/2D since the flow pathways would be forced into the DEM. The results would be inevitably (erroneously) better but not necessarily meaningful.

4.4.3 1st Method of Comparison - Time Dependent

The 1^{st} method is based on the traditional representation of the dependent variables against time. These types of graph can be plotted either with water depth (Mark, 2005) or with water flow (Bolle et al., 2006). The difficulty arises once we need to compare the 1D surface network with the 2D surface grid. Whilst the 1D model produces results at the nodes, the 2D model outputs them at the grid points. In the former, the nodes may represent a pond or a channel connection, in the latter the grid points represent a specific point on the surface which may or may not coincide with the first (i.e. location and/or element).

This method allows for the comparison of water depths and water flow propagation. It assumes that the results at the ponds and channel connections in the 1D/1D model correspond approximately to those in the 2D grid. Hence, the depths are readily available for comparison between models. The velocity, however, is harder to compare because in the 1D/2D model it is defined by two components and typically varies in space, while the velocity in 1D/1D model has a single component. Therefore, instead of looking at velocity vs. time, the arrival times of flood-peak waves are used to infer the flood flow dynamics, hence enabling the comparison between the flow propagation of both models.

To illustrate, Figure 4.25(a) shows a plan view of fictitious outputs from both 1D/1D and 1D/2D models on a regular grid with 64 elements. The two figures show two possible outputs of flow paths (from the two models) following a similar trend but with some differences. Since both models will use the same DEM it is possible to reproduce the 1D/1D and the 1D/2D results together in the same grid. Figure 4.25(b) shows the comparison

between the two models at three out of the four different locations shown in Figure 4.25(a). Points A, C and D locations coincide in both models hence the comparison is straightforward. Point B belongs to a branch of water which does not share the same grid points. In this case the modeller has to assume a correspondence between the two, either based on the proximity between points or on the distance to the coinciding points of a same branch. Figure 4.25(b) is divided into three sections. The top section shows the resulting levels from the 1D/1D model, the second shows the differences in peak elevations, time of occurrence and filling sequence of ponds (order numbers-on), the third section presents the results from the 1D/2D model. The top and bottom sections allow for a visual comparison of the hydrographs' propagation, as the flood advances with time. Those two sections also allow to qualitatively infer the models' agreement over the characteristics of the flood wave such as delay, early arrival or exact prediction, which are herein referred to as "lagging", "overshooting" and "coincident". The middle section quantifies those characteristics. The results from both models are not plotted on the same graph to make the visual comparison of the flow routing effect easier between models.

4.4.4 2nd Method of Comparison - Level-of-Resolution

The method proposed in this subsection, allows for comparing the agreement between models on the extent of the flood-inundation, and for quantifying the effect of decreasing the level-of-resolution (increasing the grid size for interpreting the results) to improve the agreement between both models, whilst keeping the accuracy of the results with the base grid in which they were first produced. This procedure enables flood managers to set-up a minimum level of resolution required, according to the objectives of a particular study, and therefore increasing their confidence in the results. The method makes use of the visualisation techniques developed in section 4.1.3 to produce grid-cell inundation-extents based on the 1D/1D model. Therefore, no difficulty arises during the comparison since they both output the results on the same grid. However, as it stands the method only allows for comparison of the models in terms of water depths and does not enable comparison of flow velocities. Unlike the previous method, this method requires pre-processing data from both the 1D/1D and the 1D/2D output results. The pre-processing can be summarized in the following five stages:

1. Transform (i.e. rasterize) the water levels from the 1D/1D surface network into a grid with the same base resolution as the 1D/2D model (e.g. $\Delta x = 1$ and $n_{cells} = 64$) using the algorithms developed in section 4.1.3.

2. Generate two matrices based on the results from the two models, with values "1" if

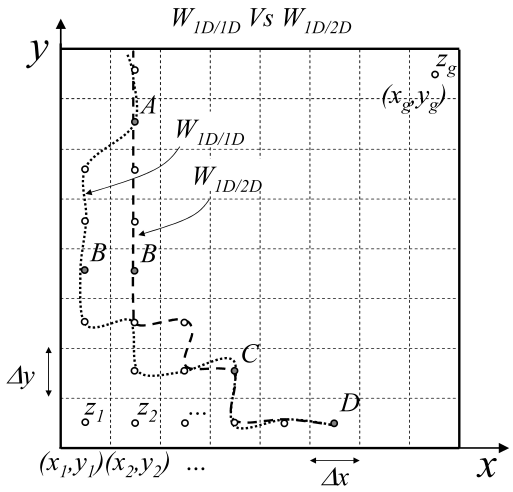

(a) Plan view (x, y) of the models outputs on a fictitious example using a grid with 64 elements.

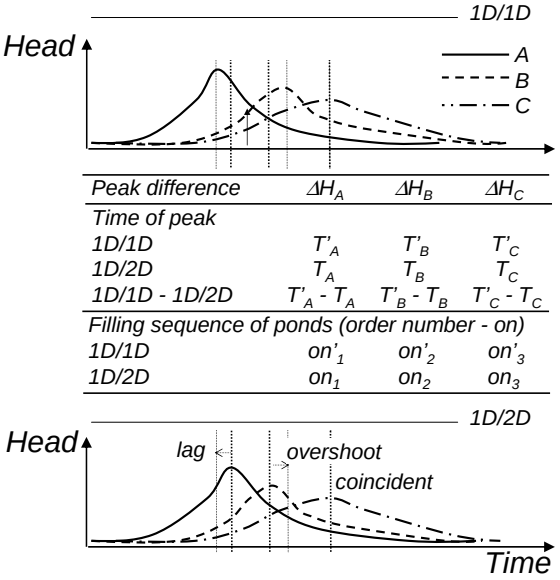

Peak difference	ΔH_A	ΔH_B	ΔH_C
Time of peak			
1D/1D	T'_A	T'_B	T'_C
1D/2D	T_A	T_B	T_C
1D/1D - 1D/2D	$T'_A - T_A$	$T'_B - T_B$	$T'_C - T_C$
Filling sequence of ponds (order number - on)			
1D/1D	on'_1	on'_2	on'_3
1D/2D	on_1	on_2	on_3

(b) Comparison of the water depth and flow propagation vs. time between for points A, B and C.

Figure 4.24: Illustration of the 1^{st} method-"Time Dependent" for comparing 1D/1D vs. 1D/2D models

water depth is greater than a minimum h_{min}, and "0" if water depth is less than or equal to h_{min}.

3. Define the set of grid resolutions (e.g. $\{64, 16, 4, 1\}$ Figure 4.25).

4. Generate similar matrices as in stage 2, for all elements in the set defined in the previous step.

5. Plot the resolution graph (Δx,F) and the downgrading of number of cells graph ($\Delta x, n_{cells}$).

Where in the above five stages:

- F is the measure of fit defined by:

$$F = \frac{100 \times \sum_{\mathrm{g}} \left(W_{1D/1D} \cap W_{1D/2D}\right)}{\sum_{\mathrm{g}} \left(W_{1D/1D} \cup W_{1D/2D}\right)} \tag{4.32}$$

- $W_{1D/1D}$ " is assigned the value of "1" if only the 1D/1D model grid point, g, is flooded and a value of "0" otherwise (similarly for the 1D/2D model);

- $\left(W_{1D/1D} \cap W_{1D/2D}\right)$ is assigned the value of "1" if both models are flooded at the grid point, g, and a value of "0" if dry;

- $\left(W_{1D/1D} \cup W_{1D/2D}\right)$ is assigned the value of "1" if at least one of the two models is flooded at the grid point, g, and a value of "0" otherwise;

- h_{min} is the minimum depth considered for plotting the flood-inundation-extent.

Equation (4.32) gives a value of 100 % for perfect agreement between models and 0% for total disagreement (Pender et al. (2004) defined a similar expression).

The resolution graph includes a line of best fit, a second degree polynomial curve (f). Urban flood managers can use the measure of fit (retrieved by the polynomial curve) to check whether a minimum level-of-resolution (grid size) meets a defined standard required in a particular case study. Depending on that, the 1D/1D model would be validated or not.

Finally, the five steps can be repeated for several h_{min}, and the Resolution graph obtained for each depth lumped together, to form a family of polynomial curves as a function of the h_{min}.

Figure 4.26(a) shows a plan view of the outputs from the 1D/1D and 1D/2D models on the same fictitious example used in the 1^{st} method. Figure 4.26 shows the stages in the pre-processing. Starting with figure 4.27(a) where the base grid (stage 1) and the

matrices (stage 2) are defined. Figures 4.27(b),4.27(c) and 4.27(d) show the generation of the matrices (stage 4) for the elements of the grid set previously defined in stage 3. Figure 4.26(b) presents the graphs obtained in stage 5.

With Figure 4.26(b) the flood manager is in control to define a desired level of resolution. The figure allows for defining a minimum level of resolution Δx_{lim} which is required by a given project. Moreover the graph provides with an indicator F that ranges from "0" to "100", no agreement to perfect agreement between models. In this way the method enables the boundary/limits to be set for applying the 1D/1D model, on the criterium of the resolution required satisfying the level of agreement demanded by the flood manager.

4.4.5 Conclusions

A methodology to setup equivalent 1D/1D and 1D/2D models has been presented to ensure a meaningful comparison. Two methods for comparing the models' performance have been introduced. The 1^{st} method-"Time Dependent" produces a thorough comparison of both water levels and flow propagation with time. The 2^{nd} method-"Level-of-Resolution" is a more flexible method which allows for selecting a level of resolution to produce maps of the extent of the flood-inundation. In this Thesis both methods are used to compare the results between the 1D/1D and the 1D/2D model. However, they can also be applied with the aim of validating the results against real data. To some extent, it is possible to interpretate the comparison as a validation of the 1D/1D model if we allow ourselves to consider the 1D/2D model results as real data. The two methods will be applied in two case studies, sections 5.2.8 and 5.3.8.

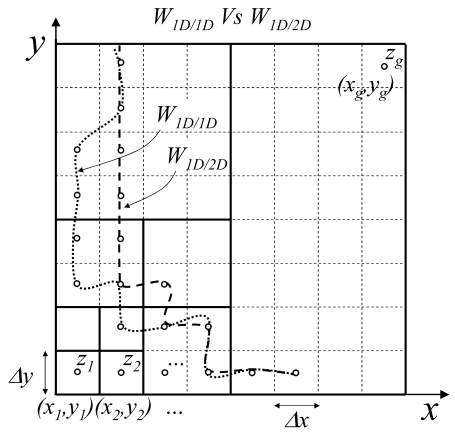

(a) Plan view (x, y) of the models outputs on a fictitious example using a grid with 64 elements. Pre-visualization of a possible set of grid sizes.

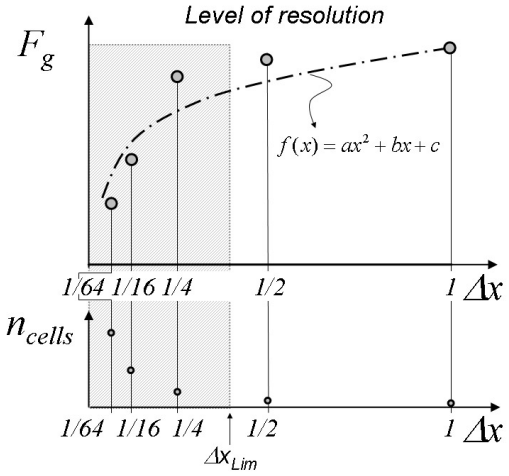

(b) Level-of-resolution graph (Δx,F), downgrading of number of cells graph $(\Delta x, n_{cells})$, with the minimum level of resolution Δx_{lim}.

Figure 4.25: Illustration of the 2^{nd} method-"Level-of-Resolution" for comparing 1D/1D vs. 1D/2D models.

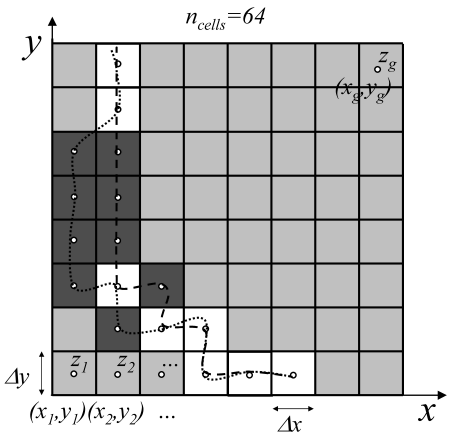

(a) Plan view (x, y) of the matrix and grid with 64 elements.

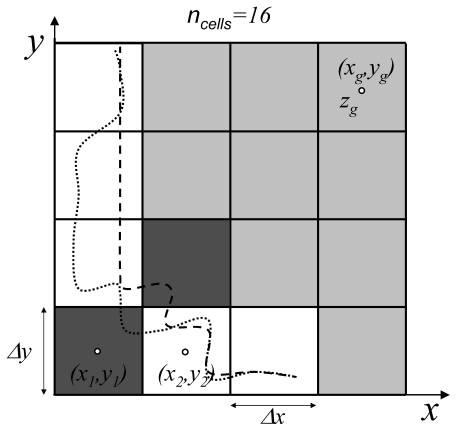

(b) Plan view (x, y) of the matrix and grid with 16 elements.

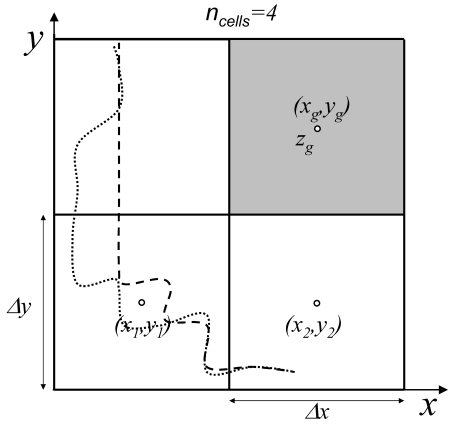

(c) Plan view (x, y) of the matrix and grid with 4 elements.

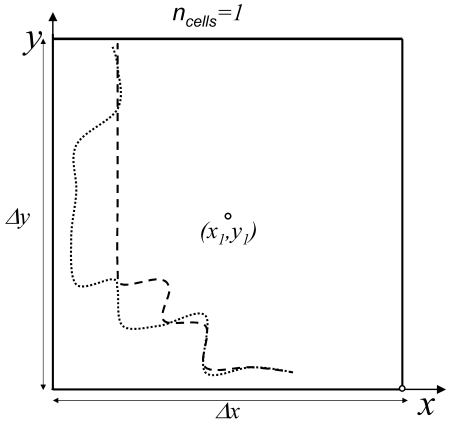

(d) Plan view (x, y) of the matrix and grid with 1 element.

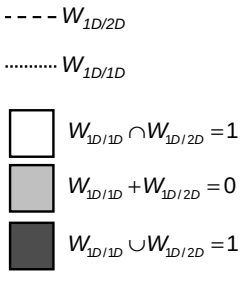

(e) legend.

Figure 4.26: Illustration of the intermediate stages in the 2^{nd} method-"Level-of-Resolution".

Chapter 5

Case Studies

5.1 Introduction

To demonstrate the suitability of the 1D/1D model to retrieve flood inundation maps, two distinctly different case studies were selected and a thorough comparison is done against a state-of-the-art 1D/2D model. In the first case study (Stockbridge area) the water surcharged by the sewer network is ponded at the surface. In the second case (Guard House School) the surcharge water is carried as overland flow to flood areas further downstream. Both case studies are located in Keighley, a town that has a recurrent history of flooding over the past years. All the results from the 1D/2D model (SIPSON/UIM) were generated by Dr. Albert Chen, hence, the author of this Thesis had no interference on the outputs from that model. The 2D Urban Inundation Model (UIM) model uses a two-step AD explicit method (Hsu et al., 2000) to solve the 2D non-inertia flow equations (see section 2.1) in the major system, while SIPSON solves implicitly the 1D St. Venant equations in the minor system. Furthermore, the 1D/1D and the 1D/2D model do not share the same linkage model, while the former uses the MLE the latter uses weir and orifice equations (Chen et al., 2007).

5.2 Stockbridge Case Study

5.2.1 Introduction

Keighley is a town located in the region of West Yorkshire (Bradford, UK) (Figure 5.2(a)). The River Aire and the railway bound the area on the North and on the South respectively. On the West and East, it is bordered by the A629 road and by a tributary of the River Aire (Figure 5.2(b)). The Stockbridge area is located in a relatively flat area with mainly residential dwellings. Due to topographical features, the area is likely to flood; in the early morning of 30th October 2000 the Stockbridge area was flooded by the River Aire.

The flooding in this part of the town is characterized by a filling up of large ponds, which depending on a higher or lower river level can have more or less severe damaging-impact. Two major flooding areas can be identified; the first can be flooded by either the rising waters of the River Aire or by the surcharge water-flow from the sewer system, or a combination of both; the second is flooded by the surcharge water-flow from the sewer system, which can nevertheless be aggravated by higher levels of the river Aire downstream of the catchment.

The Sewer network. The sewer network is divided into the main network and the detailed network. The main sewer network consists of 45 sewer pipes with a total length of $6km$, which covers an area of approximately $3.5km^2$. The sewer pipe diameters range from 300 to $1500mm$ and the slopes range from 0 to 10% (with an average of 1%). The detailed sewer network has a total of 74 sewer pipes with a length of $3.0km$ distributed in an area of $0.2km^2$. The diameters in the detailed network range from 100 to $900mm$, while the slopes range from 0% to 15% (with an average of 2%). Figure 5.2 shows the sewer network and the urban mesh within the boundaries of the study area.

5.2.2 Set-up of the 1D/1D and the 1D/2D Model

Following the steps from the methodology outlined in section 4.4.2:

Step 1. Sets the same sewer network in both models as defined in Figure 5.2. Sets the DEM with a resolution of 2x2m (Figure 5.3). Sets the boundary of the DEM as the detailed area.

Justification. The detailed sewer network is defined as the complete drainage system of that area, because it is directly responsible for the surcharge and drainage of the study area during a flood event. The main sewer network consists of the drainage pipes responsible for collecting the surface-runoff from the upstream catchments and for conveying the water to the outlets downstream of the detailed area. This network is however not allowed to surcharge hence it is only used to convey the surface runoff in the sewer pipes. As discussed in the Introduction 5.2.1, the flooding is expected to be localized and within the detailed area, therefore, that area is selected as the DEM boundary. It is assumed that a width of at least 2x2m grid is accurate enough to capture all the main topographic features such as buildings and main roads. Coarser grids would lead to inaccuracies due to averaging of these features. This is in agreement with the work of Maksimovic and Prodanovic (2001) where values in the order of 1-2m are said to be sufficient for capturing these features.

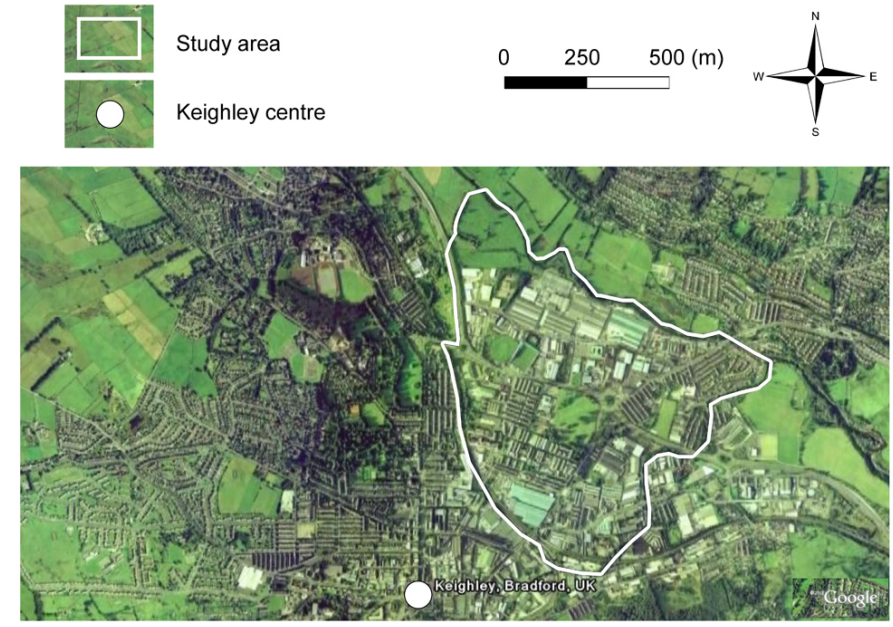

(a) Location of the Stockbridge area in relation to the Keighley town centre.

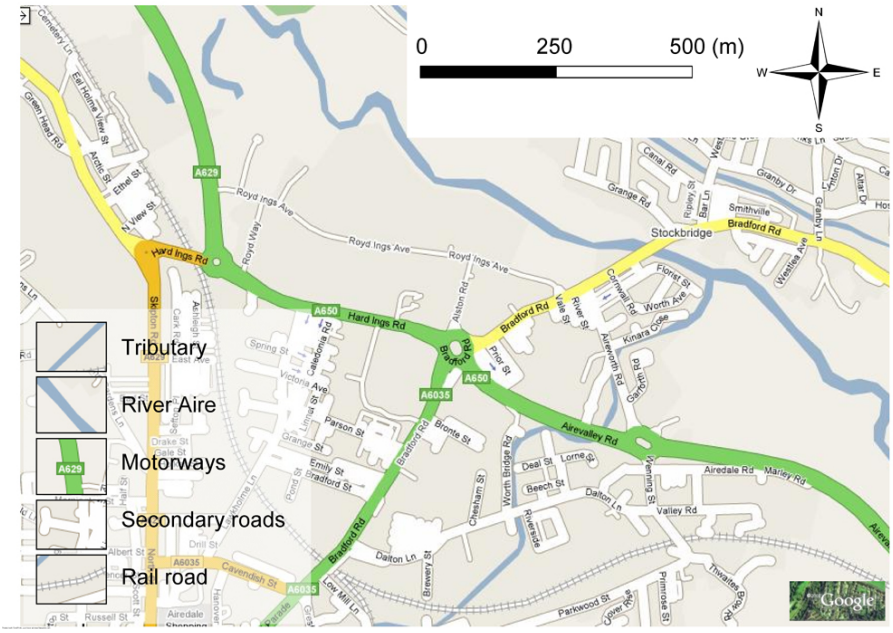

(b) Location of the Stockbridge area.

Figure 5.1: Location of the first case study.

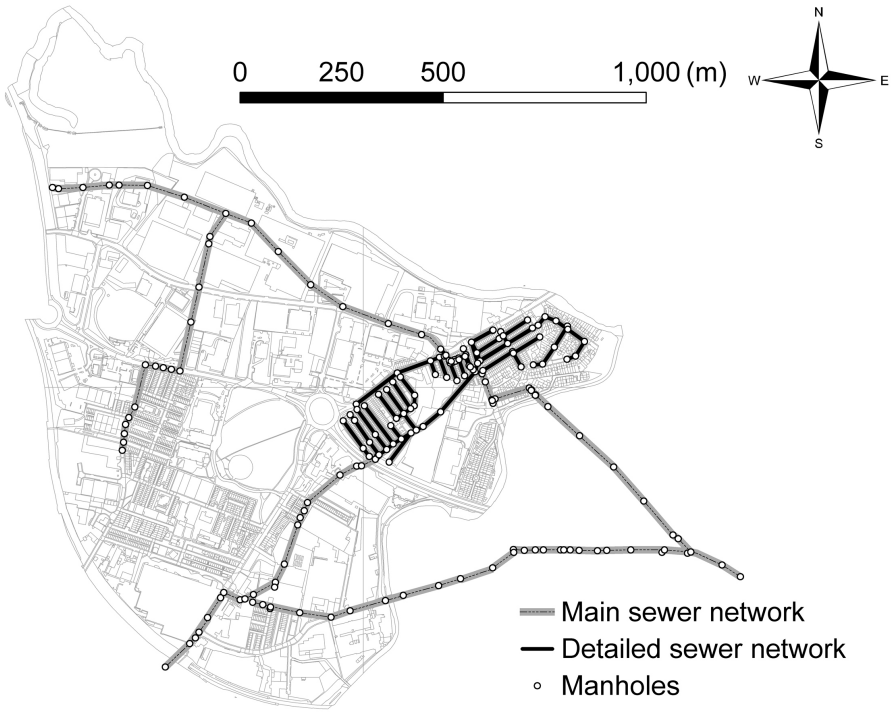

Figure 5.2: Map of the Stockbridge sewer network and boundaries of the study area.

Step 2. Generates the 1D surface network (Figure 5.4): 34 irregular cross-section channels with a total length of $2.4km$; the slopes range from -0.08% to 7% (with an average of 1%); 22 ponds. Sets 10 MLE links between ponds and manholes, 7 weir links between ponds and ponds or ponds and pathways.

Justification. The number of MLE links are set based on the proximity from the manholes to the pathways identified by the GIS tool. The remaining links are set based on the modelling details outlined in the next section 5.2.3.

Step 3. Sets to 4 inlets per manhole the MLE parameters in the 1D/1D model, Neq_j.

Justification. In this case, as in most case studies, this type of data is not available. Setting 4 inlets as an initial guess, has little influence on the final result since this will be the parameter used for calibration in the last step (see note at the end of section 4.4.2).

Step 4. Sets a synthetic block rainfall of $52mm$ in one hour, which corresponds to a 200 year return period event.

Step 5. Calibrates the 1D/1D model using the DOF/LSB algorithm. The calibration uses Neq_j in the 10 MLE links as the α_k^j (decision variables); the other parameters of the algorithm are further explained in subsection 5.2.5.

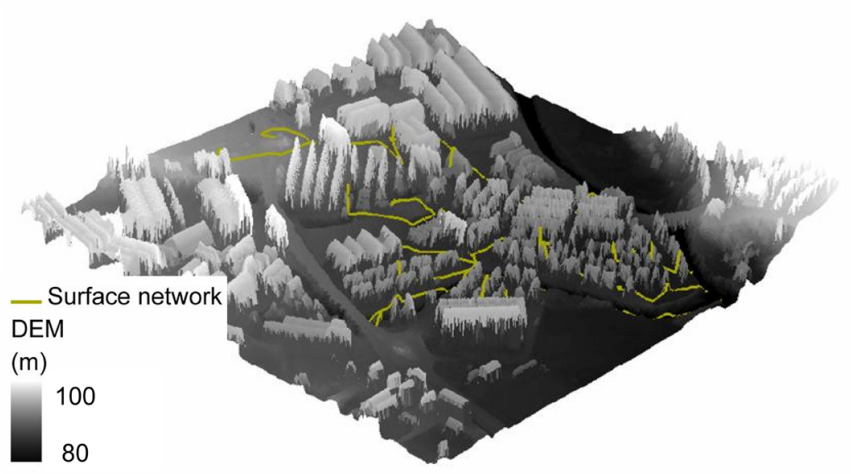

Figure 5.3: Three-dimensional view of the DEM (2x2m resolution) and the surface network with the vertical scale amplified (5x).

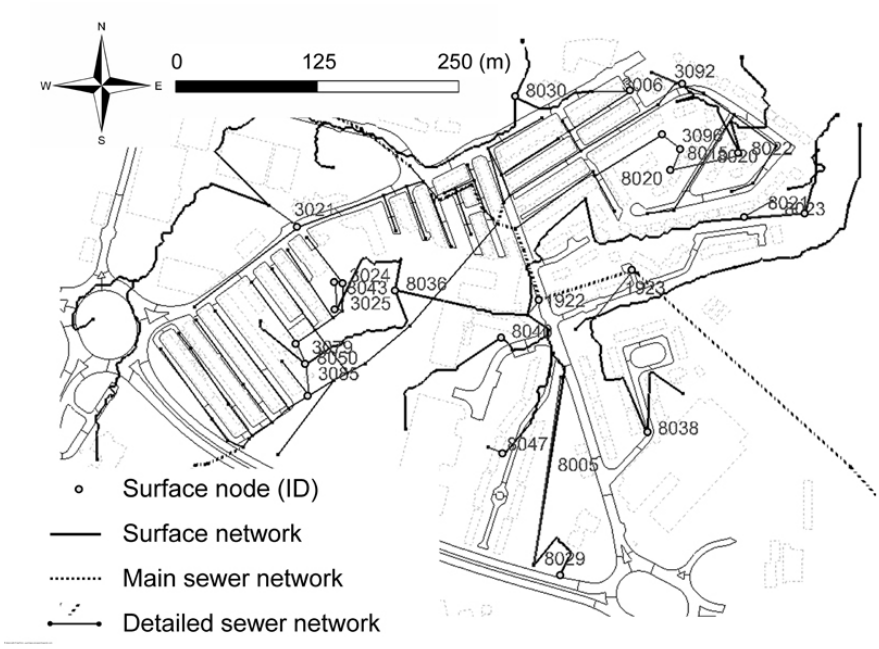

Figure 5.4: Top zoomed view of the study area. The sewer network and the 1D surface network.

5.2.3 Modelling Details

Setting up a 1D/1D model requires special care in the modelling details. One of the major drawbacks of 1D/1D models is their inherent vulnerability to schematization errors (Verwey, 2007). These errors arise during the model setup whenever the modeller misjudges the flow complexity and fails to capture its hydraulic behaviour. Three cases particularly difficult to model, analysed in this case study, are now explained in detail. The first and second cases deal with modelling the connection between manholes and ponds, as a function of their ground elevations and proximity to the edge of the pond. The third case models the connection of a small pond within a larger one. All these cases typically happen whenever flooding occurs in a relatively flat areas as a consequence of manholes surcharging, producing several localized pondings.

1. If the distance between a manhole and the edge of a pond is long enough to require a flow routing of the surcharged hydrograph from the manhole, then a virtual manhole (VM) is created between the two. The MLE is used to connect the manhole to the VM and a channel is used to convey the flow from the VM to the pond. The VM is set with an intermediate bottom elevation. The VM bottom elevation will control the discharge rate in the MLE, which otherwise would become unrealistically large if the pond bottom elevation was used instead. The channel connecting the VM to the pond will provide the necessary flow routing. Figure 5.6(a) illustrates the modelling details for connecting manholes with ponds. This figure shows the connections between pond 8050 and manholes 3079 and 3085.

2. If the distance between a manhole and the edge of the pond is considered short (few meters) and the bottom elevation of the pond is close to the top elevation of the manhole (few centimetres), then a VM is created between the two. The MLE is used to connect the manhole to the VM and a weir is used to connect the VM to the pond. As in the previous case, if the two were connected without the VM, the discharge rate would be calculated based on the water level at the pond instead of the water level at the surface next to the manhole. In this way unrealistic discharges between the manhole and pond are made realistic by considering a water level and a ground elevation in a location closer to the manhole (as in the 2D model). These form the second modelling case illustrated in Figure 5.6(b). This figure shows the connection between pond 8031 and manhole 3092.

3. The third and last case is used for modelling a small pond within a larger one. This case is modelled by connecting ponds with weir equations, either submerged or

non-submerged (depending on the levels in both ponds). Different crest levels are needed depending on the exit levels of each pond. Figure 5.6(c) illustrates the case where pond 8015 is located within pond 8020. The first connection uses the MLE from the manhole with ID 3096 to the pond 8015. The second connection uses a weir to connect pond 8015 to pond 8020. The third and last connection is a weir connection from pond 8020 to pond 8022. The weir connections are justified by the short distance between the ponds edges.

The author wishes to emphasise that the use of VM in this context has the sole objective of bringing the discharge rates from the surcharged manholes closer to the 1D/2D model (presumably more realistic). It is not to control a possible unstable behaviour of the linking element nor to enable more connections to the sewer network as in the work of Schmitt et al. (2004), where the concept of VM was also applied.

5.2.4 IRG Examples

From all the 34 surface pathways, four are selected to illustrate the use of the IRG algorithm developed in section 4.1.2. Figure 5.6 shows the cross-section of the four selected surface pathways. Figure 5.7 shows the resulting hydraulic radius (Hr) with and without the use of the IRG, with the horizontal axis as the 150 units in which the vertical cross-section is divided.

5.2.5 Calibration LSB vs. DOF

LSB and DOF parameters. The DOF and LSB parameters (section 4.3) are set as:

- The $\overline{\lambda}_k \rightarrow \left\{ f_k^j > 6000, \overline{\lambda}_k = 0.3 \; ; f_k^j > 3600, \overline{\lambda}_k = 0.2; f_k^j < 3600, \overline{\lambda}_k = 0.1; \right.$
- Interval of uncertainty $\alpha_k^j \in [0.5; 6.0]$;
- The β parameter equals $\max\{5, k-1\}$;
- The Ts, θ and MS are set to 0.95, 6 and 100.

The step length is made dependent on the objective function value in order to speed the convergence of both algorithms.

The interval of uncertainty is constrained by $lb = 0.5$ and $ub = 6$. The ub constraint is set because of the maximum physical number of Neq_j per manhole, and the lb constraint is justified for cases where partial blockage may reduce the Neq_j to less than 1.

β and Ts control the amount and quality of past iterations to be used. By setting β equal to the iteration number minus one, we are using all the information available from

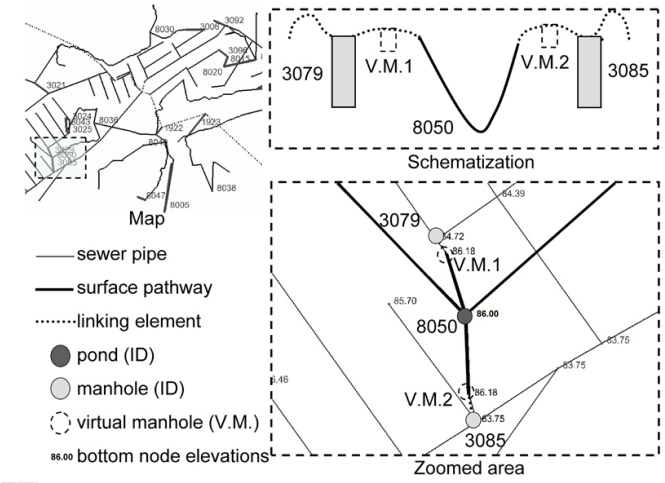

(a) Modelling details for connecting manholes with ponds (1).

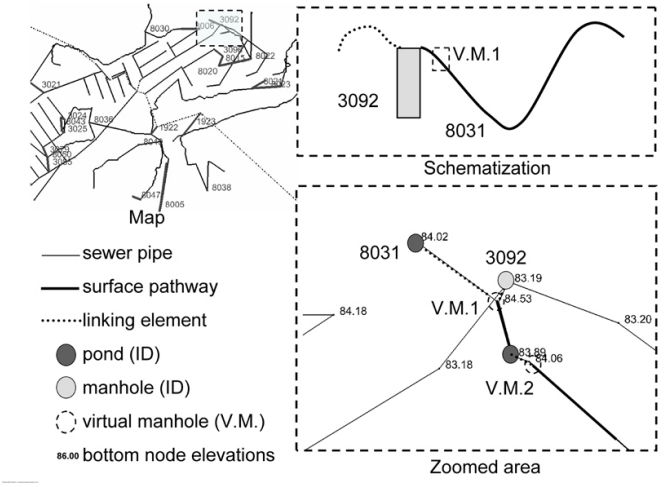

(b) Modelling details for connecting manholes with ponds (2).

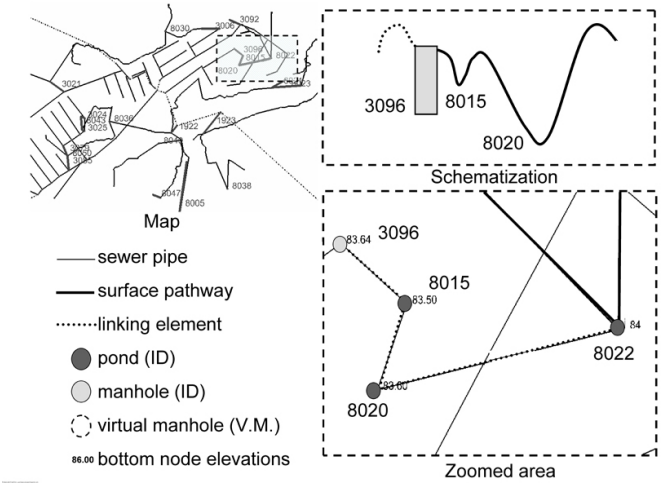

(c) Modelling details for connecting ponds to ponds (3).

Figure 5.5: Particular modelling details of the Stockbridge case-study.

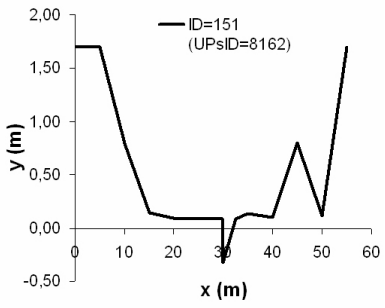

(a) Surface pathway with ID 151.

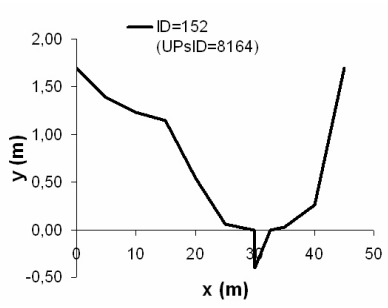

(b) Surface pathway with ID 152.

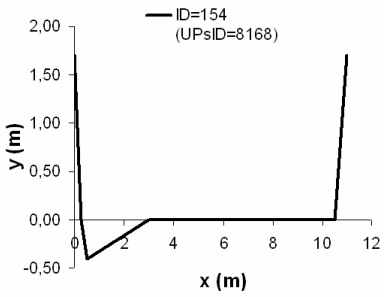

(c) Surface pathway with ID 154.

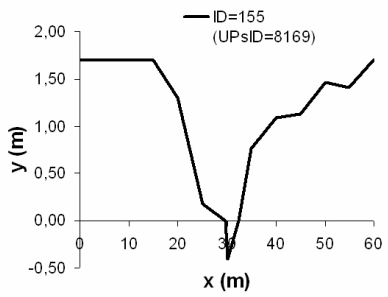

(d) Surface pathway with ID 155.

Figure 5.6: Four typical cross-sections of the Stockbridge 1D surface network.

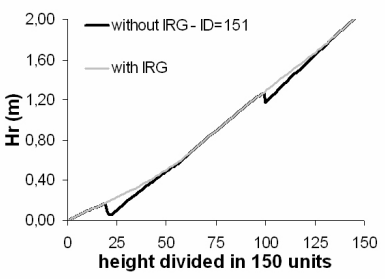

(a) Surface pathway with ID 151.

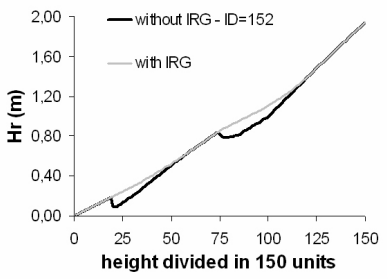

(b) Surface pathway with ID 152.

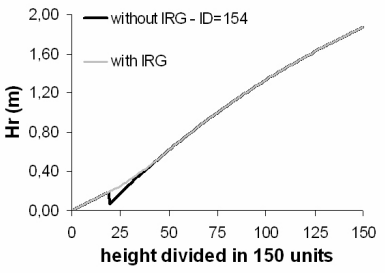

(c) Surface pathway with ID 154.

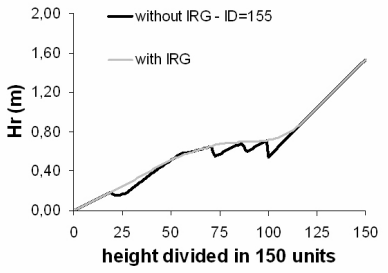

(d) Surface pathway with ID 155.

Figure 5.7: Four corrected Hydraulic Radius curves from the Stockbridge 1D surface network.

Alg.	LBS	DOF	LBS	DOF	LBS	DOF	LBS	DOF
I.guess	1	1	2	2	3	3	4	4
f_k^j	9501	9478	9306	9297	9140	10687	19345	12675
iter.	17	25	34	62	36	114	26	43

Table 5.1: Summary of the comparison between the calibration algorithms LSB vs. DOF as a function of the number of iterations (iter.) to obtain the optimum value f_k^j, and the initial guess (I.guess).

the past runs (however it was set a minimum of 5 initial runs to replace the LBS with the DOF for assuring a minimum of valuable information to calculate the Ccm, "warm up period"). The set of such a threshold (Ts) assures that only the highly linearly correlated f_k^j will be used to construct the f_k^j in the DOF.

θ cannot be too high otherwise we risk losing sensibility in tracking when the f_k^j enters or leaves the state of "possible convergence". Due to the oscillatory behaviour of the DOF algorithm the Ms cannot be set to 0, therefore a minimum value had to be used.

Many other combinations of parameters could be suggested and tried, with a possible gain in the efficiency of the algorithms (speed of convergence or/and better optimum achieved), however the values suggested were found to give good results, which indicates that a sensitivity analysis on these parameters may not have a dramatic improvement.

LSB Vs DOF results. In order to compare the performance of both calibration algorithms, four runs were set-up with four different initial values of the control variables. Table 5.1 summarises the results of the comparison based on the optimum value and the number of iterations to obtain it, for each calibration algorithm. Table 5.2 summarises the Neq_j obtained by each calibration algorithm, and the average $\bar{x}$ and standard deviation δ of the LSB and the DOF. The tables shows the number of upstream manhole IDs (UPsID) of each of the ten Neq_j. The reader should note that because Neq_js with UPsID equal to 3021 and 3025 have "0" flow throughout the whole simulation, they are kept unchanged.

The next set of plots compare the results from both algorithms, using the example with initial guess equal to 4. Figure 5.9(a) shows a plot of the objective function f_k^j as function of the k^{th} iteration. Figure 5.9(b) shows the control/decision variables Neq_j in a polar graph, for the first 50 iterations. The Ccm grid can be plotted either with its values in a matrix as a function of the k^{th} iteration, or alternatively it can be split individually into each of the ten control variables and the correlation values plotted as a function of the k^{th} iteration, as in Figure 5.9. Note that UPsID:3025 and 3021 do not display any values because the flow is 0 in both models.

Alg.	3096	3079	3024	3025	1922	3092	3085	3021	3006	1923
LBS(1)	3.6	1.9	1.8	-	1.8	2.7	1.0	-	2.2	0.6
DOF(1)	3.4	1.9	1.8	-	1.6	2.7	1.0	-	2.2	0.6
LBS(2)	4.6	1.8	1.9	-	2.5	2.7	1.1	-	2.3	0.6
DOF(2)	5.4	1.8	1.9	-	3.1	2.7	1.1	-	2.3	0.6
LBS(3)	5.5	2.0	1.9	-	3.5	2.7	1.1	-	2.3	0.6
DOF(3)	5.4	6.0	2.1	-	1.9	2.9	1.1	-	2.3	0.6
LBS(4)	5.9	2.2	4.6	-	3.3	3.5	1.1	-	4.3	0.7
DOF(4)	5.0	2.0	3.2	-	4.6	3.0	1.2	-	4.8	0.8
$\bar{x}_{LSB}$	4.9	2.0	2.6	-	2.8	2.9	1.1	-	2.8	0.6
$\bar{x}_{DOF}$	4.8	2.9	2.3	-	2.8	2.8	1.1	-	2.9	0.7
δ_{LSB}	1.0	0.2	1.4	-	0.8	0.4	0.1	-	1.0	0.1
δ_{DOF}	1.0	2.1	0.7	-	1.4	0.2	0.1	-	1.3	0.1

Table 5.2: Summary of the Neq_j obtained in each run of both calibration algorithms (identified by the UPsID), and the average $\bar{x}$ and standard deviation δ of the LSB and the DOF results

5.2.6 MLE Before and After Calibration

The results from the manhole discharges illustrate the MLE behaviour and the improvement in using the calibration on the 1D/1D model. Figures 5.10 and 5.11 show the 8 working MLEs discharge flow rates before and after calibration.

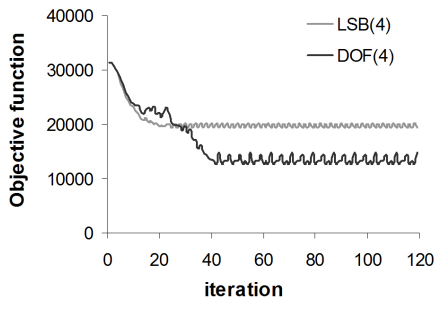

(a) Objective function $f_k = \sum f_k^j$ comparison.

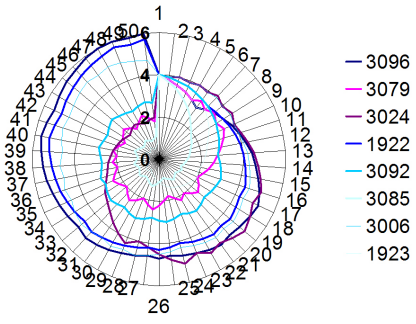

(b) Polar graph of the control variables α_k^j (number of equivalent elements Neq_j) identified by the UPsID (DOF algorithm).

Figure 5.8: Calibration outputs of the objective function and control variables.

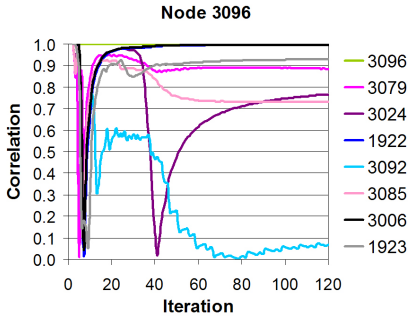

(a) Ccm with UPsID 3096.

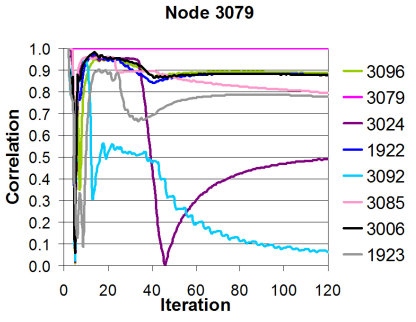

(b) Ccm with UPsID 3079.

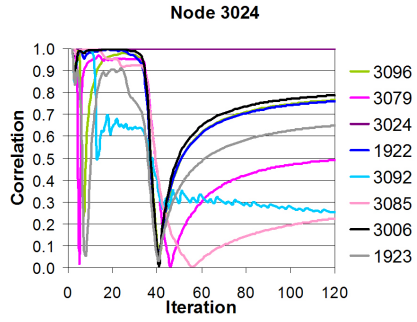

(c) Ccm with UPsID 3024.

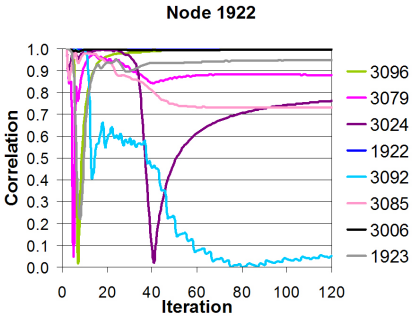

(d) Ccm with UPsID 1922.

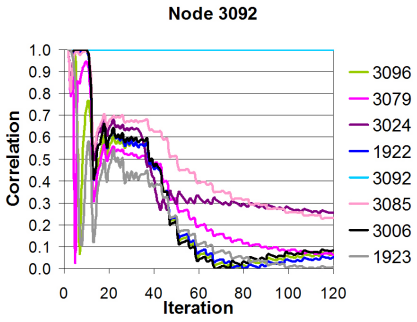

(e) Ccm with UPsID 3092.

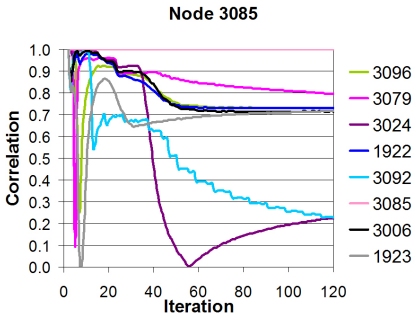

(f) Ccm with UPsID 3085.

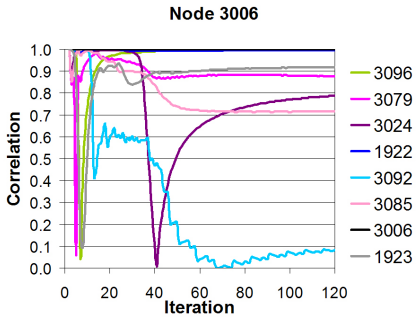

(g) Ccm with UPsID 3006.

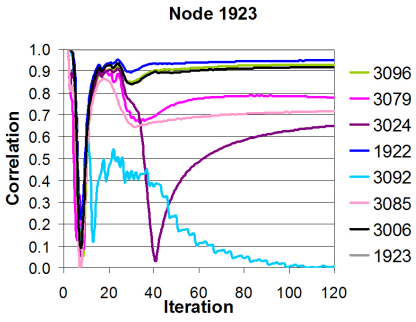

(h) Ccm with UPsID 1923.

Figure 5.9: Cross-correlation matrix values for each control variable.

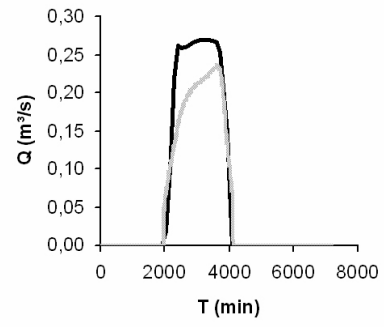

(a) UpsID 3024 before calibration.

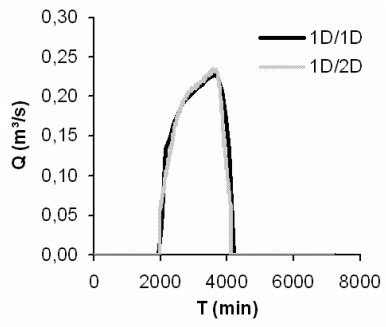

(b) UpsID 3024 after calibration.

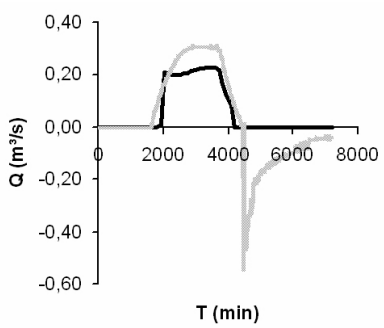

(c) UpsID 3079 before calibration.

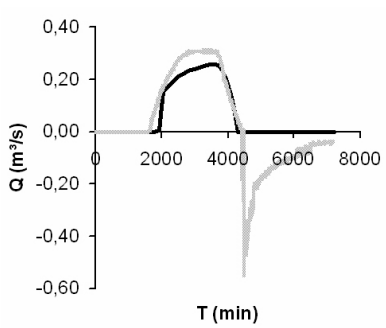

(d) UpsID 3079 after calibration.

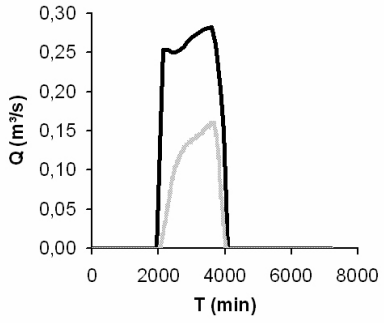

(e) UpsID 3085 before calibration.

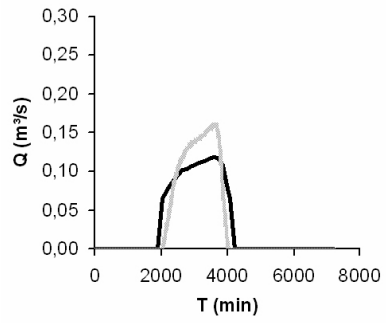

(f) UpsID 3085 after calibration.

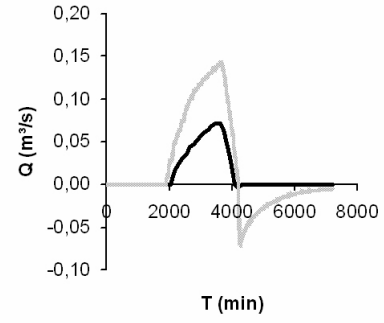

(g) UpsID 1922 before calibration.

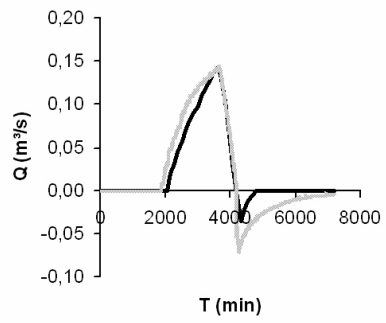

(h) UpsID 1922 after calibration.

Figure 5.10: First four MLE discharge flow rates before and after calibration, from the Stockbridge 1D surface network.

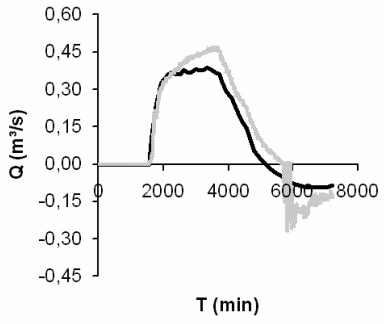

(a) UpsID 3096 before calibration.

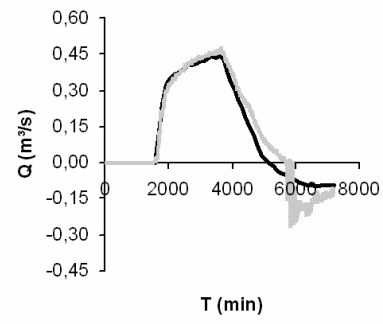

(b) UpsID 3096 after calibration.

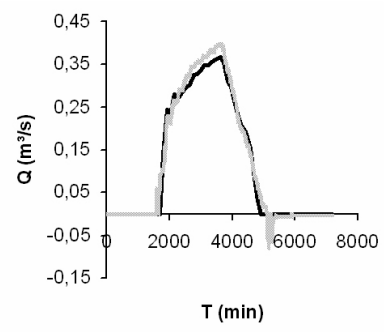

(c) UpsID 3092 before calibration.

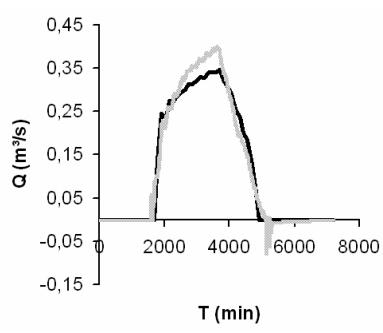

(d) UpsID 3092 after calibration.

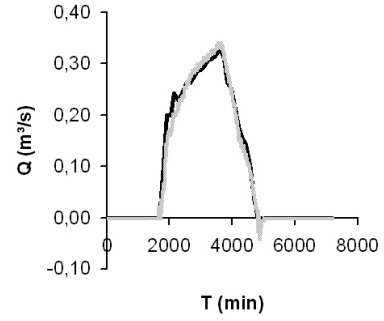

(e) UpsID 3006 before calibration.

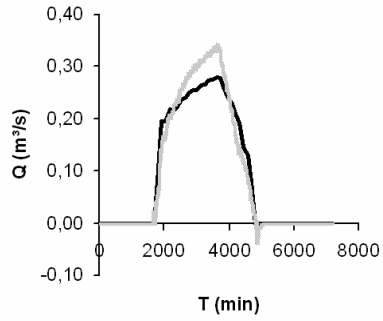

(f) UpsID 3006 after calibration.

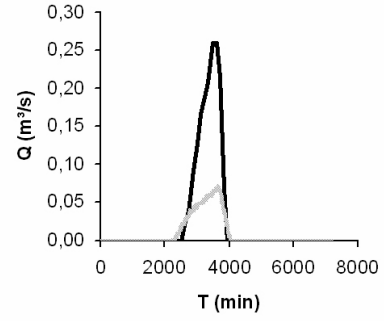

(g) UpsID 1923 before calibration.

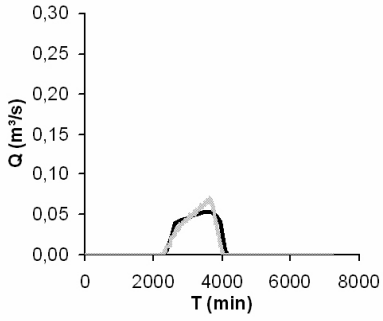

(h) UpsID 1923 after calibration.

Figure 5.11: Last four MLE discharge flow rates before and after calibration, from the Stockbridge 1D surface network.

5.2.7 Maps of Flood Inundation Extents

With the Visualization algorithm developed in section 4.1.3 it is possible to obtain the urban flood-inundation-extents. Figure 5.12 shows the maximum flood-inundation-extents obtained with the 1D/1D and 1D/2D models, for the event used for calibration.

Figures 5.13 and 5.14 show the flood inundation-extents obtained with the 1D/1D and 1D/2D models, for a 150 and 100 year return period.

Appendix A presents a complete list of the flood-inundation-extents produced for the FRMRC project. These depict the 1D/1D model suitability for producing flood-inundation-extents with different boundary conditions, and with different return periods and durations. The effect of ignoring the flooding defences (or assuming their failure) is clear on the flood-inundation-extents, highlighting the rather conservative approach assumed by the UK Government (2006) when defining the Flood Zones (zones at risk of flooding).

5.2.8 Models Comparison

1^{st} **method - Time dependent.** Figure 5.12 shows two major flooded areas located at the Southwest and Northeast sections of the detailed area. These areas are selected for comparing the surface flow propagation and water levels between both models.

Figure 5.15 shows the comparison of water levels and time of peak flows at the lowest point of the major ponds, in the 1D/1D and the 1D/2D models. The top section shows the results as described in section 4.4.3. The bottom section of the figure shows the geographic location of the nodes.

Figure 5.16(a) shows the water levels at ponds 8050 and 8043, and the surcharged manholes 3024, 3079 and 3085 (the latter manholes coincide with the ones having UPsIDs of the links shown in Figure 5.10). Figure 5.16(b) shows the time and peak levels being clearly captured in both ponds as well as a good agreement in the general shape of the water level profile. The length of the channels modelled downstream of the surcharged manholes predict accurately the routing flood hydrograph from the manhole to the pond. Therefore, both models agreed on the timing of flood propagation. The locations of ponds are in agreement with the results in Figure 5.12. Focusing on pond 8050, the analysis shows that after surcharging and a maximum peak is attained, the sewer starts to drain the water from the surface to the pipe network. It also shows that the crest levels in both models are in good agreement. Pond 8043 shows similarly good agreement; however in this case the water just remains on the surface and does not return to the sewer. Pond 8052 does not receive any water, because neither the manhole 3025 surcharges, nor the weir

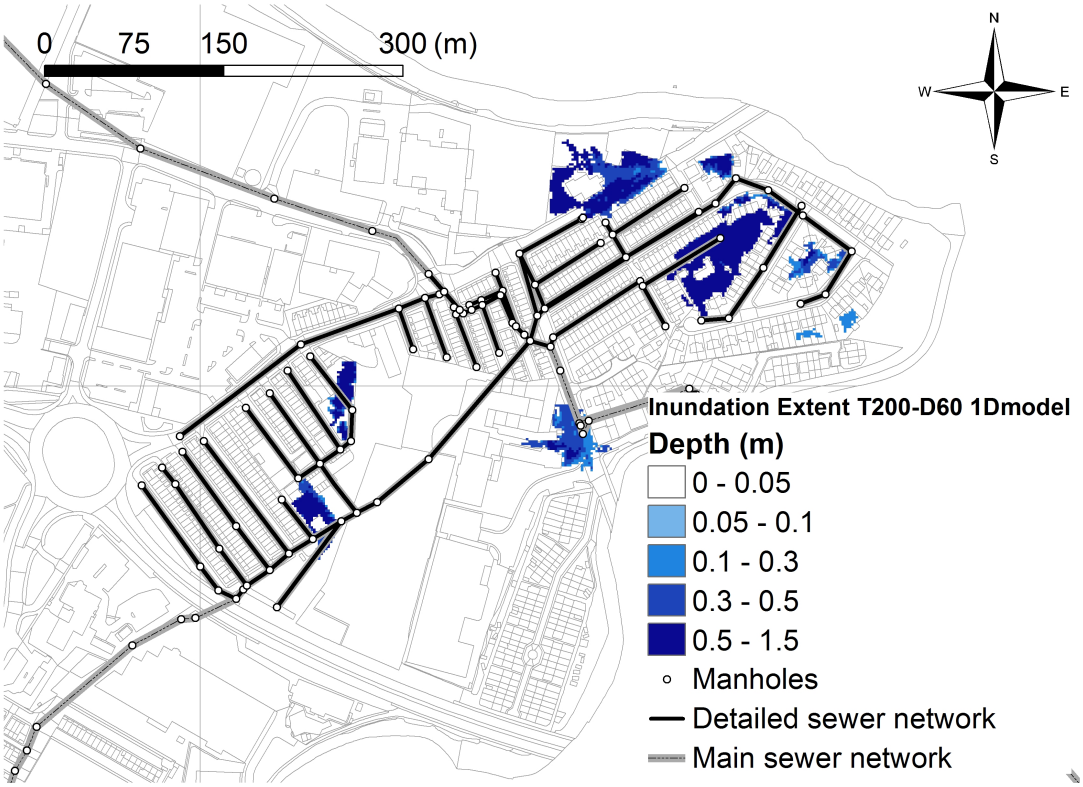

(a) Obtained with the 1D/1D model.

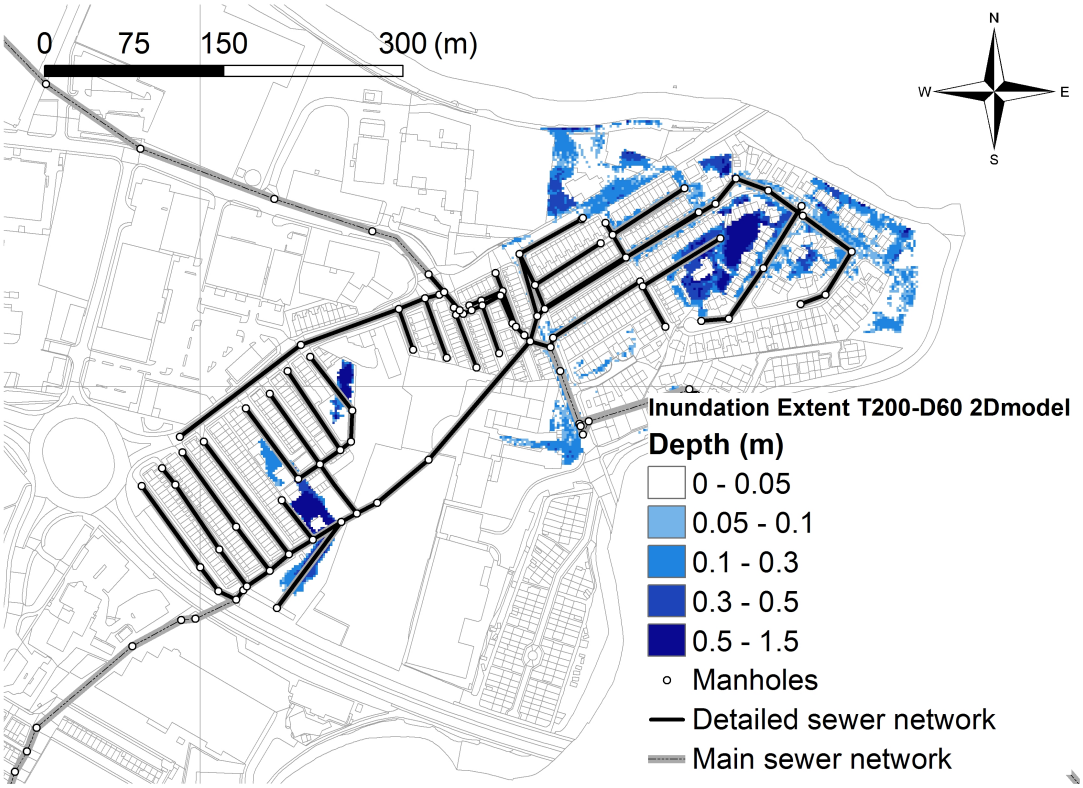

(b) Obtained with the 1D/2D model.

Figure 5.12: Stockbridge, maximum flood inundation extents for a 200 year return period event with 60 minutes duration.

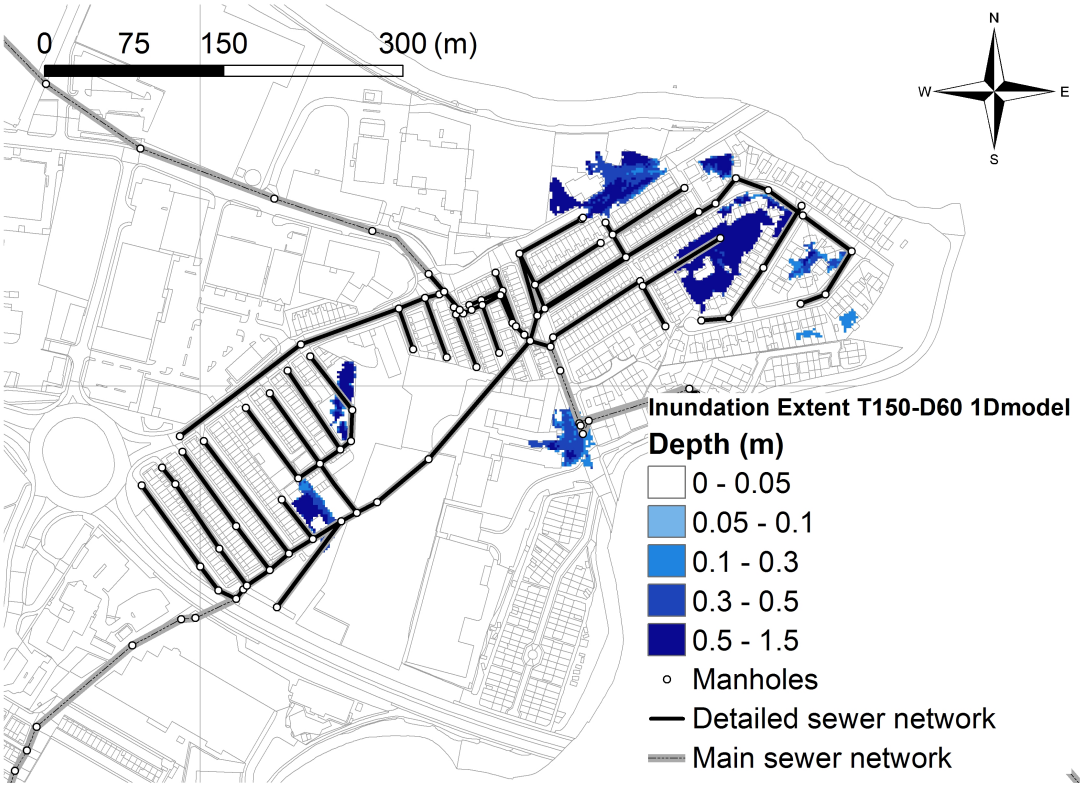

(a) Obtained with the 1D/1D model.

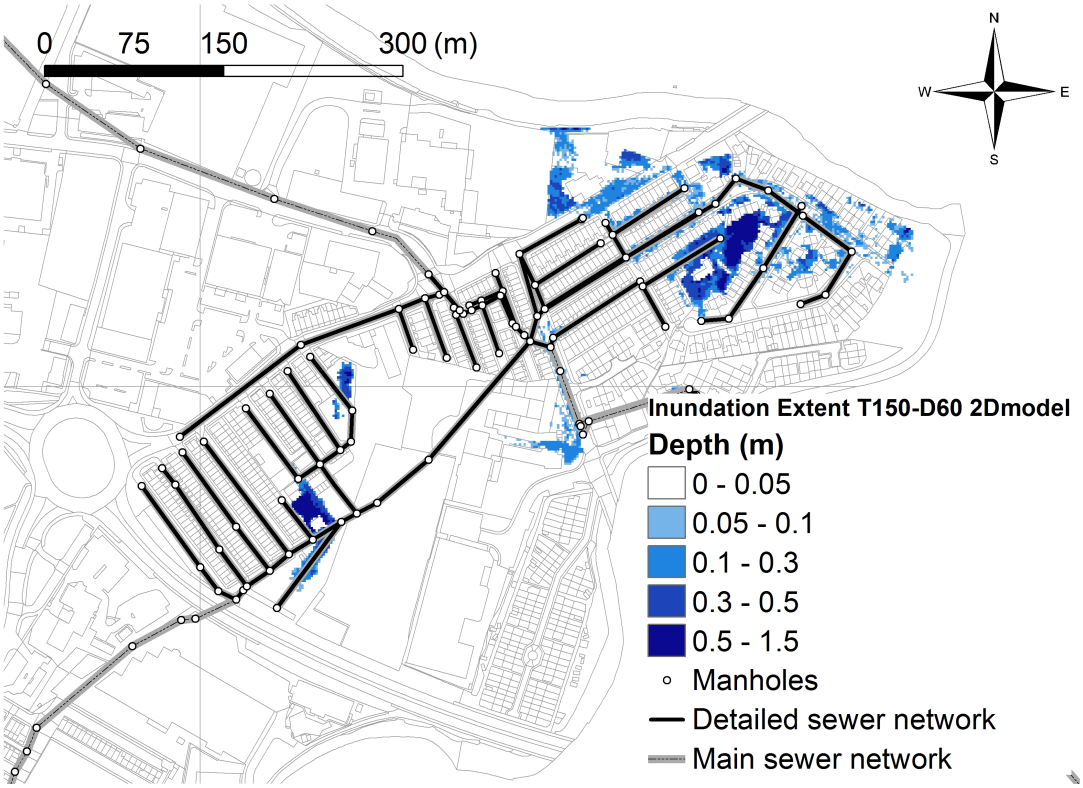

(b) Obtained with the 1D/2D model.

Figure 5.13: Stockbridge, maximum flood inundation extents for a 150 year return period event with 60 minutes duration.

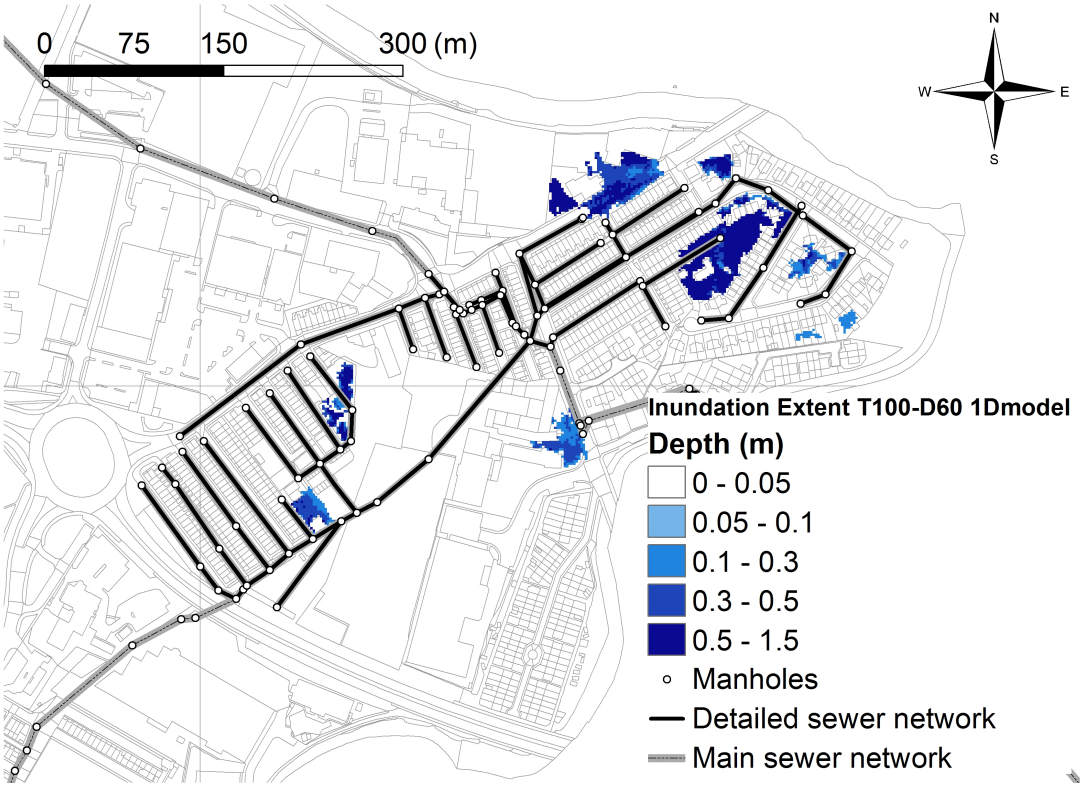

(a) Obtained with the 1D/1D model.

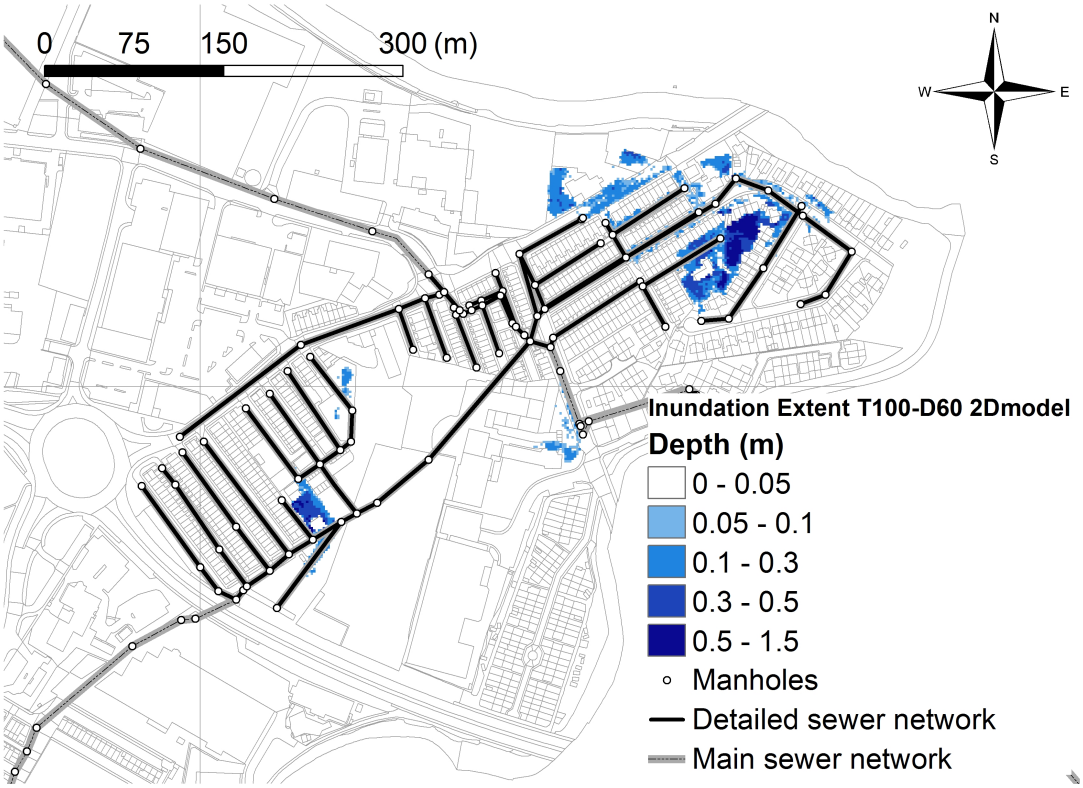

(b) Obtained with the 1D/2D model.

Figure 5.14: Stockbridge, maximum flood inundation extents for a 100 year return period event with 60 minutes duration.

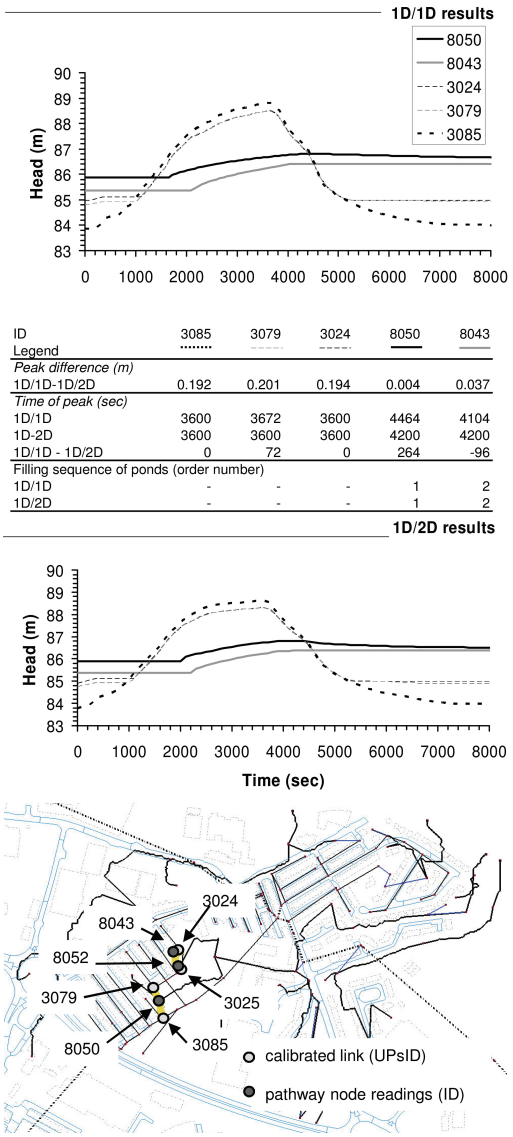

ID	3085	3079	3024	8050	8043
Legend					
Peak difference (m)					
1D/1D-1D/2D	0.192	0.201	0.194	0.004	0.037
Time of peak (sec)					
1D/1D	3600	3672	3600	4464	4104
1D-2D	3600	3600	3600	4200	4200
1D/1D - 1D/2D	0	72	0	264	-96
Filling sequence of ponds (order number)					
1D/1D	-	-	-	1	2
1D/2D	-	-	-	1	2

(a) 1D/1D and 1D/2D model results at the south-west flooded area.

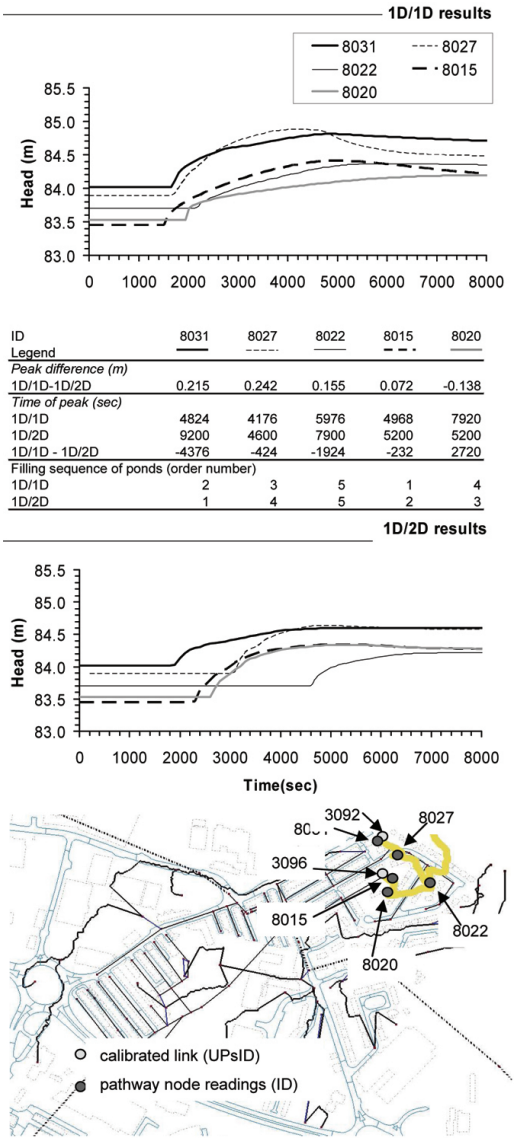

ID	8031	8027	8022	8015	8020
Legend					
Peak difference (m)					
1D/1D-1D/2D	0.215	0.242	0.155	0.072	-0.138
Time of peak (sec)					
1D/1D	4824	4176	5976	4968	7920
1D/2D	9200	4600	7900	5200	5200
1D/1D - 1D/2D	-4376	-424	-1924	-232	2720
Filling sequence of ponds (order number)					
1D/1D	2	3	5	1	4
1D/2D	1	4	5	2	3

(b) 1D/1D and 1D/2D model results at the north-east flooded area.

Figure 5.15: Stockbridge, model comparison using the 1^{st} method - Time dependent, for a 200 year return period event with 60 minutes duration.

connection with the neighbouring pond 8043 overflows. This figure shows that, for the selected ponds, the 1D schematization of the ponds and channels, as well as the modelling discretization used (Figure 5.6(a)) were indeed effective in reproducing the 2D features of the 1D/2D model.

Figure 5.16(b) shows water levels at ponds 8031, 8027, 8015, 8020 and 8022, and the surcharged manholes 3092 and 3096 (the latter manholes coincide with the UPsID's of the links shown in Figure 5.11). This figure shows that the peak levels were generally in better agreement than the times of peak. The selected area is severely flooded during the simulations as can be seen in Figure 5.12. The flow spreads over the whole area (i.e. it is distinctly two-dimensional). The 1D/1D model fails to predict the correct flow paths and, therefore, the filling sequence of ponds.

For ponds 8015 and 8020 (Figure 5.6(c) shows the modelling details) the time and peak level for the first pond are both well predicted. The 1D/1D model in the second pond shows the water level slightly underestimated and a lagged peak time when compared to the 1D/2D model. One of the possible explanations for the discrepancy in pond 8020 is the overestimation of the volume-depth curve, which would cause a peak delay and consequently prevent the correct peak level being obtained.

The pond 8022 in the 1D/1D model shows an overshoot of both peak time and water level. At first it may appear that an incorrect modelling assumption was used for linking ponds 8020 and 8022 (Figure 5.6(b)). However, if a channel is used for connecting the two ponds, it would result in an overlap of flooding areas due to the proximity of their edges. The schematization error in this case may have resulted from failing to consider the delay effect of filling up the smaller ponds. The error could also be exaggerated due to the absence of multiple exit points at ponds 8020 and 8022 in the 1D/1D model. A closer look into the 1D/2D results supports this explanation, showing that the filling of several small ponds precedes the filling of the lowest point in the 2D model, where the pond 8022 is located in the 1D/1D model. Since only one large pond was identified in the 1D/1D model (i.e. pond 8022) it directly starts filling without having the delay effect caused by the surrounding smaller ponds.

Figure 5.6(a) shows the modelling details for Pond 8027. The pond results show the time to peak and the peak levels reasonably well predicted, however, the instant when the pond starts to fill is overshot in the 1D/1D model. In this case, it may be concluded that a similar schematization error has occurred to that seen earlier for pond 8022. Nevertheless, the modelling detail used here seems to allow a good prediction of peak time and the volume-depth curve to enable a good agreement on the peak level.

Pond 8031 show a good general agreement in the profile shape for both models. This

pond illustrates the second case in the modelling details (Figure 5.6(b)). Because of the short distance between the pond exit and the manhole, the VM connects to the pond using a weir. The good prediction of the exact moment when the flooding starts is an indicator that there was no need to considerer a channel for connecting the manhole and the pond. However, an overshoot of the peak level in the 1D/1D model indicates either an underestimation of the volume-depth curve or a need to include an extra exit point in pond 8031.

Before concluding this subsection, the author wishes to make a remark on the delay effect of filling up surrounding ponds. There is a contribution to that effect due to the choice of governing equations used in the 2D surface model (thought difficult to quantify). Since the 2D model is a non-inertial based model (table 2.1) an inherent lagging in the surface flow propagation exists (Lin et al., 2006) and will contribute to that delay effect.

2^{nd} **method - Level of Resolution.** Figures 5.16 and 5.17 show the comparison of flood inundation-extents results between the 1D/1D and the 1D/2D models, for grid sizes (dx) equal to 2, 4 and 8, and 12, 16 and 20. The dx changes only the level-of-resolution and not the grid size in which the simulation results were produced. The flood inundation extent is obtained considering only water depths greater than 0.05m. The colour code is:

- White - both models have water on the grid node;
- Black - only one of the models has water on the grid node;
- Grey - both models are dry on the grid node.

Figure 5.18 shows the level-of-resolution graph considering only water depths greater than 0.05m, and dxs from 1m to 50m. Figure 5.19 shows the 2nd degree polynomials obtained by the level-of-resolution graph considering water depths greater than 0.000, 0.025, 0.050, 0.075 and 0.100m, and dxs from 1m to 50m.

The first two figures (5.16 and 5.17) show the visual impact of decreasing the level of resolution on the flood inundation-extents. For each grid size of resolution the colour code indicates if the models agree on whether the cells will or will not be partially flooded, with a depth greater than the minimum depth considered.

Looking at Figure 5.18, the level-of-resolution corresponding to $dx = 2$ (base resolution) has 40% of the total cells flooded agreeing in both models. This initial high percentage gives a strong confidence in the results from both models. As the dx increases (and the grid gets coarser) this percentage rises, though more slowly for the first values.

A sensitivity analysis on the h_{min} values (Figure 5.19), reveals a strong influence on the measure-of-fit F (see equation (4.32)), particularly in the area of the higher levels-

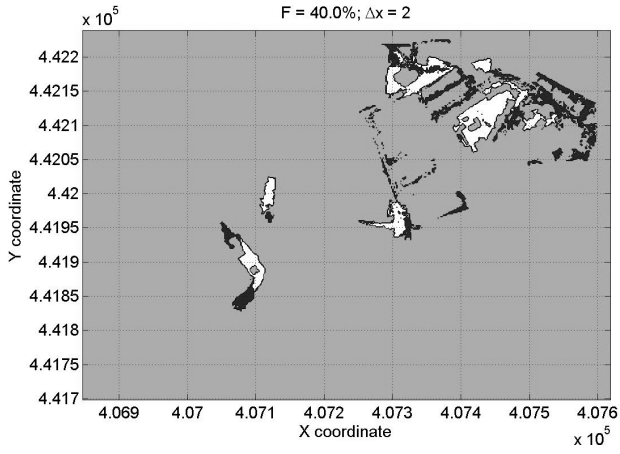

(a) 1D/1D and 1D/2D model results using $dx = 2$.

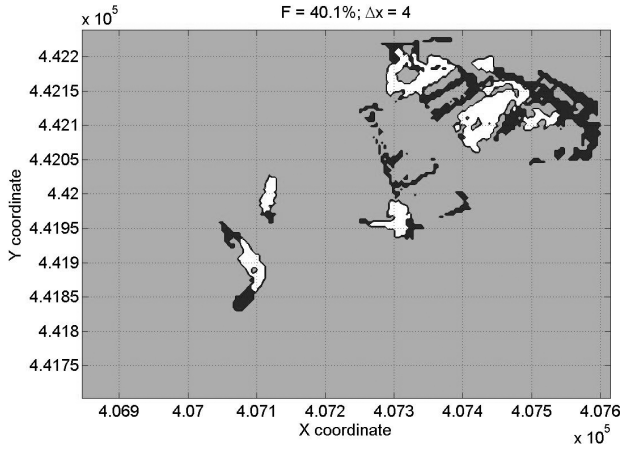

(b) 1D/1D and 1D/2D model results using $dx = 4$.

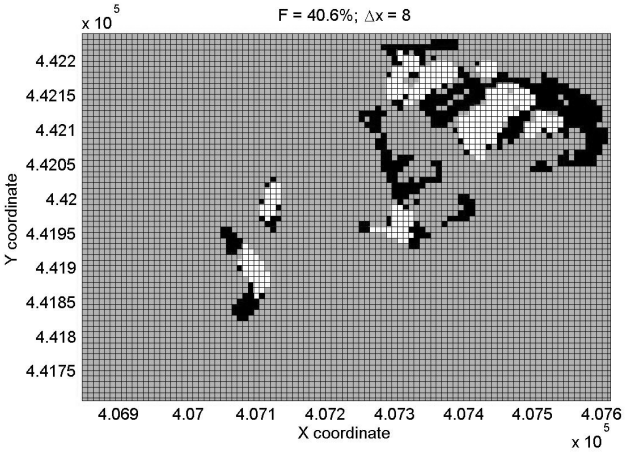

(c) 1D/1D and 1D/2D model results using $dx = 8$.

Figure 5.16: Stockbridge, model comparison using the 2^{nd} method - Level-of-Resolution, for dxs equal to 2, 4 and 8, and for a 200 year return period event with 60 minutes duration.

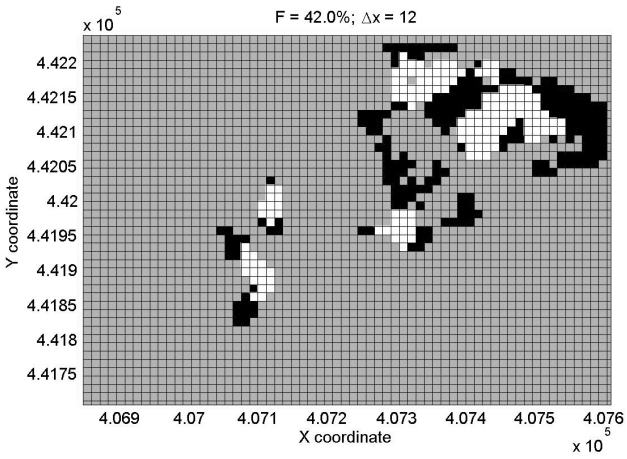

(a) 1D/1D and 1D/2D model results using $dx = 12$.

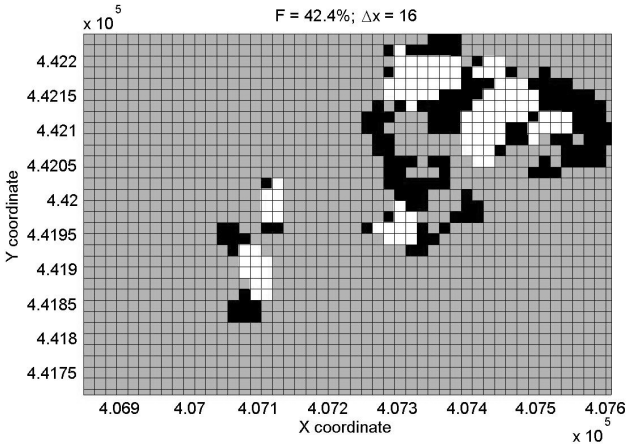

(b) 1D/1D and 1D/2D model results using $dx = 16$.

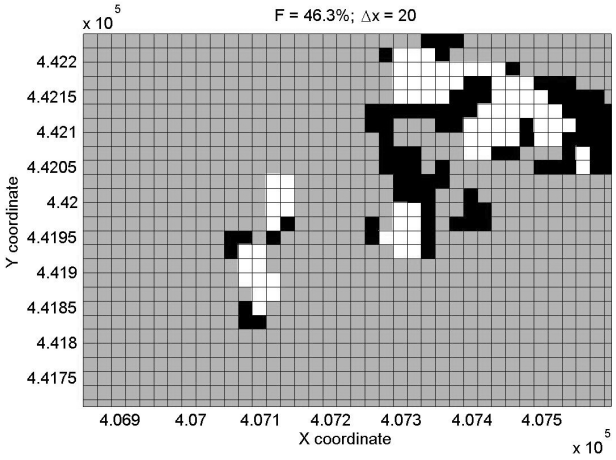

(c) 1D/1D and 1D/2D model results using $dx = 20$.

Figure 5.17: Stockbridge, model comparison using the 2^{nd} method - Level-of-Resolution, for dxs equal to 6, 8 and 10m, and for a 200 year return period event with 60 minutes duration.

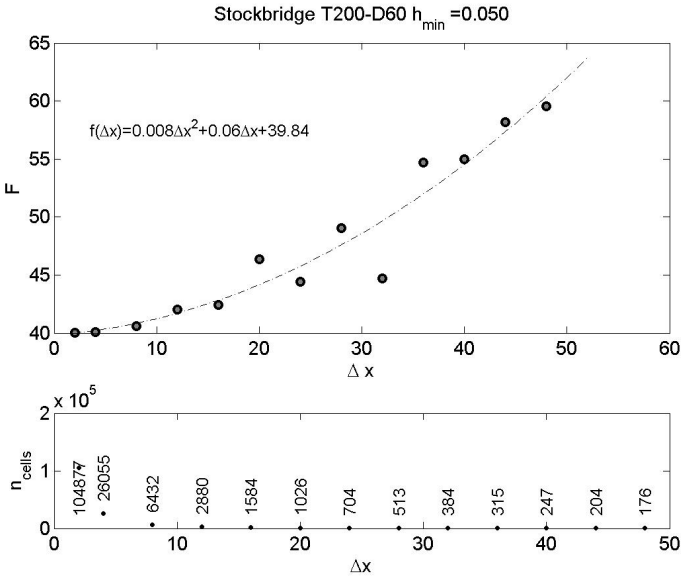

Figure 5.18: Stockbridge, level-of-resolution graph for water depths greater than 0.05m.

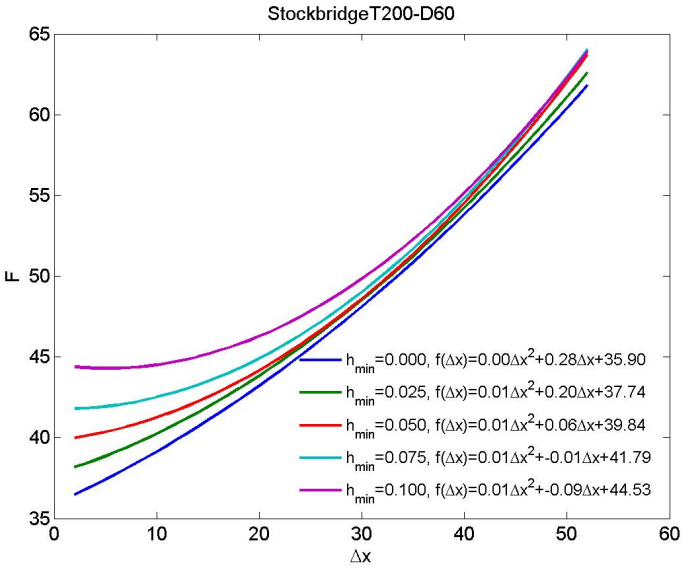

Figure 5.19: Stockbridge, level-of-resolution graph for water depths greater than 0.000, 0.025, 0.050, 0.075 and 0.100m.

of-resolution (dx between 1 and 30). This effect is stronger when using finer grids for visualization, where from raising the minimum depth from $h = 0$ to $h = 0.10m$ the percentage of cells in agreement has a gain of nearly 10%. However as the grid is made coarser than $dx = 30m$ this influence becomes negligible, as F becomes almost independent of h_{min} (Figure 5.19). For grids coarser than $dx = 30m$ and up to $dx = 50m$ F rises from 50% to 63%. This shows that the agreement on the flood-inundation-extent improves as h_{min} moves away from the very small water depths. The monotonic behaviour of the polynomial curves, both in relation to dx and h_{min} (the last only in the area of the higher levels-of-resolution), is an indicator that the two models converged to a similar flood-inundation-extent. Increasing dx invariably increases F, whereas increasing h_{min} increases F only in the area of higher levels-of-resolution.

It must be emphasized that this method only changes the resolution in which we analyse the results, whilst keeping the fine grid in which they were first produced. Therefore, in this method, the coarsening of the grid has no effects such as of smoothing of topographic features as described by Maksimovic and Prodanovic (2001).

5.3 Guard House School Case Study

5.3.1 Introduction

Guard House School is a primary school with capacity for 300 students. It is located to the North West of Keighley town centre, in a hillside area (Figure 5.21(a)). Since 2003 the school has been subject to flooding caused by extreme rainfall events, with the drainage sewers unable to cope with the flooded water. The school creates an artificial barrier to the overland flow, preventing the water from draining naturally from the higher northern area towards the lower southern part.

Two major flooding areas can be identified near the school; one at the North-Eastern end at the boiler house and a second at the North-Western end (Figure 5.21(b)). The first area is mainly flooded by the overland flow coming along Braithwaite Avenue into Braithwaite Grove and then into the driveway to the boiler house. The second area is flooded by the overland flow from the hillside on the Northwest of the school.

The sewer network. The sewer network is divided into the main network and the detailed network. The main sewer network consists of 50 sewer pipes with a total length of $4km$, which covers an area of approximately $0.4km^2$. The sewer pipe diameters range from 150 to $800mm$ and the slopes range from 1% to 21% (with an average of 6%). The detailed sewer network has a total of 20 sewer pipes with a length of $0.5km$ distributed in an area of $0.01km^2$. The diameters in the detailed network range from 100 to $150mm$, while the slopes range from 0% to 12% (with an average of 5%). Figure 5.21 shows the sewer network and the urban mesh within the boundaries of the study area.

5.3.2 Set-up of the 1D/1D and the 1D/2D Model

Following the steps from the methodology outlined in section 4.4.2:

Step 1. Sets the same sewer network in both models as defined in Figure 5.21. Sets the DEM with a resolution of 1x1m (Figure 5.22). Sets the boundary of the DEM as the case study area.

Justification. The detailed sewer network is the drainage system of the Guard House School. The main sewer network consists of the drainage pipes responsible for surcharging and generating the overland flow responsible for flooding the school and the drainage pipes downstream of the detailed area leading to the outlets. Unlike the previous case study, here both networks are allowed to surcharge. Given the type of flooding discussed in the Introduction 5.2.1, the whole case study area is used as the DEM boundary. Unlike the

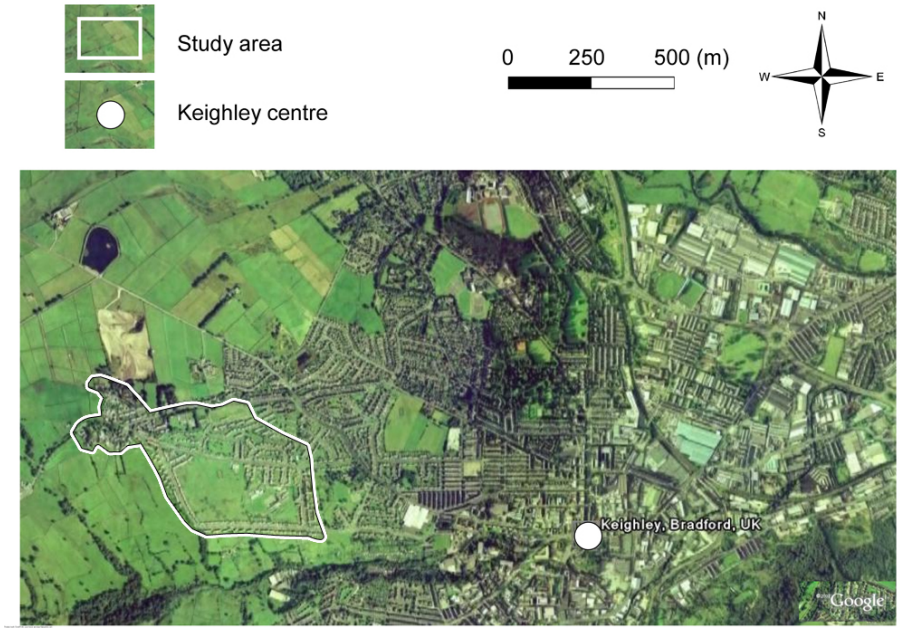

(a) Location of the Guard House School area in relation to the Keighley town centre.

(b) Location of Guard House School.

Figure 5.20: Location of the second case study.

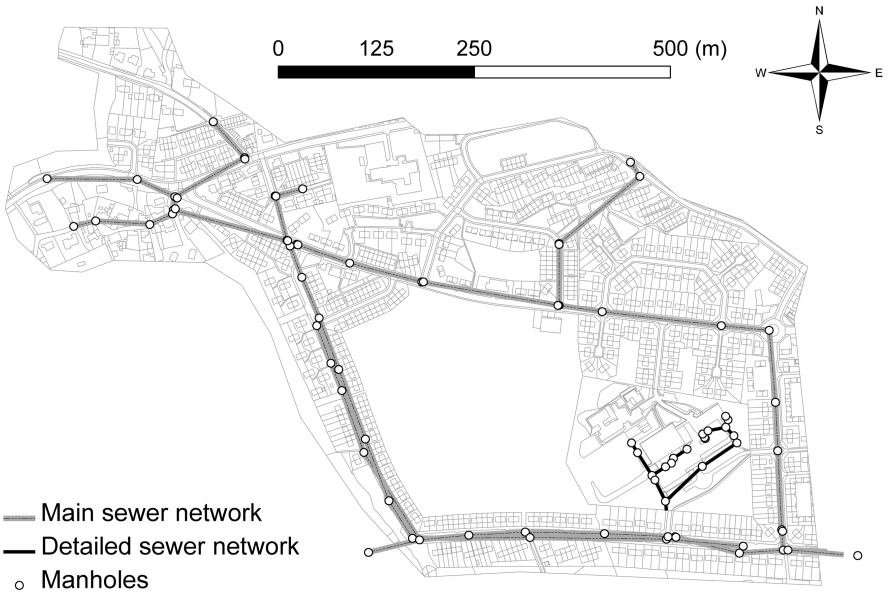

Figure 5.21: Map of the Guard House School sewer network and boundaries of the study area.

previous case study, here a 1x1m grid is used; the highest level of resolution available. This allow conclusions to be drawn on the computational efficiency of both models.

Step 2. Generates the 1D surface network (Figure 5.23): 59 irregular cross-section channels with a total length of 2.3km; the slopes range from 0% to 22% (with an average of 6%); 14 ponds. Sets 11 MLE links between ponds and manholes, 9 weir links between ponds and ponds or ponds and pathways.

Justification. The number of MLE links are set based on the proximity from the manholes to the pathways, and on the possibility of the water surcharged from the manholes contributing to the school flooding.

Step 3. This step is similar to the previous case study.

Step 4. Sets a synthetic block rainfall of 52mm in one hour with a 200 year return period event, where part of it is input into the surface system.

Justification. Because there is a large non urbanized area without a sewer network, circumscribed by the Braithwaite Avenue, North Dean Avenue and North Dean Road, it was decided that the runoff in that area would be input into the surface system (unlike the rest of the area where the runoff is input into the pipe network nodes).

Step 5. This step is similar to the previous case study.

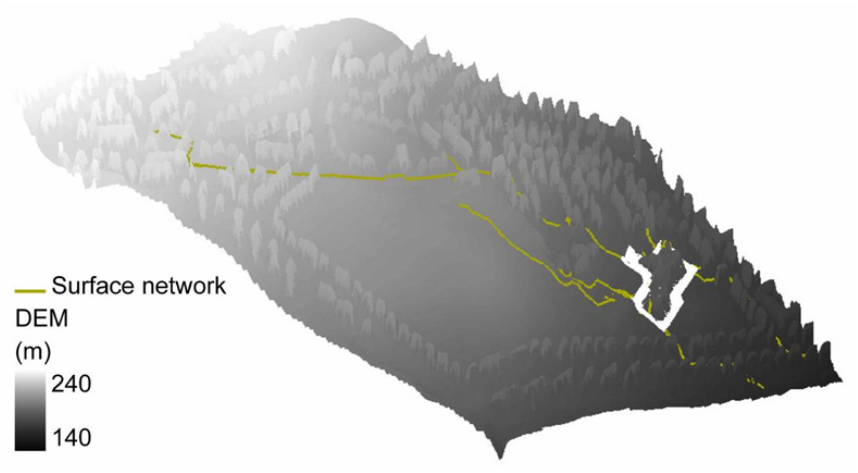

Figure 5.22: Three-dimensional view of the DEM (1x1m resolution) and the surface network with the vertical scale amplified (5x).

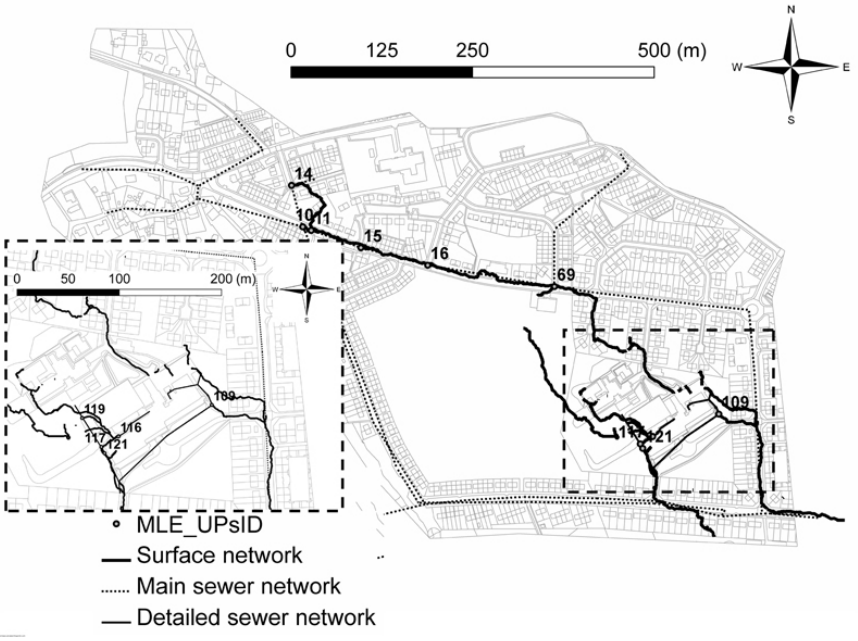

Figure 5.23: Top zoomed view of the study area. The sewer network and the 1D surface network.

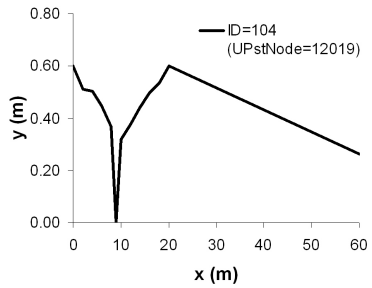

(a) Surface pathway with ID 104.

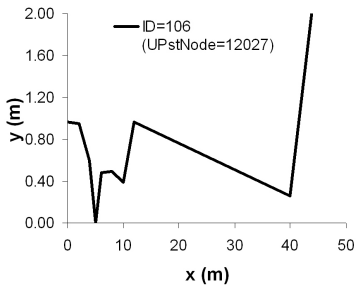

(b) Surface pathway with ID 106.

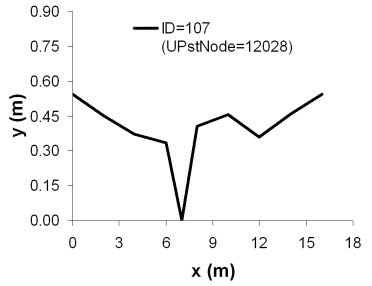

(c) Surface pathway with ID 107.

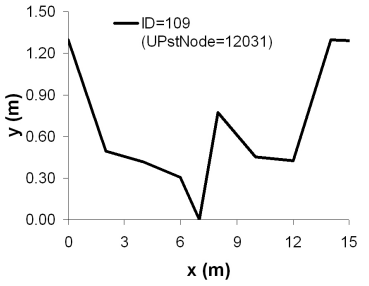

(d) Surface pathway with ID 109.

Figure 5.24: Four typical cross-sections of the Guard House School 1D surface network.

5.3.3 Modelling Details

The flooding in the Guard House School case study is entirely different from the one that affects the Keighley case study. The ponding seen in Stockbridge, is not the driving factor in Guard House. In this case, the flow is entirely conveyed by the surface network between ponds. The special care that had to be taken in this case, was to try and minimise the influence on results of the initial depth assumed in the SIPSON model . For that, the weir crests of the surface channels to ponds were raised by the minimum depth of each respective channel to prevent an earlier fill-up of the ponds. Moreover, when the surface results were used to generate the flood inundation maps, they were only displayed once the depths were greater than the original minimum depths of each channel.

5.3.4 IRG Examples

Figure 5.24 shows the cross-section of four selected surface pathways. Figure 5.25 shows the resulting hydraulic radius (Hr) with and without the use of the IRG, with the horizontal axis as the 150 units in which the vertical cross-section is divided.

5.3.5 Calibration LSB Vs DOF

LSB and DOF parameters. The DOF and LSB parameters are set with the same values as in the previous case study (section5.2.5), except for the interval of uncertainty

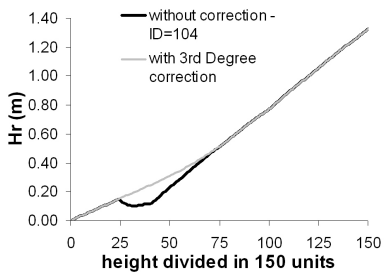

(a) Surface pathway with ID 104.

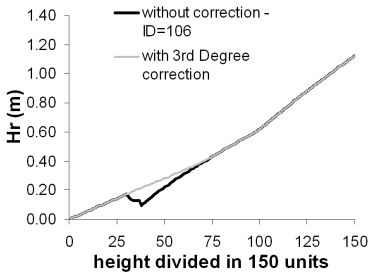

(b) Surface pathway with ID 106.

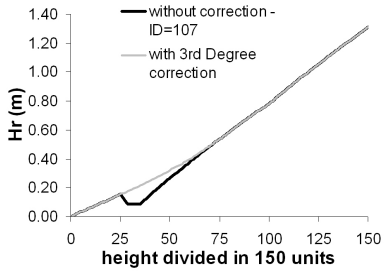

(c) Surface pathway with ID 107.

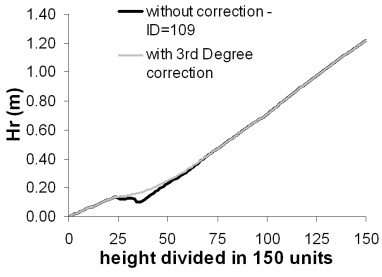

(d) Surface pathway with ID 109.

Figure 5.25: Four corrected Hydraulic Radius curves from the Guard House School 1D surface network.

and the grid length $\overline{\lambda}_k$:

- The $\overline{\lambda}_k \rightarrow \left\{ f_k^j > 6000, \overline{\lambda}_k = 0.3 \; ; f_k^j > 3600, \overline{\lambda}_k = 0.2; f_k^j < 3600, \overline{\lambda}_k = 0.01; \right.$
- Interval of uncertainty $\alpha_k^j \in [0.01; 10.0]$;

The interval of uncertainty is instead constrained by $lb = 0.01$ and $ub = 10$. This case study showed larger differences in the behaviour of both models, namely with some manholes inlets working in one model and not working in the other. In a real case this could represent an inlet blockage, reducing considerably the inlet capacity of a given manhole or a displacement of the manhole cover which would have the reverse effect. Therefore in this case study the ub constraint is set to a higher value (10), and the lb constraint is set with a value closer to 0.

The grid length used herein gave better results than the one used on the previous case study, hence its use.

LSB Vs DOF results. As in the previous case study four runs were set-up with four different initial values of the control variables. Table 5.3 summarises the comparison results on the optimum value and the number of iterations to obtain it by each calibration algorithm. Table 5.4 summarises the Neq_j obtained by each calibration algorithm, and the average $\bar{x}$ and standard deviation δ of the LSB and the DOF. The tables show the

Alg.	LBS	DOF	LBS	DOF	LBS	DOF	LBS	DOF
I.guess	1	1	2	2	3	3	4	4
f_k^j	13899	13749	13670	13619	13576	13636	13491	13550
iter.	147	149	148	150	150	150	150	147

Table 5.3: Summary of the comparison between the calibration algorithms LSB vs. DOF as a function of the number of iterations (iter.) to obtain the optimum value f_k^j,and the initial guess (I.guess).

Alg.	10	11	14	15	16	69	109	116	117	119	121
LBS(1)	2.42	0.90	-	-	2.44	2.44	-	0.01	0.01	0.02	-
DOF(1)	2.42	0.89	-	-	2.68	2.68	-	0.90	0.01	0.04	-
LBS(2)	3.45	1.79	-	-	3.45	3.39	-	0.01	0.01	0.02	-
DOF(2)	3.43	1.77	-	-	3.43	3.39	-	1.20	0.01	0.03	-
LBS(3)	4.47	2.99	-	-	4.47	3.41	-	0.01	0.01	0.03	-
DOF(3)	4.14	2.97	-	-	4.14	3.40	-	1.00	0.01	0.03	-
LBS(4)	5.47	3.99	-	-	5.47	2.95	-	0.01	0.01	0.02	-
DOF(4)	5.11	4.31	-	-	5.11	3.10	-	1.10	0.01	0.02	-
$\bar{x}_{LSB}$	3.95	2.42	-	-	3.96	3.05	-	0.01	0.01	0.02	-
$\bar{x}_{DOF}$	3.77	2.49	-	-	3.84	3.14	-	1.05	0.01	0.03	-
δ_{LSB}	1.31	1.35	-	-	1.31	0.46	-	0.00	0.00	0.01	-
δ_{DOF}	1.14	1.49	-	-	1.04	0.34	-	0.13	0.00	0.01	-

Table 5.4: Summary of the Neq_j obtained in each run of both calibration algorithms (identified by the UPsID), and the average $\bar{x}$ and standard deviation δ of the LSB and the DOF results

number of the upstream manhole IDs (UPsID) of each of the ten Neq_j. The Neq_js with UPsID equal to 14, 15 and 109 have "0" flow hence they are kept unchanged. The Neq_j with UPsID equal to 121, has "0" flow only on the 1D/2D model because the water does not reach this node on this model, however in the 1D/1D it works as a flow-sink hence it is set to "0" flow. By reducing the number of Neq_js which do not contribute to the overall improvement, the algorithms' efficiency is improved.

The next set of plots compare the results from both algorithms, using the example case with an initial guess equal to 3 for that purpose. Figure 5.27(a) shows a plot of the objective function f_k^j as a function of the k^{th} iteration. Figure 5.27(b) shows the control/decision variables Neq_j in a polar graph, for the first 35 iterations.

The Ccm grid can be plotted either with its values in a matrix as function of the

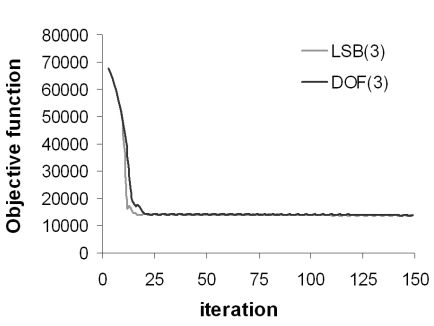

(a) Objective function $f_k = \sum f_k^j$ comparison.

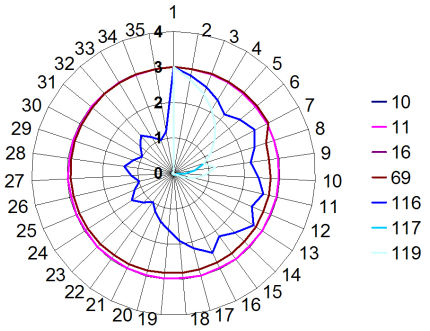

(b) Polar graph of the control variables α_k^j (number of equivalent elements Neq_j) identified by the UPsID (DOF algorithm).

Figure 5.26: Calibration outputs of the objective function and control variables.

k^{th} iteration (this is more suitable for a video animation), or alternatively it can be split individually into each of the eight control-variables working, and the correlation values plotted as a function of the k^{th} iteration, as in Figure 5.27. Note that UPsID equal to 14, 15, 109 and 121 do not display any values because the flow is 0 in the 1D/2D model.

5.3.6 MLE Before and After Calibration

Figures 5.28 and 5.29 show the 7 working MLEs discharge flow rates before and after calibration.

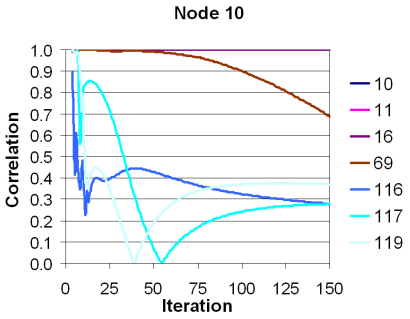

(a) Ccm with UPsID 10.

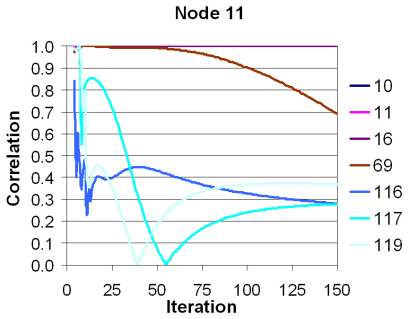

(b) Ccm with UPsID 11.

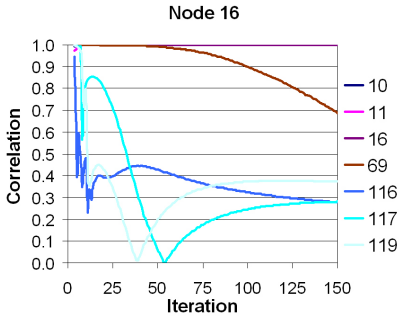

(c) Ccm with UPsID 16.

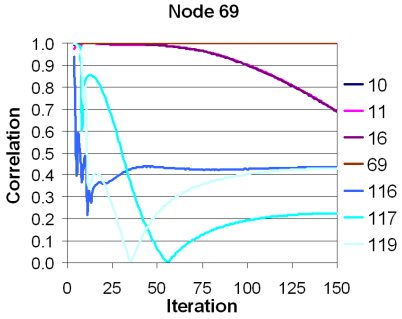

(d) Ccm with UPsID 69.

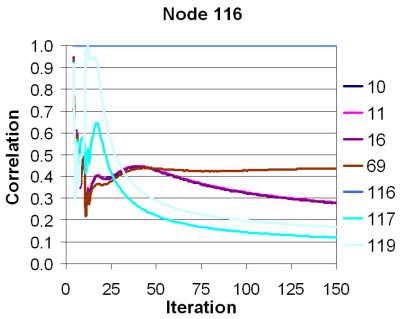

(e) Ccm with UPsID 116.

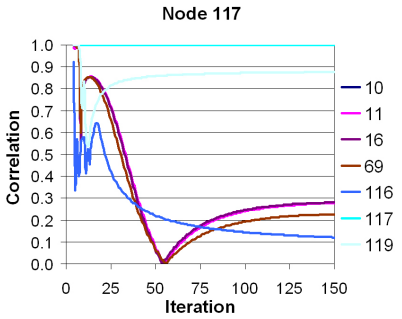

(f) Ccm with UPsID 117.

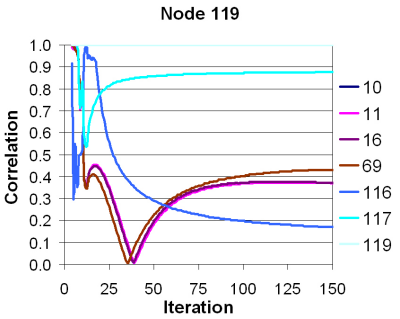

(g) Ccm with UPsID 119.

Figure 5.27: Cross-correlation matrix values for each control variable.

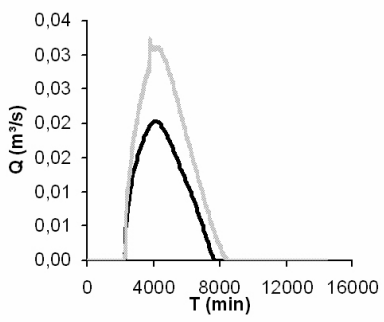

(a) UpsID 10 before calibration.

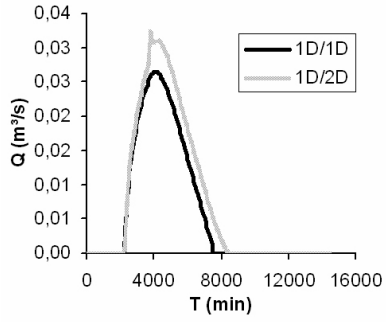

(b) UpsID 10 after calibration.

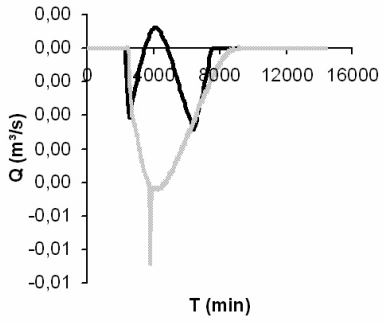

(c) UpsID 11 before calibration.

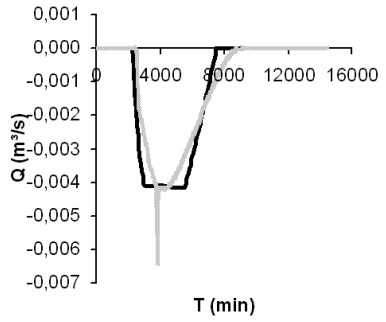

(d) UpsID 11 after calibration.

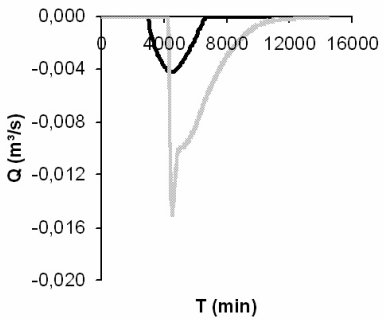

(e) UpsID 16 before calibration.

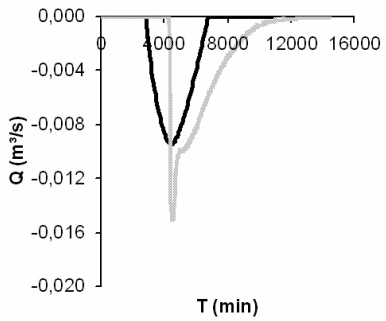

(f) UpsID 16 after calibration.

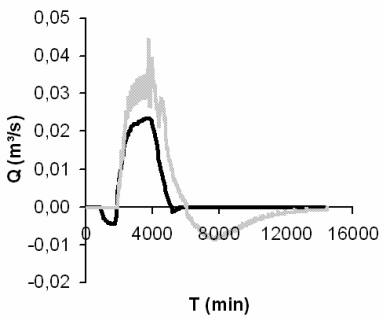

(g) UpsID 69 before calibration.

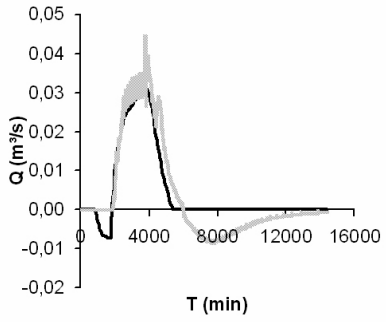

(h) UpsID 69 after calibration.

Figure 5.28: First four MLE discharge flow rates before and after calibration, from the Guard House School 1D surface network.

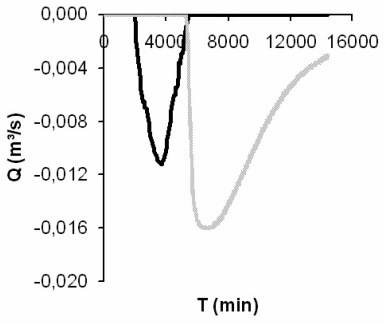

(a) UpsID 116 before calibration.

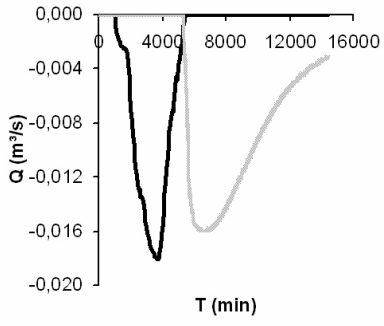

(b) UpsID 116 after calibration.

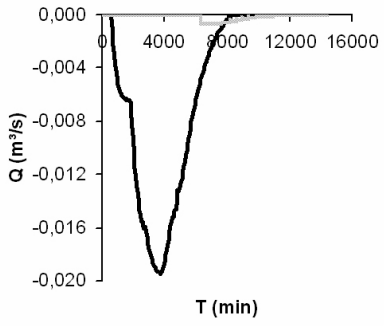

(c) UpsID 117 before calibration.

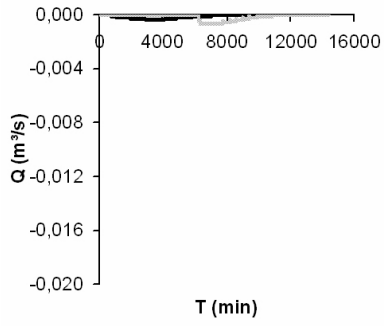

(d) UpsID 117 after calibration.

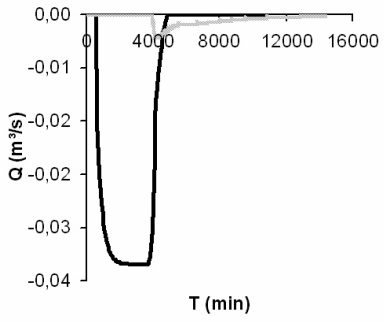

(e) UpsID 119 before calibration.

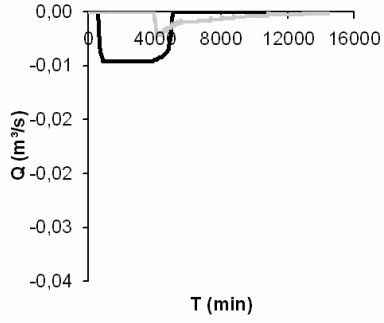

(f) UpsID 119 after calibration.

Figure 5.29: Last three MLE discharge flow rates before and after calibration, from the Guard House School 1D surface network.

5.3.7 Maps of Flood Inundation Extents

With the Visualization algorithm developed in section 4.1.3 it is possible to obtain the urban flood-inundation-extents in the Guard House School case study. Figure 5.30 shows the maximum flood-inundation-extents obtained with the 1D/1D and the 1D/2D models, for the event used for calibration.

Figures 5.31 and 5.32 show the flood inundation-extents obtained with the 1D/1D and 1D/2D models, for a 150 and 100 year return period.

5.3.8 Models Comparison

1^{st} **method - Time dependent.** Figure 5.30 shows the pond at the Northeast side of the school being flooded by surface flow coming along Braithwaite Avenue into Braithwaite Grove and then into the driveway to the boiler house. That pathway and pond are selected for comparing the surface flow propagation and water levels between both models.

Figure 5.33 shows the comparison of water levels and time of peak flows (of the 1D/1D and the 1D/2D models) at several points along the surface pathways, while Figure 5.34 shows three ponds located near the Guard House School Northeast side. The top section shows the results as described in section 4.4.3. The bottom section of the figure shows the geographic location of the nodes.

Figure 5.34(a) shows the water levels at nodes 12006, 12019, 10027 and 10008. The time to peak is well captured as well as the general shape of the water level profiles. The peak height, however, shows large differences. Although both the flooding pathway (Figure 5.30) and the timing of flood propagation are well identified, the 1D/2D model shows much smaller water depths when compared with the 1D/1D model. A possible explanation, lies in the need to consider an initial depth in the 1D/1D model whereas in the 1D/2D model this is not necessary. Because the water depths are indeed small, the initial depth considered becomes more visible, resulting in an overshoot of the water depths in the 1D/1D model (waves travelling faster).

Figure 5.34(a) shows the water levels at ponds 10316, 10314 and 10047. A lagging on the time of peak on the 1D/2D is visible. The water level peak difference is larger than in the previous nodes. Looking at the flood-inundation-extents in Figure 5.30, both models agree in location of the ponds, however they disagree in the magnitude of the water depths. The difference in time of peak can be explained looking at the difference in water depths observed earlier on the pathways. The greater the depth the faster propagations travel on the surface, i.e. celerity, hence in the 1D/1D model the flood propagation seems to travel faster than the 1D/2D model. Moreover we also need to consider the added

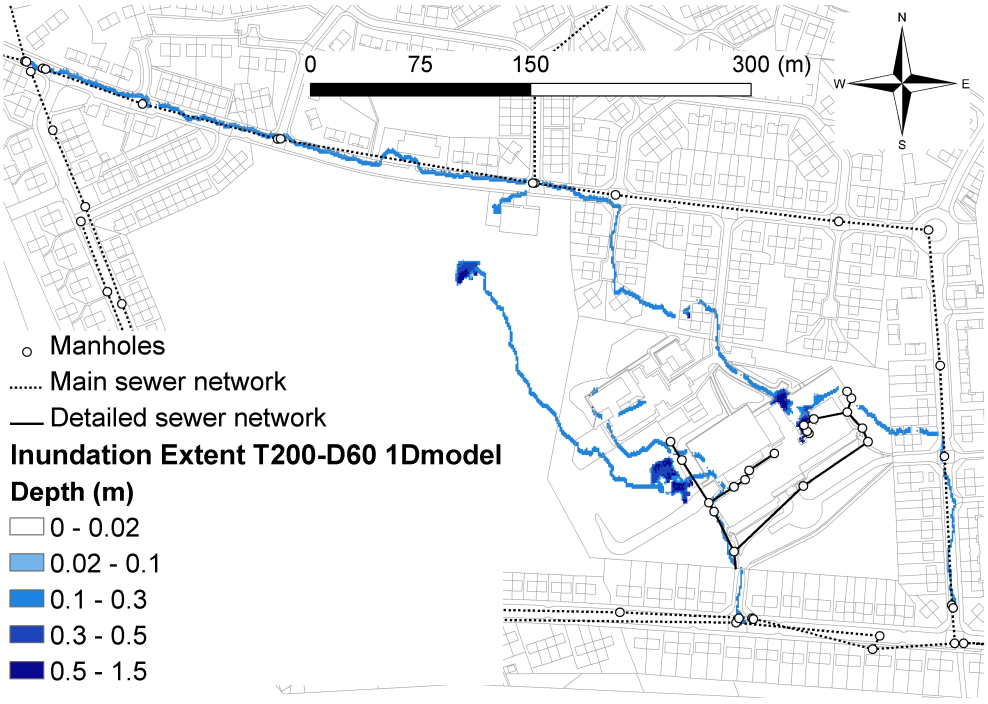

(a) Obtained with the 1D/1D model.

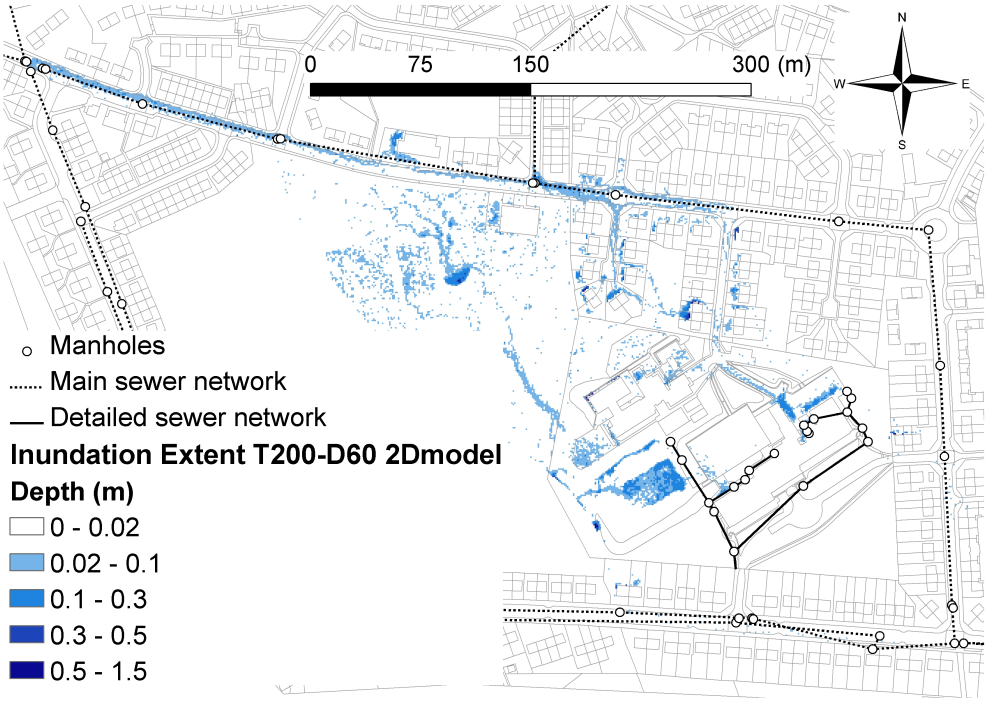

(b) Obtained with the 1D/2D model.

Figure 5.30: Guard House School, maximum flood inundation extents for a 200 year return period event with 60 minutes duration.

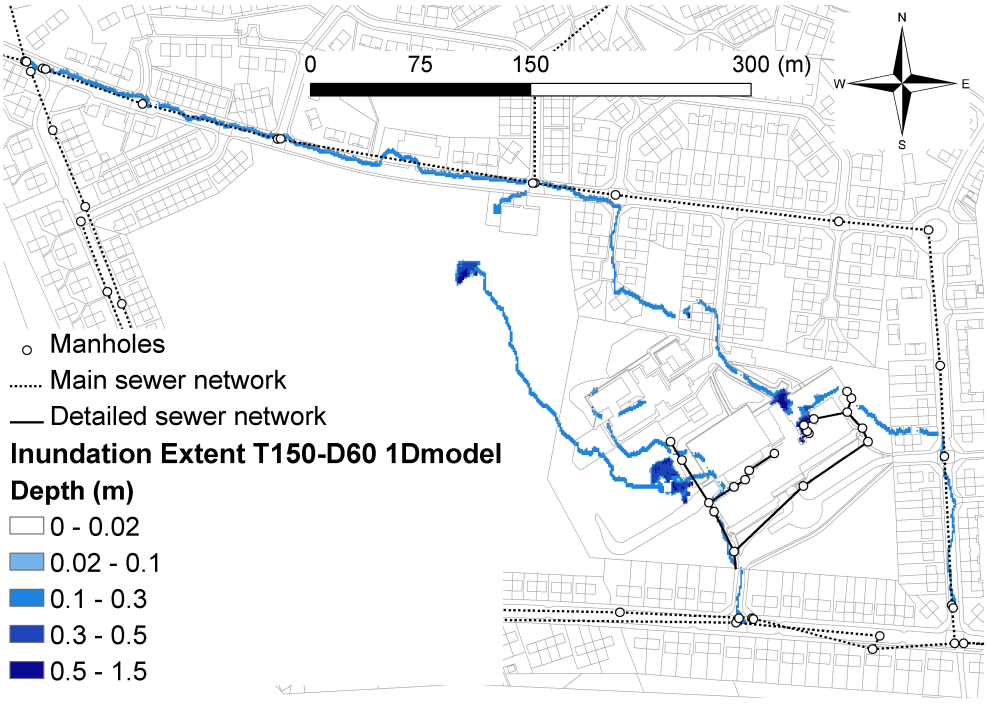

(a) Obtained with the 1D/1D model.

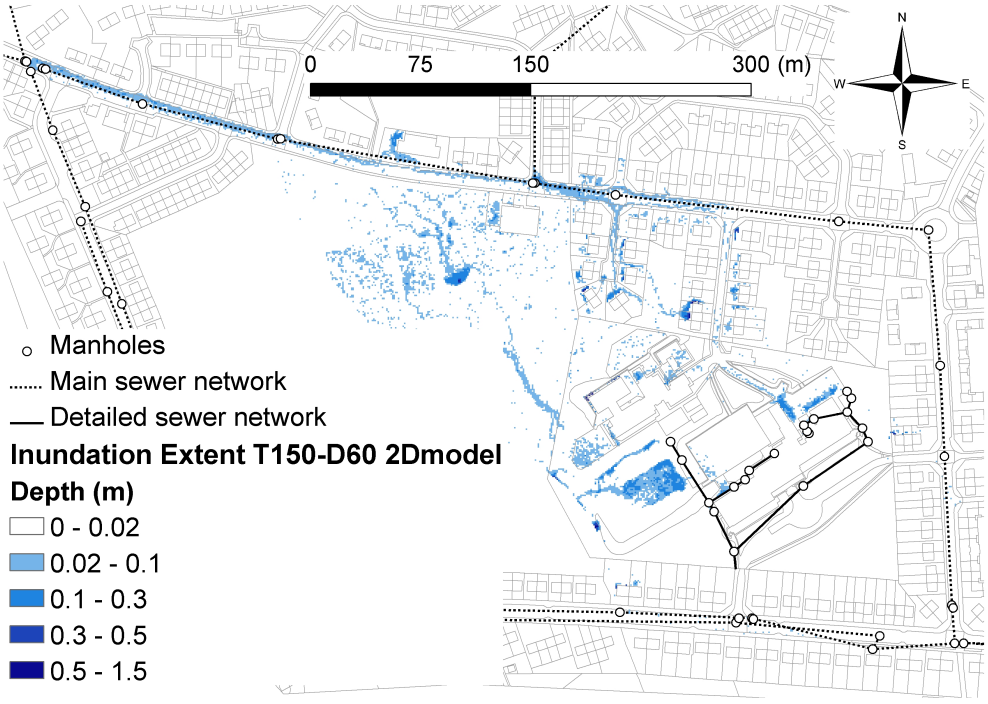

(b) Obtained with the 1D/2D model.

Figure 5.31: Guard House School, maximum flood inundation extents for a 150 year return period event with 60 minutes duration.

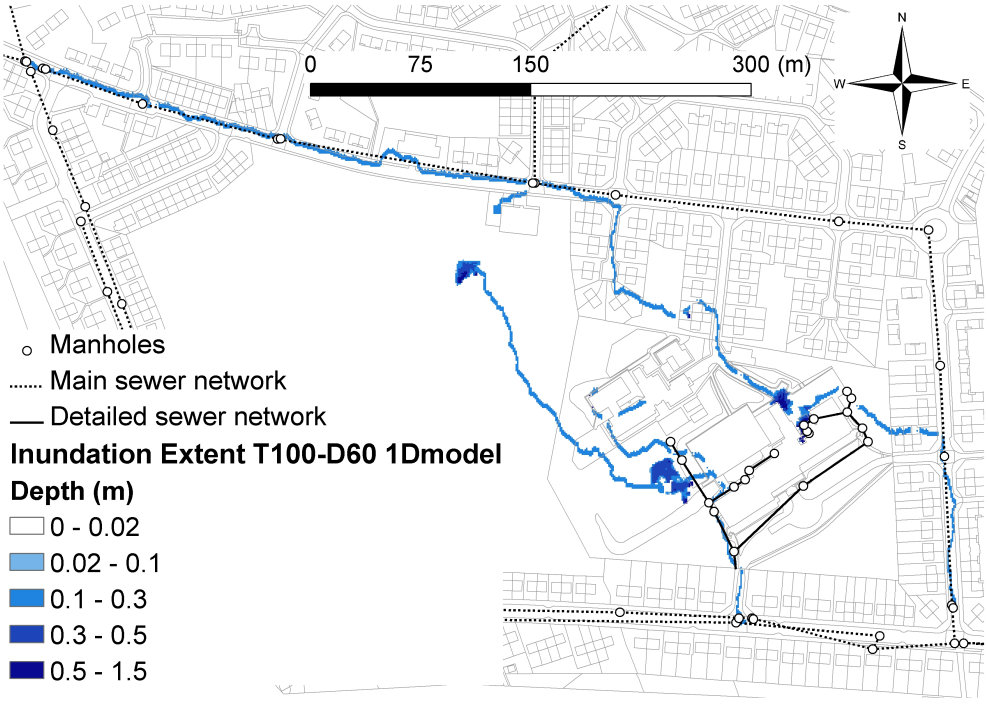

(a) Obtained with the 1D/1D model.

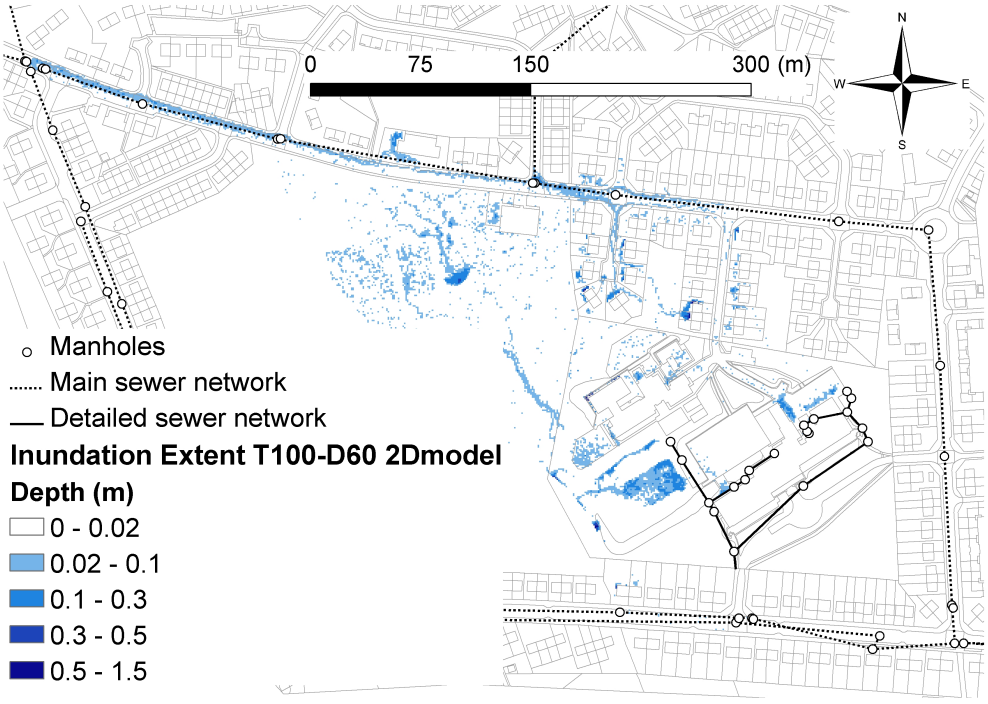

(b) Obtained with the 1D/2D model.

Figure 5.32: Guard House School, maximum flood inundation extents for a 100 year return period event with 60 minutes duration.

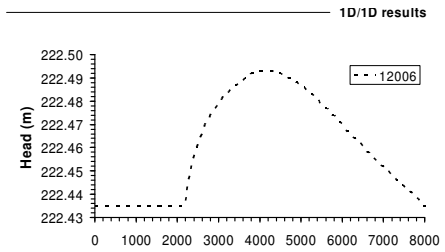

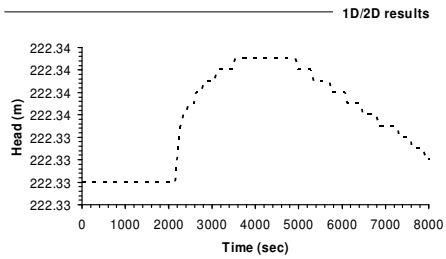

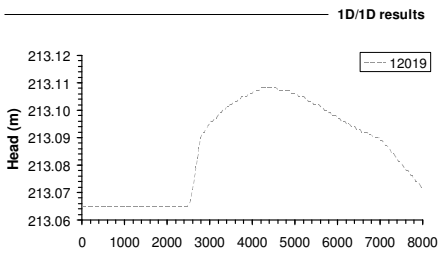

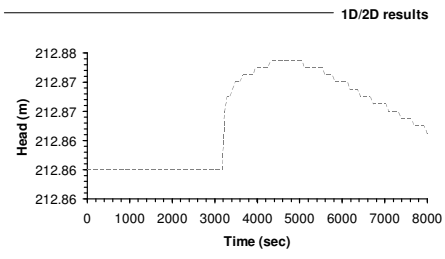

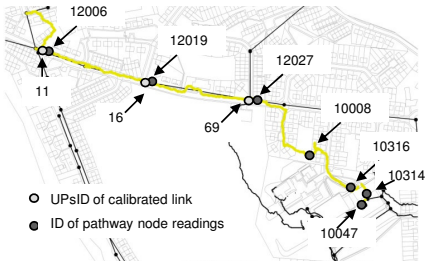

(a) 1D/1D and 1D/2D model results at the Braithwaite Avenue.

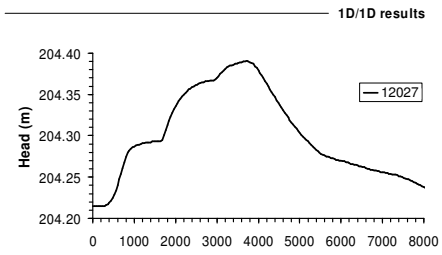

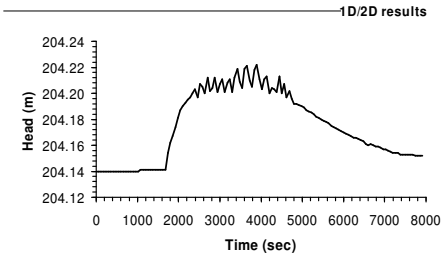

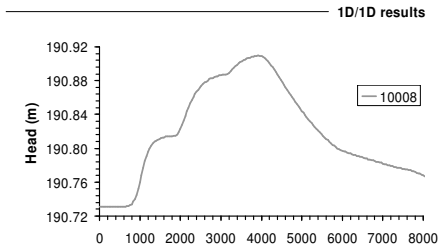

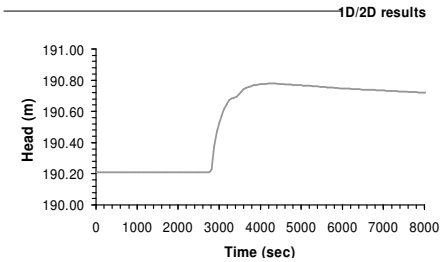

Data compare

ID	12006	12019	12027	10008
Legend	.....	- - - -	- - - -	———
Peak difference (m)				
1D/1D-1D/2D	0.152	0.233	0.169	0.132
Time of peak (sec)				
1D/1D	3920	4200	3720	3920
1D/2D	3540	4320	3900	4200
1D/1D - 1D/2D	380	-120	-180	-280
Filling sequence of ponds (order number)				
1D/1D	3	4	1	2
1D/2D	2	4	1	3

(b) 1D/1D and 1D/2D model results at the Braithwaite Grove.

Figure 5.33: Guard House School, model comparison using the 1^{st} method - Time dependent, along the pathways, for a 200 year return period event with 60 minutes duration.

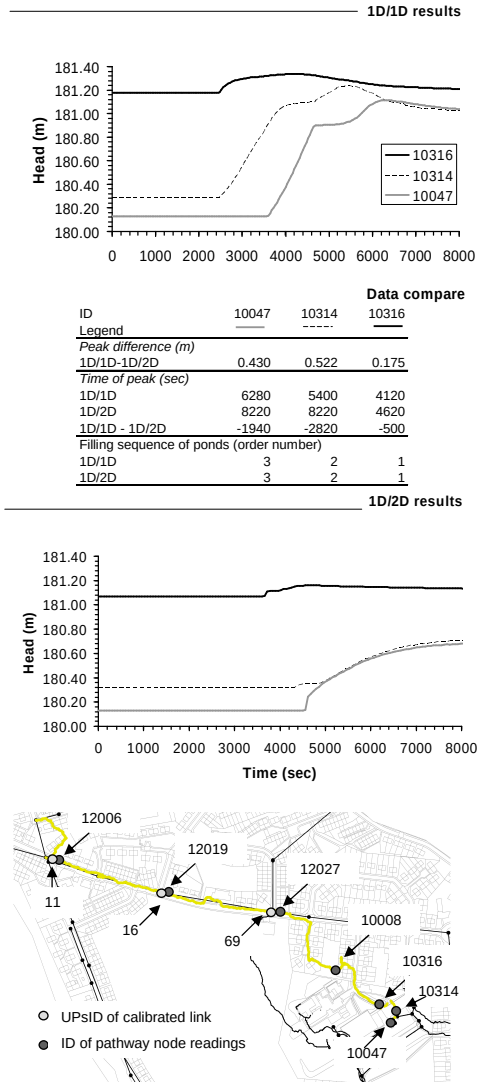

Figure 5.34: Guard House School, model comparison using the 1^{st} method - Time dependent, near the boiler house, for a 200 year return period event with 60 minutes duration.

effect of the 2D model non-inertial based model as mentioned at the end of paragraph 5.2.8. Finally the overall effect of filling up of smaller ponds in the 2D model, seems to contribute not only to the time delay but also to the damping of the peak, since the water is seen stored along the pathways of the 2D grid and not reaching the ponds near the boiler house (Figure 5.30).

2^{nd} **method - Level of Resolution.** Figure 5.30 shows two flooded areas located at the Northwest and Northeast of the Guard House School, and two main flooded pathways. The first follows Braithwaite Avenue into Braithwaite Grove and then into the driveway to the boiler house. The second follows the overland flow from the hillside at the Northwest of the school.

Figures 5.35 and 5.36 show the results of the comparison of flood inundation-extents

in the 1D/1D and the 1D/2D models, for grid sizes (dx) equal to 1, 2 and 4m, and 10, 12 and 14m. The dx changes only the level-of-resolution and not the grid size in which the simulation results were produced. The flood inundation extent is obtained considering only water depths greater than 0.02m. The colour code is:

- White - both models have water on the grid node;
- Black - only one of the models has water on the grid node;
- Grey - both models are dry on the grid node.

Figure 5.37 shows the level-of-resolution graph considering only water depths greater than 0.02m, and dxs from 1m to 50m. Figure 5.38 shows the 2^{nd} degree polynomials obtained by the level-of-resolution graph considering water depths greater than 0.00, 0.02, 0.04, 0.06, 0.08 and 0.10m, and dxs from 1m to 50m.

The first two figures (5.35 and 5.36) show the visual impact of downgrading the level of resolution on the flood inundation-extents. For each grid size resolution the colour code indicates if the models agree on whether the cells will or will not be partially flooded, with a depth greater than the minimum depth considered. Looking at Figure 5.37, the level of resolution corresponding to $dx = 1m$ (base resolution) has 22% of the total cells flooded agreeing in both models. This initial low percentage indicates some disagreement in both results of the models. The existence of overland flow on the hillside at the Northwest of the school, where the rainfall was directly input on the surface (section 5.3.2- step 4 of the methodology), may explain the low values found for the first elements in the set of grid sizes. The 1D surface network is unable to simulate the runoff on that area, due to the large multiplicity of the 2D surface pathways.

In contrast to the Stockbridge case study, decreasing the level-of-resolution has a strong initial gradient effect on the F. With $dx = 20m$ $F = 43.1\%$, a value greater than the initial value for Stockbridge, and with $dx = 40m$ $F = 58.3\%$, showing a better agreement than for Stockbridge, with the same level-of-resolution. Also as h_{min} increases, the percentage of cells in agreement does not necessarily increase (Figure 5.38). Nonetheless, independently of h_{min}, the percentage of cells in agreement rises strongly as the grid is coarsened. Unlike the Stockbridge area, in Guard House School there is a smaller degree of monotonic behaviour of the polynomial curves. The curves still show a similar behaviour as the dx changes (as mentioned before), however they do not follow a similar pattern as the h_{min} increases.

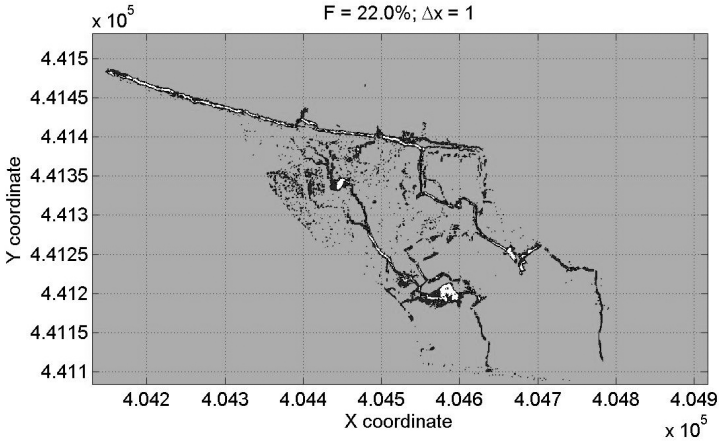

(a) 1D/1D and 1D/2D model results using $dx = 1$.

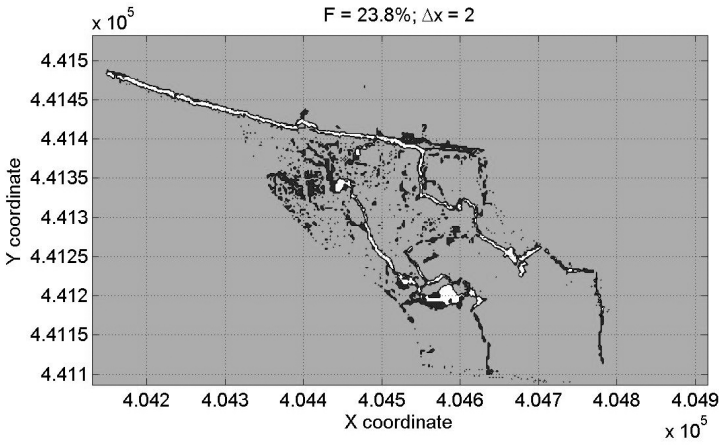

(b) 1D/1D and 1D/2D model results using $dx = 2$.

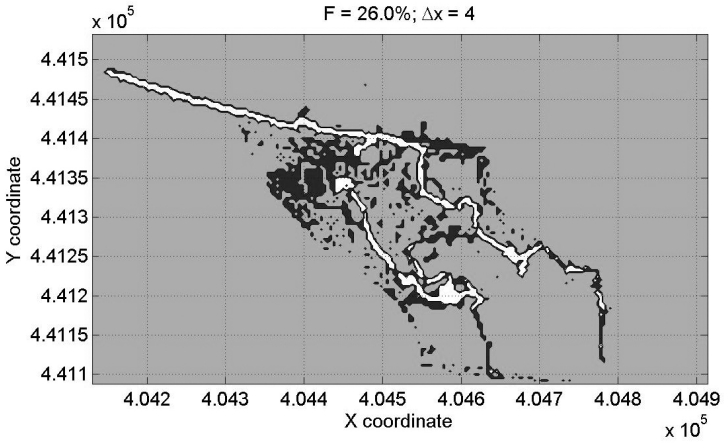

(c) 1D/1D and 1D/2D model results using $dx = 4$.

Figure 5.35: Guard House School, model comparison using the 2^{nd} method - Level-of-Resolution, for dxs equal to 1, 2 and 4, and for a 200 year return period event with 60 minutes duration.

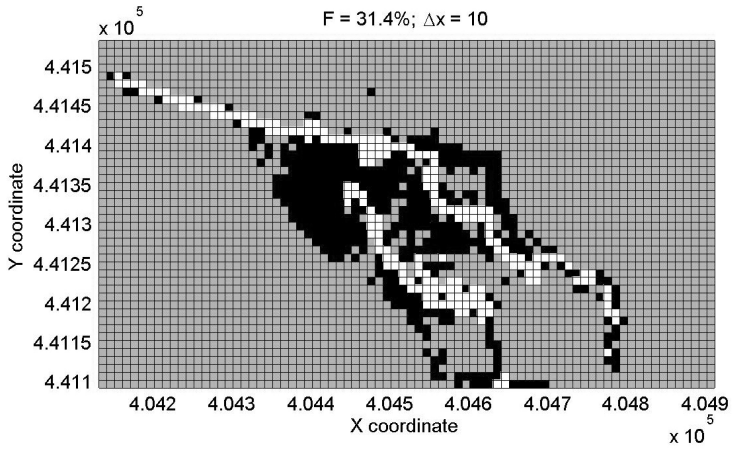

(a) 1D/1D and 1D/2D model results using $dx = 10$.

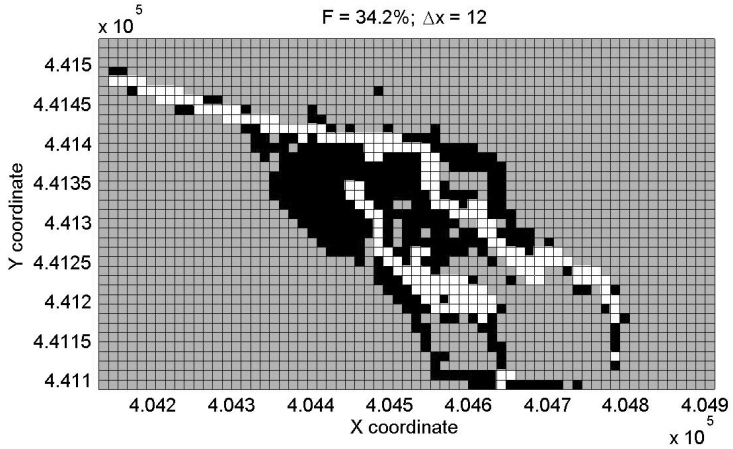

(b) 1D/1D and 1D/2D model results using $dx = 12$.

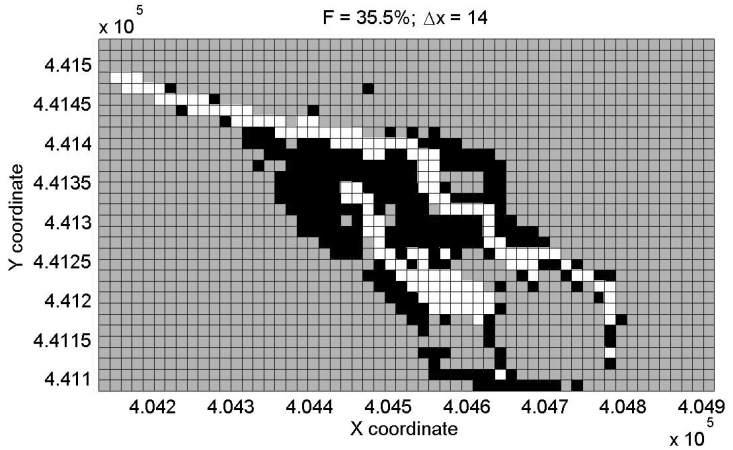

(c) 1D/1D and 1D/2D model results using $dx = 14$.

Figure 5.36: Guard House School, model comparison using the 2^{nd} method - Level-of-Resolution, for dxs equal to 10, 12 and 14, and for a 200 year return period event with 60 minutes duration.

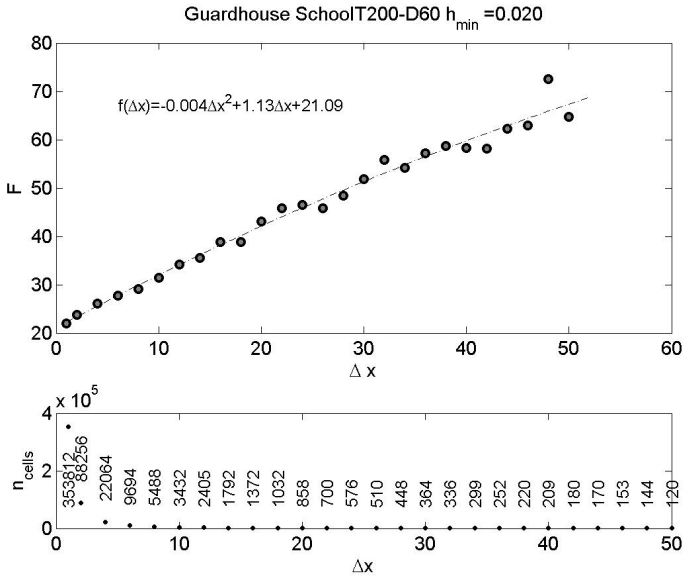

Figure 5.37: Guard House School, level-of-resolution graph for water depths greater than 0.02m.

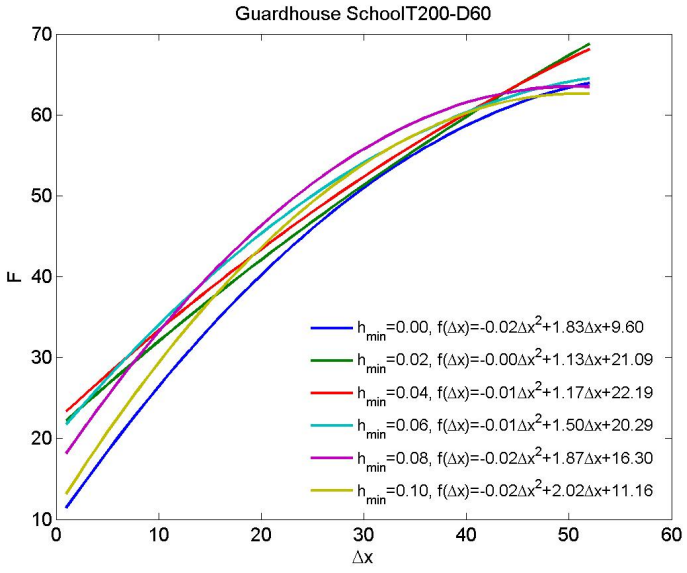

Figure 5.38: Guard House School, level-of-resolution graph for water depths greater than 0.00, 0.02, 0.04, 0.06, 0.08 and 0.10m.

Chapter 6

Discussion and Conclusions

6.1 Introduction

As stated in the first chapter, this Thesis is driven by the need for flood modelling tools able to produce flood-inundation-extents while keeping a good balance between accuracy and computational efficiency. The flood incidents in the UK and across Europe, initiated an immediate reaction from the European Union to try to reduce the hazards to the communities at-risk (clearly stated in the EU directive 2007/60 (European Parliament and Council of The European Union, 2007)). In turn, this Thesis aims to contribute to the response in tackling the flood problem.

To recall, the three major questions when assessing flooding are: Where, when, and to what extent will it flood? Section 6.2.1 discusses the case study results in the light of the above questions, keeping in perspective the hypothesis of this Thesis:

> "The inundation extent of urban flooding can be reproduced by 1D/1D models in good agreement with the 1D/2D models if the results are kept within certain limits of resolution and under certain conditions"

Section 6.3 draws the overall conclusions looking at the previous sections of chapter 4 and the needs that form the motivation of the research question in chapter 3. Section 6.4 presents a summary of the contributions. Section 6.5 concludes this final chapter with the Author recommendations and suggestions for future research.

6.2 Discussion

6.2.1 Case Studies Results

The two selected case studies show two distinctly different types of flooding. Whilst in the Stockbridge area, flooding is mostly due to ponding of water on top of the surcharged

manholes, in the Guardhouse School it is mostly surcharged water carried as overland flow to flood areas further downstream. In both cases, the 1D/1D and the 1D/2D models provided results of flood inundation extents, whereas the level of agreement between both is dependent on the case study considered and on the level of resolution adopted. The results show that urbanized and flatter areas will provide better agreement between models than hillside rural areas with steeper slopes. This is in agreement with other authors' recent results (e.g. Vojinovic and Tutulic, 2008).

The maximum flood inundation extents (Where will it flood?) visually seem to be well identified in both models across the three return periods tested (Figures 5.12 to 5.14 and Figures 5.30 to 5.32). Both 1D/1D features of channels and ponds seem to match with the 1D/2D locations, however, the actual extent might show some differences, particularly in the second case study. Broadly speaking the 1D/1D model gives smaller inundation extents with higher depths when compared to the 1D/2D model. The calibrated event shows visually a better agreement than the other events tested. When the return period considered moves away from the calibrated event the agreement decreases. However one should point out that, as the return period reaches the design event of the sewer system, both models will provide similar results again, simply because the surcharge will then be nil, and a 100 % match will be obtained. This shows that there are always two events bounding the level of agreement: the calibrated event and the no surcharge event. In turn, when judging the return period used for calibration there is compromise to be reached on the purpose of the modelling.

Trying to quantify the question of "How well can 1D/1D reproduce 1D/2D flood inundation maps?" two methods were developed, the Time dependent and the Level of Resolution. The 1^{st} method, allows for comparison of water depths and water flow propagation vs. time. This is one of the advantages of this method over the second; it shows how both models behave in terms of rates of rising water and water flow (When will it flood?). The flood information is given at predefined pin-point locations on the grid. The method highlights the good agreement between models in the first case study, in both water depths and water flow propagation (Figure 5.15). It also made possible the earlier detection of schematization errors and the definition of modelling details to improve the surface flow simulation (section 5.2.3). The influence of the base flow is seen to influence the results of the 1D/1D in the second case study (5.34), however this should become less significant as the surcharge flow increases or if the base flow is reduced.

The 2^{nd} method, complements the first method, in the way that it allows for answering the question: "To what extent will it flood?". It also gives a better answer to "Where?", however it does not state "When?". Unlike the previous method, this one is

unable to judge on the 1D/1D model predictability (over time) to detect schematization errors (hence help with the definition of modelling details). Looking at the maximum flood inundation extents, the method highlighted (and quantified) the better agreement between models in the first case study (Figure 5.18) than in the second case study (Figure 5.37). The worst performance in the second case study, could be explained by the non-urbanized hillside area on the Northwest side (Figures 5.35), which clearly accounts for a large portion of the measure of fit F. However, coarsening the grid increases the level of agreement, although at different rates as discussed in sections 5.2.8 and 5.3.8. More important, is the ability of this method, for enabling urban flood managers to define the minimum level-of-resolution (grid size) required and depending on the F, to decide if the 1D/1D model (or the 1D/2D, if comparison is done against real data) can or cannot be used in a particular case study. It must be re-emphasized that this method only changes the resolution in which we analyse the results, whilst keeping the fine grid in which they were firstly produced. Therefore, it would be wrong to attribute the effect of smearing topographical-features due to the decreasing of the grid size to this method.

6.2.2 Validation of the Comparison

The application of the methodology developed in section 4.4.2 assures the validation of the comparison. The methodology allows for producing a surface 1D network equivalent (steps 1 to 3) to the 2D grid (Figures 5.23 and 5.4), with similar external (step 4 - rainfall inputs) and internal (step 5 - calibration) boundary conditions. The results in the Stockbridge area show that the five-step methodology allows the 1D/1D model to identify the main ponds responsible for flooding, while in the Guardhouse School they show that it is possible to identify the main channels responsible for conveying the surface flow. However the latter case shows that the assumptions taken in the fourth step influence the previous ones, namely the definition of the surface network (steps 2 and 3). The assumption of direct input of the rainfall on the sewer manholes, reduces the overall number of surface channels needed on the 1D/1D model. In other words, that assumption helps the definition of the 1D surface network and the overall agreement. Moreover, the hillside area in Guardhouse School shows that, applying the rainfall directly on the surface, creates a large multiplicity of channels which in turn makes it difficult to provide a good agreement (with the 2D model results) using the 1D model schematization (Figure 5.30). Nevertheless, it is also true that most of those "channels" on the 2D model will be working with such small depths that they can be omitted on an urban-flooding context.

The first step in the methodology decides the DEM resolution. The finer grid resolution

of 1 meter used in the Guardhouse School (Figure 5.22) instead of the 2 meter grid used in Stockbridge area (Figure 5.3) has a strong impact on the computational time. The Stockbridge case study takes 60 sec on the 1D/1D model and 3 hours on the 1D/2D model to complete a full run with a duration of 120 minutes. The Guardhouse School case study takes 3 min on the 1D/1D model and 3 days on the 1D/2D model to complete a full run with a duration of 240 minutes.[1] The computational time increase in the second case study is a result of a smaller time step in the 1D/1D model, to account for instabilities, and a smaller grid size (hence also a smaller time step), used for testing the 1D/2D model. Those computational times illustrate the benefit of using the 1D/1D model. Urban flood managers need to take into account the fine balance between accuracy and computational time, when deciding on which model to use.

The benefits of the calibration (fifth step) on the discharges of the surcharged manholes are clear in both the Stockbridge (Figures 5.10 and 5.11) and the Guardhouse School areas (Figures 5.28 and 5.29). The two calibration algorithms (LSB and DOF) achieved a good fit regardless of the initial guess (Tables 5.1 and 5.3). Although in both case studies the LSB obtains the best fit, the DOF outperforms the former in 50 % of the tests. Yet the DOF generally took more runs to achieve the best fit (in the Stockbridge area). Except for the Neq_j with ID 116, 117 and 119 of the second case study, all control/decision variables converge to values within the upper and lower bounds (Tables 5.1 and 5.4). The exceptions had virtually nil 2D discharges, hence the values were fairly close to the lower bounds (Figure 5.29). The Ccm grids illustrate the strong linear correlation between different individual objective functions (Figure 5.9 e.g. nodes 3096, 3006, and Figure 5.27 e.g. nodes 10, 11, 16 and 69), and how these relations change with time as the control variables converge to their final values. The Ccm is responsible for the DOF outperforming the LSB in 50% of the tests.

The results obtained after calibration support the choice made of (1) the calibrated parameter and (2) the variable optimized. The parameter chosen for calibration (decision variable) has a strong influence on the discharge curves obtained and allowed for improving the agreement of the internal boundary conditions from both coupled models. Similarly, in the case of real data this calibration parameter will allow for defining the number of equivalent elements working in each manhole, hence be closer to the reality.

A remark must be made on the ground-truthing technique. Hankin et al. (2008) recognizes that some level of ground-truthing has to be applied to the DEM in order to ensure that the flow on the pathways is correctly represented. However, there is no information on the degree of ground-truthing to be applied. In this Thesis, the lack of

[1] The computational times are for a PC with: Pentium 4, CPU 3.00GHz and 1GB of RAM

information on that technique, combined with the aim of making an unbiased comparison between the two coupled models led the Author to the disregard such technique. The Author of this Thesis agrees that ground-truthing should be used, but is of the opinion that more research needs to be done on that technique before it can be applied meaningfully to the DEM.

6.2.3 Visualisation Tool and Improved SIPSON

The 2D flood inundation maps, obtained with the visualisation tool, are responsible for the fresh look given to the 1D/1D results, while the Improved SIPSON allows to be applied with a wider range when compared to the original SIPSON model. With the visualisation tool the 1D model results can be plotted side by side with the 2D model. The tool allows for plotting ponds and channels with their corresponding depths (see Figures 5.12 to 5.14 and Figures 5.30 to 5.32). The algorithm allows the control of the unrealistic flood representation of using a blind extrapolation of water levels, seen in other works (Vojinovic and Tutulic, 2008) (Figure B.1).

The Improved SIPSON models the linkage between sewer and surface using the Multiple-Linking-Elements (MLE). The MLE adjust the discharge rate depending on the surface and sewer water levels and on the dominant control section (section 4.2.2.2). The stability control included in the MLE and the volume control, reduces the oscillations and instabilities on the 1D, still visible on the 2D elements used for modelling the linking element (Figures 5.10 and 5.11 e.g. node 3079, and Figures 5.28 and 5.29 e.g. 11,16 and 69). The model, calculates the irregular cross-sections with the IRG algorithm. The IRG can deal with highly irregular cross-sections (Figure 5.6 and 5.24). Unwanted drops in the Hydraulic Radius are easily removed (Figure 5.25), even in the case of multiple drops (Figure 5.7).

6.3 Conclusions

6.3.1 Comparison 1D/1D vs. 1D/2D

In this Thesis, a comprehensive comparison between the 1D/1D and the 1D/2D models has been presented. The two models' ability to model surcharged flood flow has been demonstrated by means of comparing water levels and time of peak flows at the lowest point of major ponds (1^{st} Method - Time Dependent) and the flood-inundation-extents (2^{nd} Method - Level of Resolution). However, this Thesis also shows that care has to be taken in the setting up and calibration of the lower order model. A methodology to setup the two equivalent models (subsection 4.4.2) is shown to be essential to assure

a meaningful comparison. The modelling details are necessary for the 1D/1D model to capture the surface flow dynamics (subsections 5.2.3 and 5.3.3). In order to achieve the similarity between boundary conditions in the surface flow throughout the entire simulation (for both 1D/1D and 1D/2D approaches), it was shown that the agreement between the flows discharged from the manholes in both models is imperative (subsection 4.3.5). The two calibration algorithms adopted (subsections 4.3.4 and 4.3.3) were shown to be effective in achieving a good level of agreement, when making use of the MLE potential to control and regulate the flows discharged from the sewer network. The SLE control sections are responsible for allowing the MLE to have such an effect on the discharged flows (subsection 4.2.2.1). The comparison of results between the 1D/1D vs. the 1D/2D model, in the two case studies, showed strong evidence of what the Author considers to be the key factors/recommendations in setting up an accurate 1D/1D model. These can be summarized as:

- The accurate definition of ponds including the volume-depth curves, bottom levels and crest levels;
- The accurate definition of the 1D surface network including, cross-sections, paths and slopes;
- To apply sensible elements for linking the sewer with surface (MLE), and ponds to ponds and ponds to pathways (weirs);
- The definition of 1D/1D modelling details capable of reproducing the 1D/2D results;
- The definition of a minimum grid resolution of 2mx2m of the DEM as a good balance of detail and computational efficiency.

The comparison also allowed for defining the range of application/limitations of the 1D/1D model:

- Better results of the flood propagation on the surface are obtained where the boundaries of the streets and buildings serve as preferential paths;
- Highly urbanized areas produce better results than in rural areas;
- Relatively flat areas having overland slopes with an average of 1% produce good results;
- Worst results are obtained over hillside areas having overland slopes with an average of 6%;

- Better results are obtained in the absence of excessive flood propagation on the surface (and as long as all the ponds are properly identified on the 1D/1D model);
- Better results are obtained when rainfall is input directly on the sewer system.

6.3.2 Improved SIPSON and MLE

This Thesis presented an improved 1D/1D model, whereby the linkage-model was changed to the MLE, a new visualisation tool was developed for plotting the 1D flood-inundation-maps in a 2D view, and an algorithm was presented to deal with irregular-cross-sections in a computationally efficient manner. With these improvements, the 1D/1D model was shown to be able to rival the more accurate 1D/2D model, especially in areas with gentle slopes.

The 2D flood inundation maps, obtained with the visualisation tool, were responsible for the fresh look given to the 1D/1D results, while other improvements allowed for a wider range of the model's applicability. With the visualisation tool, 1D results could be plotted side by side with 2D model results.

The linkage model that connects the sewer and surface was shown to adjust the discharge rate depending on the surface and sewer water levels and on the dominant control section. It was shown to change direction, to be stable and to have fewer oscillations than the equivalent in the 1D/2D model.

In conclusion:

- The visualisation tool is able to produce 2D flood-inundation-maps based on the 1D/1D modelling results;
- The linkage model becomes more stable and with smoother variations when using the MLE;
- The irregular-cross-section algorithm allows for the removal of the unwanted drops on the Hr curves.

6.3.3 Model Calibration

A novel calibration algorithm was presented for urban-flooding 1D/1D coupled-hydraulic-models. The Dynamic-objective-function (DOF) algorithm was based on a Linear-search-based (LSB) algorithm where the objective function was made dynamic, and controlled by a cross-correlation matrix (CCm). When developing the DOF algorithm, the following procedures were taken into account:

- Setting of an interval of uncertainty to avoid unrealistic values of the decision variables;
- Setting of a threshold (Ts) to control the inclusion or exclusion of a neighbouring objective function;
- β parameter for regulating the amount of information used;
- The set of a minimum slope (Ms) to determine the state of convergence of a given objective function;
- θ parameter for keeping track of when the objective function enters or leaves the state of "possible convergence".

When compared, the DOF algorithm was shown to outperform the LBS algorithm in 50 % of test runs though it took longer to reach the set of solutions. The discharge results of the 1D/1D model were greatly improved when compared with the 1D/2D results.

The case studies allowed the following conclusions to be drawn:

- The use of the MLE parameter as the calibration parameter (decision variable), allowed the discharge rates to be controlled throughout the whole model-simulation;
- The selection of the difference of the cumulative volumes discharged between models as the objective function to be minimized, enabled the calibration to retrieve similar discharge-curves from the surcharged manholes in both coupled-models;
- The agreement between coupled-models on the internal-boundary-conditions, in the sewer and surface interfaces is essential to validate/correct the 1D surface-network-model.
- The results suggest a linear relationship between some of the objective functions, validating the DOF algorithm assumption.

6.3.4 Remarks on the calibration role

Calibration must be seen as a part of a model and not as a complement or simply as an add on. To misjudge the role of calibration in flood modelling discredits the model results. Often models are applied with disregard to their underlying assumptions and principles of their use, even though parameters are known to have a great degree of uncertainty. Moreover, they represent a simplified reality that cannot account for the complete set of multiple variables in a real flood event. Calibration helps in minimizing uncertainty by fitting a rather simplified model to a real observed event. It is therefore of paramount

importance to understand where and how to apply them in a successful way. Aiming at comparing the surface flooding results from the 1D/1D and 1D/2D models, it is recognized that not only the surface pathways have to be in agreement with the flow propagation but also the flow discharges should conform. To paraphrase to my own words the comment of Horritt and Bates (2002) on a good model:

> "A good model cannot be defined as such without the agreement of the discharges from the sewer, i.e. the boundary conditions on the interfaces between the sewer network and the ground surface; only then can one validate a surface flow model, otherwise it is but a pointless endeavour."

That is, without the agreement of the volume surcharged from the minor system, it is meaningless to compare the surface flow or to validate the 1D network, without previously calibrating the discharge hydrographs of the surcharged manholes. This statement should hold for other types of coupled models whenever real data or results from a more accurate model exist.

6.3.5 Research question

The Author believes that the needs highlighted in section 3 have been successfully fulfilled:

1. The need for effective 1D/1D vs. 1D/2D model comparison has been achieved by: First developing a methodology to enable a valid comparison between the two models, and secondly with the use of two methods for comparing the surface flow results (section 4.4). The 1^{st} Method - Time Dependent, compares water depth profiles and water flow propagation. The 2^{st} Method - Level of Resolution, compares flood-inundation-extents and improves the agreement between models based on the level of resolution (grid size). The 1D/1D model is computationally much faster than the 1D/2D model.

2. The need for better visualization of 1D/1D results has been achieved by: The development of the 1D/1D visualisation tool (section 4.1.3). The fresh look at the 1D/1D model flood-inundations-extents, overcame the unrealistic maps previously seen in other works.

3. The need for a better linking element has been achieved by: The Multiple-Linking-Element (section 4.2). A methodical and systematic approach was applied which gave credibility and recognition to the MLE. The linking element is based on a typical manhole connection between the sewer and the surface.

4. The need for calibration led to the development of the Dynamic-Objective-Function algorithm (section 4.3). The faster 1D/1D model enabled the development of an effective algorithm for calibration, proving one of the strengths of the 1D/1D over the 1D/2D. Two important questions were answered: (1) Which parameters to calibrate? (2) Which variables to optimise? (Section 4.3.5). It was concluded that, without the agreement of the volume surcharged from the minor system (i.e. without previously calibrating the discharge hydrographs of the surcharged manholes) it is meaningless to do a surface flow comparison or a 1D network validation.

5. The improved 1D/1D model showed enhanced stability. This was achieved with the implementation of the MLE (section 4.2.2.4) and the volume control (section 4.1.5) as shown in the MLE results (sections 5.2.6 and 5.3.6, and the IRG algorithm 4.1.2 with the removal of the unwanted drops in the hydraulic radius curves.

6. The need for an algorithm to deal with irregular cross-sections in 1D model, was achieved with the development of the IRG algorithm 4.1.2.

6.4 Summary of Contributions

This section summarises the list of the Author's contributions:

- A methodology for setting up two equivalent 1D/1D and 1D/2D models and two methods for comparison: the Time-Dependent and the Level-of-Resolution.
- An innovative GIS technique for generating flood-inundation-maps from the 1D/1D model results combined with the DEM.
- A theoretical linkage-model of the interaction between the sewer system and the surface system: the Multiple-Linking-Element.
- A novel calibration algorithm to calibrate the 1D/1D with the 1D/2D model results: the Dynamic-Objective-Function.
- An improved 1D/1D model, in terms of increased model stability and wider range of application.

6.5 Future Research

Two main areas of future research can be identified. The first builds on improving the work presented herein, and the second is a natural extension of what could be the next stage.

The first one concerns the validation of the linkage-model, MLE, with either laboratory study or computational fluid dynamics (CFD) simulations. Discharge coefficients of the MLE could be calibrated, and a more accurate and precise element for linking sewer with surface networks would be obtained. This work is of great interest to both academia and the industry. Work on the FRMRC phase 2 has just started to study the behaviour of the manhole connections with both CFD simulations and experimental testing in a laboratory rig. The Author would like to believe that the work developed and presented in this Thesis has influenced the decision to take the 2^{nd} phase of the FRMRC in that direction.

The 2^{nd} method used for comparison could be extended to include velocity. The 1D/1D model can only provide velocity in channels and pipes, but not in ponds. Therefore, the assumptions would need to be set-up carefully to extrapolate the 1D velocity field.

Looking at the DOF, further research can be envisaged:

1. The use of variable-step-lengths based on the stored information of the objective functions, where the gradients of the objective function could be determined on previous values by using polynomial regression;

2. The possible use of different statistical parameters to measure the relationship between the sets of variables;

3. The testing of different objective functions (e.g. the mean square error).

Those experiments could benefit the performance of the DOF algorithm.

The second area looks at open future research questions. These can be seen as a list of questions that are still without a clear answer and that definitely deserve to be studied:

1. What type of models should be preferred for modelling the two layers overland/sewer?

2. How can the MLE be extended to 2D models?

3. What level of accuracy is required in both layers?

4. How to develop faster numerical schemes without compromising accuracy?

5. What is the level of resolution required for DEM driven models?

6. How should the damage and risk due to flooding be quantified?

7. How can our hydraulic models help reduce the risk of flooding (Flood evacuation plans)?

8. In the case of flood warning: What kind of data should be provided and when (Pitt, 2008)?

There are three points the Author would like to raise.

Firstly the importance of extending the MLE to 2D models. Currently the link between 1D/2D models is still based on the out-dated concepts described in the literature review. The MLE may be brought into the 2D models but some assumptions will have to be introduced. One possibility would be to use the potential flow theory. It might be interesting to think of the flow around a gutter as a sink or a source as in the theory of potential flow.

Secondly the quantification of flood risk using flood damage curves. Currently flood damage curves are independent of time. This assumption is unrealistic since the duration of flooding is not taken into account. One possibility would be to consider a time lag for the full damage cost to be obtained. An "S" shape curve could be used to delay reaching that full cost.

Thirdly and final point, the need for faster and accurate models. Currently 2D models are an accurate but rather slow tool, whereas 1D models are faster but need the surface network to be carefully defined. The promising 2D cell models could be an attractive tool to overcome the issues of accuracy, computational effort and surface delineation. One possibility would be the use of control rules to convey flow over a grid. This could prove fast enough but there are some doubts as to how accurate the results would be.

Appendix A

Flood-inundation-extents Appendix

This appendix presents some examples of flood-inundation-extents using the 1D/1D model for different return periods and considering the influence of the river and of having a flap valve at the outlet (Figure A.3(a)). Case (c.1) with flap valve and the influence of the river (Figure A.3(b)), and case (c.2) without flap valve without influence from the river (Figure A.4(a)) and with influence from the river (Figure A.4(b)). Each flood-inundation-extent is identified by "M-returnperiod(years)-D-duration(min)-riverlevel". Riverlevel=1 identifies a low river level (1y return period = 80m), riverlevel=2 (25y return period = 84.86m), riverlevel=3 (50y return period = 85.06m), riverlevel=4 (100y return period = 85.24m) riverlevel=5 identifies the high river level (200y return period = 85.45m). Figure A.1 summarises the total number of flood-inundation-extents simulated with the 1D/1D model.

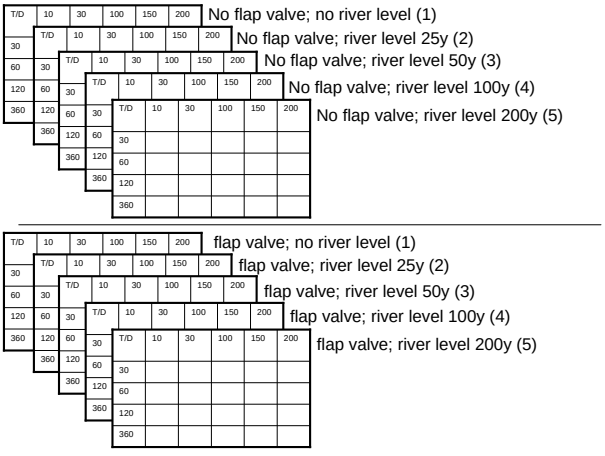

Figure A.1: Matrix of events run with the 1D/1D model.

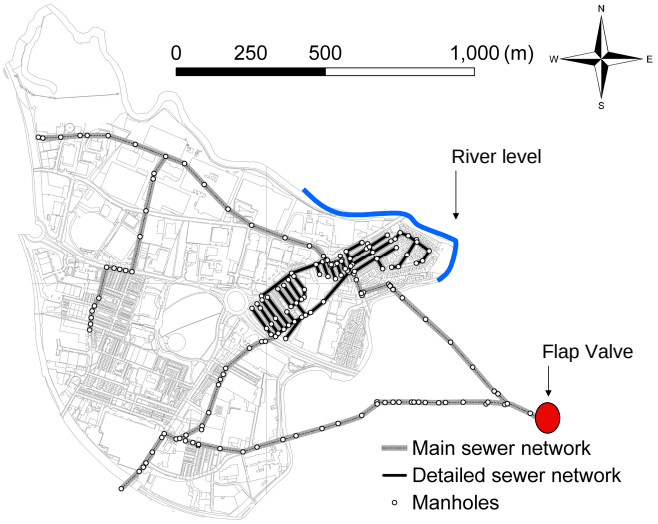

(a) The two types of events considered: River Level and Flap Valve.

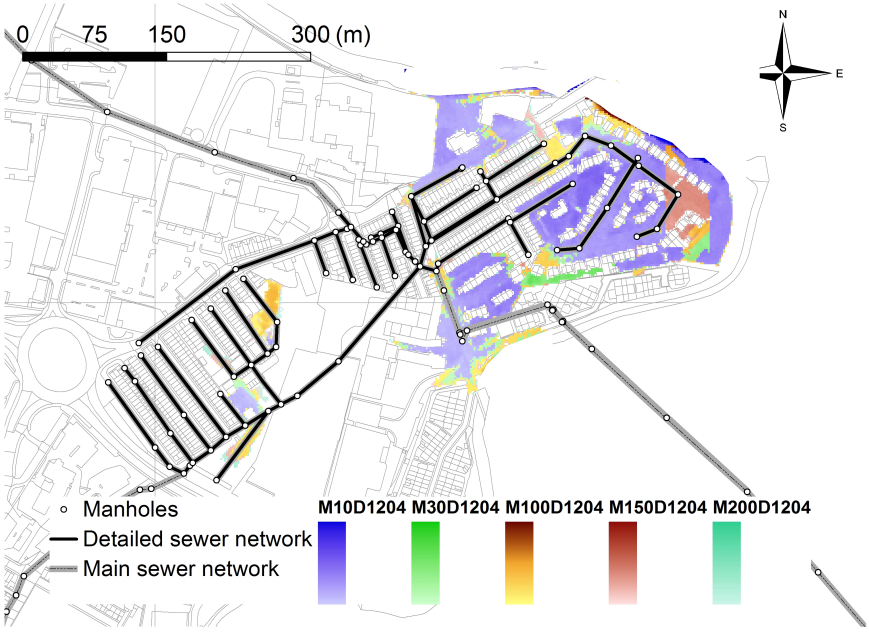

(b) Obtained with the 1D/1D model considering the influence of the river level.

Figure A.2: Stockbridge area, maximum flood inundation extents for studying the influence of the river level with flap valve - c.1.

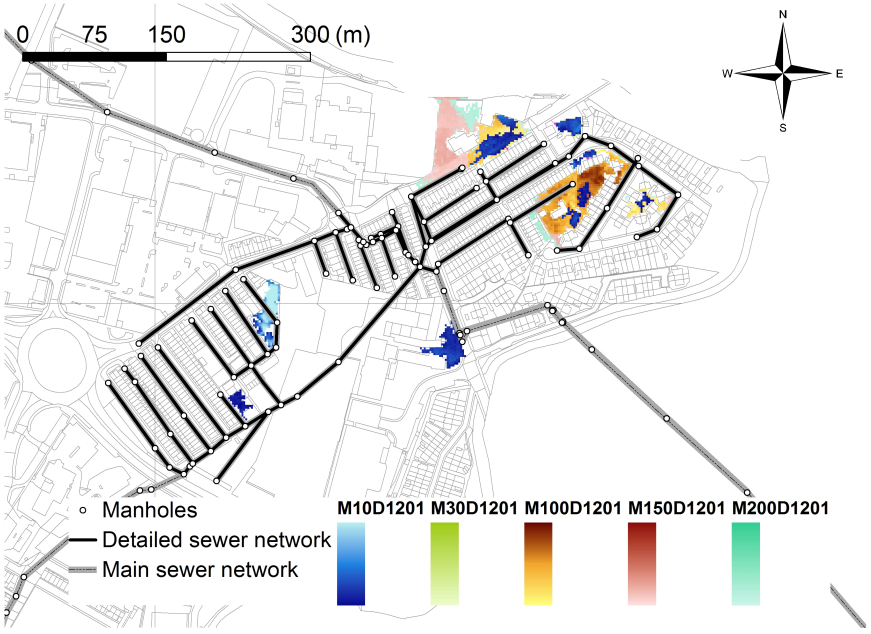

(a) Obtained with the 1D/1D model without considering the influence of the river level.

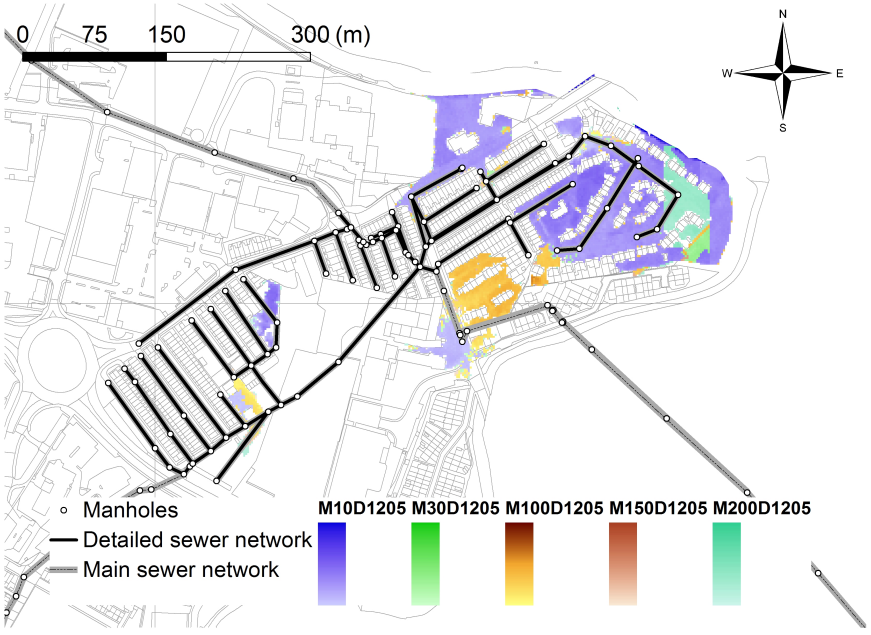

(b) Obtained with the 1D/1D model considering the influence of the river level.

Figure A.3: Stockbridge area, maximum flood inundation extents for studying the influence of the river level without flap valve - c.2.

Appendix B

Visualisation Appendix

This appendix intends to illustrate unrealistic procedures for producing flood-inundation extents using 1D models. The first is a blind extrapolation of water levels in the Guardhouse School case study. The steeper slopes in the second case study makes this area the perfect candidate for exaggerating the unrealistic results of blind extrapolation of the water levels. The same event used for calibration is presented in Figure B.1.

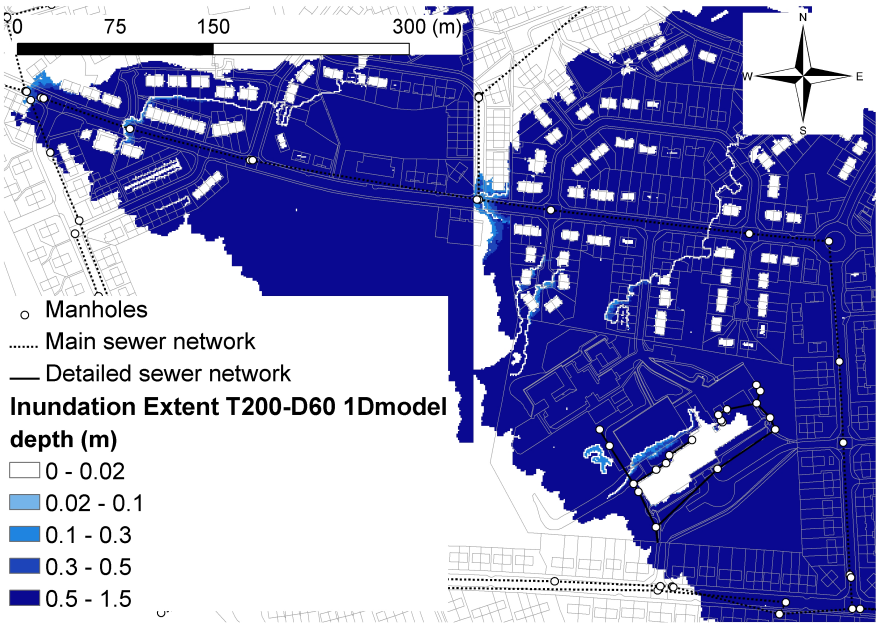

Figure B.1: Unrealistic maximum flood inundation extents for a 200 year return period event with 60 minutes duration.

The second and third are examples of the use of flooding compartments (Figures B.3 B.2).

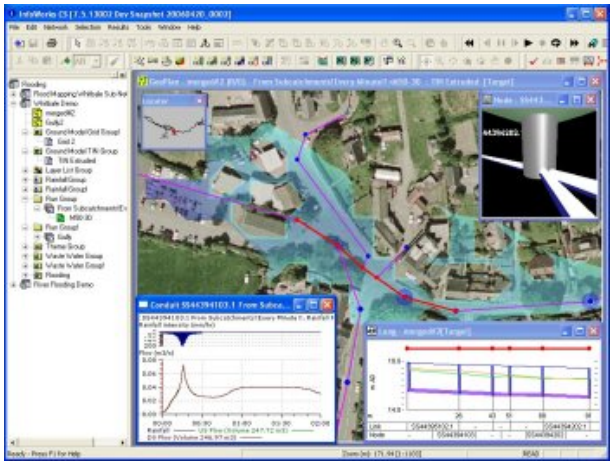

Figure B.2: Output results from Infoworks CS (Wallingford Sofware) of an Inundation map from a sewer network. (www.water-simulation.com/ wsp/ category/ water-simulation-packages/ on 5/05/2008)

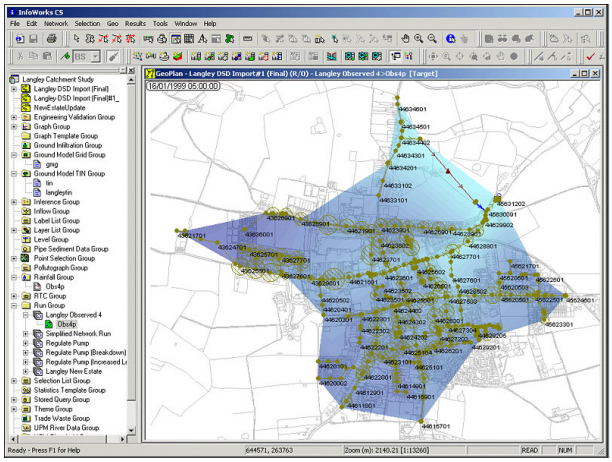

Figure B.3: Output results from Infoworks CS (Wallingford Sofware) of an Inundation map from a sewer network. (www.wallingfordsoftware.com on 28/01/2008)

References

Abbott, M. B., 1979. Computational Hydraulics - Elements of the theory of free surface flows. Pitman.

ABI, 2007. Summer Floods 2007: Learning the lessons. Association of Brithish Insurers.

Abou-Seida, M. M., Quaraishi, A. A., 1976. A flow equation for submerged rectangular weirs. Proceedings of the Institution of Civil Engineers, Water Management 61, 685–696.

Akan, A. O., Houghtalen, R. J., 2003. Urban hydrology: Hydraulics and storm water quality. Engineering applications and computer modelling. John Wiley & Sons.

Almeida, B., 1983. Master lectures in transient flows.

Aronica, G., Bates, P., Horritt, M., 2002. Assessing the uncertainty in distributed model predictions using observed binary pattern information within glue. Hydrological Processes 16, 20012016.

Aronica, G. T., Lanza, L. G., 2005. Drainage efficiency in urban areas: a case study. Hydrological Processes 19, 1105–1119.

Balmforth, D., Digman, C., Kellagher, R., Butler, D., 2006. Designing for exceedance in urban drainage - good practice. CIRIA.

Bazaraa, M. S. Sherali, H. D., Shetty, C. M., 1993. Nonlinear programming. John Willey & Sons, New York.

BBC, 2004. http://news.bbc.co.uk/1/hi/england/west-yorkshire/3697790.stm, (as seen on 29/Spet/2004).

BBC, 2007a. http://news.bbc.co.uk/1/hi/business/7034293.stm, (as seen on 8/Oct/2007).

BBC, 2007b. http://news.bbc.co.uk/1/hi/world/americas/7072554.stm, (as seen on 7/Nov/2007).

Beffa, C., Painter, D. J., Connell, R. J., 2001. Two-dimensional flood plain flow. i: Model description. Journal of Hydrologic Engineering 6(5), 397–399.

Bellman, R. E., Dreyfus, S. E., 1962. Applied Dynamic Programming. Princeton University Press, Princeton, New Jersey.

Bertsekas, D. P., 2000. Dynamic programming and optimal control: 1. Athena Scientific, 2nd edition.

Beven, K., Binley, A., 1992. The future of distributed models: model calibration and uncertainty prediction. Hydrological Processes 6, 279298.

Bolle, A., Demuynck, A., Willems, P., Bouteligier, R., Bosch, S., Verwey, A., Berlamont, J., 2006. Hydraulic modelling of the two-directional interaction between sewer and river systems. In: Urban Drainage Modelling and Water Sensitive Urban Design, Melbourne.

Boonya-Aroonnet, S., Maksimovic, C., Prodanovic, D., Djordjevic, S., 2007. Urban pluvial flooding: Development of GIS based pathways model for surface flooding and interface with surcharged sewer model. Proceedings of the 6th NOVATECH international conference, Lyon, France, 481–488.

Butler, D., Davies, J. W., 2000. Urban Drainage. E & FN Spon.

Cambridge Dictionary, 2008. http://dictionary.cambridge.org/. Tech. rep., Cambridge.

Carr, R. S., Smith, G., 2006. Linking of 2D and pipe hydraulic models at fine spatial scales. In: Urban Drainage Modelling and Water Sensitive Urban Design, Melbourne.

Chanson, H., 1999. The hydraulics of open channel flow - An introduction. Butterworth-Heinemann, London.

Chaudhry, M. H., 1987. Applied hydraulic transients. Second edition, Van Nostrand Reinhold, New York.

Chaudhry, M. H., 1993. Open-Channel flow. Prentice-Hall, Englewood Cliffs.

Chen, A., Djordjevic, S., Leandro, J., Savic, D., 2007. The urban inundation model with bidirectional flow interaction between 2D overland surface and 1D sewer networks. Proceedings of the 6th NOVATECH international conference, Lyon, France.

Chen, A. S., Hsu, M. H., Chen, T. S., Chang, T. J., 2005. An integrated inundation model for highly developed urban areas. Water Science and Technology 51(2), 221–229.

Courant, R., Friedrichs, K., Lewy, H., 1967. On the partial difference equations of mathematical physics. IBM J. 11, 215–234.

Cunge, J. A., Holly, F. M., Verwey, A., 1980. Practical aspects of computational river hydraulics. Pitman Publishing, London.

de Saint-Venant, A. J. C. B., 1871. Thorie du mouvement non-permanent des eaux avec application aux crues des rivires et l'introduction des mares dans leur lit. C. R. Hebd. Seances Acad. Sci. 73, 148154.

Dey, A., Kamioka, S., 2006. An integrated modelling approach to predict flooding on urban basin. ICMS Pty Ltd-Urban Drainage Modelling and Water Sensitive Urban Design.

DHI, 2007a. "mike-21.", http://www.dhigroup.com/.

DHI, 2007b. "mike-storm.", http://www.dhigroup.com/.

Djordjevic, S., 2001. A mathematical model of the interaction between surface and buried pipe flow in urban runoff and drainage. Ph.D. thesis, Faculty of Civil Engineering, University of Belgrade.

Djordjevic, S., Prodanovic, D., Maksimovic, C., 1999. An approach to simulation of dual drainage. Water Science and Technology 39(9), 95–103.

Djordjevic, S., Prodanovic, D., Maksimovic, C., Ivetic, M., Savic, D., 2005. SIPSON - simulation of interaction between pipe flow and surface overland flow in networks. Water Science and Technology 52, 275–283.

Djordjevic, S., Prodanovic, D., Walters, G. A., 2004. Simulation of transcritical flow in pipe/channel networks. Journal of Hydraulic Engineering 130(12), 1167–1178.

Dorini, G., Jonkergouw, P., Kapelan, Z., Khu, S. T., Savic, D., 2006. An efficient algorithm for sensor placement in water distribution systems. In: Water Distribution System Analysis, Cincinnaty, Ohaio.

Elliot, A. H., Trowsdale, S. A., 2007. A review of models for low impact urban stormwater drainage. Environmental Modelling Software 22, 394–405.

Ellis, J., McBean, E., Mulamoottil, G., 1982. Design of dual drainage systems using SWMM. Journal of the Hydraulics Division 198(HY10), 1222–227.

European Parliament and Council of The European Union, 2007. Directive 2007/60/EC of the European Parliament and of the Council of 23 october 2007 on the assessment and management of flood risks. Tech. rep., Official Journal of the European Union.

Falconer, R., 1980. Numerical modelling of tidal circulation in harbours. Journal of Hydraulic Engineering, ASCE 106, 31–48.

Farmani, R., Walters, G. A., Savic, D., 2006. Evolutionary multi-objective optimization of the design and operation of water distribution network: total cost vs. reliability vs. water quality. Journal of Hydroinformatics 8(3), 165–179.

Fennema, R. J., Chaudhry, M. H., 1987. Simulation of one-dimensional dam-break flows. Journal of Hydraulic Research 25(1), 41–51.

Ferreira, R. M., 2005. River morphodynamics and sediment transport conceptual model and solutions. Ph.D. thesis, IST/DECivil, UTL.

Ferziger, J. H., Peric, M., 2002. Computational Methods for Fluid Dynamics. Springer, New York.

Fletcher, C. A. J., 1991. Computational Techniques for Fluid Dynamics 2: Specific Techniques for Different Flow Categories - Volume II. Springer-Verlag.

Franco, A., 1988. Simulao de cheias provocadas por roturas de barragens em srie. Master's thesis, IST/DECivil, UTL, Lisbon.

Franco, A. B., 1996. Modelao computacional e experimental de escoamentos provocados por roturas de barragens. Ph.D. thesis, IST/DECivil, UTL, Lisbon.

Garcia-Navarro, P., Alcrudo, F., Saviron, J., 1992. 1-D open channel flow simulation using TVD-MacCormack scheme. Journal of Hydraulic Engineering 118-(10), 1359–1372.

Hankin, B., Waller, S., Astle, G., Kellagher, R., 2008. Mapping space for water: screening for urban flash flooding. Journal of Flood Risk Management 1(1), 13–22.

Harten, A., 1983. High resolution schemes flow hyperbolic conservation laws. Journal of computational physics 49, 357–393.

Hicks, F., Peacock, T., 2005. Suitability of HEC-RAS for flood forecasting. Canadian Water Resources Journal.

Horritt, M., Bates, P. D., 2002. Evaluation of 1D and 2D numerical models for predicting river flood inundation. Journal of Hydrology 268, 87–99.

Horritt, M. S., 2006. A methodology for the validation of uncertain flood inundation models. Journal of Hydrology 326, 153–165.

Hosoda, T., Tada, A., Iwata, M., Furuhachi, T., 2002. Fundamental studies on hydraulic transients with interaction between overland sruface flows and underground channels flows. In: Internatiional conference on Urban Hydrology for the 21st Century 14-16 October, Kuala Lumpur.

Hsu, M. H., Chen, S. H., Chang, T. J., 2000. Inundation simulation for urban drainage basin with storm sewer system. Journal of Hydrology 234, 21–37.

Hsu, M. H., Teng, W. T., Huang, C. H., 1999. A study on flood and indundation models for river basins. In: 8th International Conference on Urban Storm Drainage, Sidney, Australia, 857-865.

Huber, W. C., Dickinson, R. E., 1988. Storm Water Management Model. Athens, Georgia, U.S.A., Athens, Georgia, U.S.A.

Hunter, N., Horrit, M., Bates, P., Wilson, M., Werner, M., 2005a. Improved simulation of flood flows using storage cell models. Proceedings of the Institution of Civil Engineers, Water Management 159, 9–18.

Hunter, N., Horritt, M., Bates, P., Wilson, M., Werner, M., 2005b. An adaptive time step sollution for raster-based storage cell modelling of floodplain inundation. Advances in Water Resources 28, 975–991.

Hunter, N. M., Bates, P. D., Neelz, S., Pender, G., Villanueva, I., Wright, N. G., Liang, D., Falconer, R. A., Lin, B., Waller, S., Crossley, A. J., Mason, D. C., 2008. Benchmarking 2D hydraulic models for urban flooding. Proceedings of the Institution of Civil Engineers, Water Management 161(1), 13–30.

Inoue, K., Toda, K., Tanino, T., Hayashi, H., 1999. Hydraulic study of overland flood flows in an urban area with underground space. In: International Symposium on Flood Control, November 10-13, 1999 Beijing China, 249-256.

Jean-Philippe, V., Sabine, M., Jean-Baptiste, F., Denis, D., 2005. Towards a reasoned 1D river model calibration. Journal of Hydroinformatics 7(2), 91–104.

Jha, A. K., Akiyama, J., Ura, M., 1995. First-order and 2nd-order flux-difference splitting schemes for dam-break problem. Journal of Hydraulic Engineering 121(12), 877–884.

Klawitter, A., Ostrowski, M., 2006. A modelling system for improved discharge simulation in small urbanized catchements. In: Urban Drainage Modelling and Water Sensitive Urban Design, Melbourne.

Klonidis, A. J., Soulis, J. V., 2002. An implicit scheme for steady two-dimensional free-surface flow calculation. Journal of Hydraulic Research 39(4), 393–401.

Konig, A., Saegrov, S., Schilling, W., 2002. Damage assessment for urban flooding. In: 9th International Conference on Urban Drainage, Portland, Oregon.

Krupka, M., Pender, G., Wallis, S., Sayers, P., Mulet-Marti, J., 2007. A rapid flood inundation model. In: 32nd Congress of IAHR - Harmonizing the Demands of Art and Nature in Hydraulics, Venice.

Lal, A. M. W., 1998. Performance comparison of overland flow algorithms. Journal of Hydraulic Engineering April, 342–348.

Lancaster, J. W., Preene, M., Marshall, C. T., 2004. Developement and flood risk - guidance for hte construction industry (C624). Classic House of London http://www.ciria.org.uk/.

Leendertse, J. J., 1967. Aspects of a computational model for well mixed estuaries and coastal seas. RM-5294-PR. The Rand Corp.

Lhomme, J., Bouvier, C., Mignot, E., Paquier, A., 2006. One-dimensional GIS-based model compared to two-dimensional model in urban floods simulations. Water Science and Technology 54(6-7), 83–91.

Liang, D., Lin, B., , Falconer, R., 2007. A boundary-fitted numerical model for flood routing with shock-capturing capabil. Journal of Hydrology 332, 447–486.

Lin, B., Wicks, J. M., Falconer, R. A., Adams, K., 2006. Integrating 1D and 2D hydrodynamic models for flood simulation. Proceedings of the Institution of Civil Engineers, Water Management 159, 19–25.

Maksimovic, C., Prodanovic, D., 2001. Modelling of urban flooding - breakthrough or recycling of outdated concepts. In: Urban Drainage Modelling, Orlando, Florida, USA.

Mark, O., 2005. Urban flooding modelling by coupling a 1D sewer system model to a 2D surface model. Tech. rep., DHI Water & Environment.

Mark, O., Weesakul, S., Apirumanekul, C., Aroonnet, S. B., Djordjevic, S., 2004. Potential and limitations of 1D modelling of urban flooding. Journal of Hydrology 299, 284–299.

Merriam Webster Dictionary, 2008. http://www.merriam-webster.com. Tech. rep., Merriam-Webster.

Meselhe, E., Holly, F., 1997. Invalidity of Preissmann scheme for transcritical flow. Journal of Hydraulic Engineering 123(7), 652–655.

Microsoft, 2006. Configuring windows hotstart. Tech. rep., 2006 Microsoft Corporation.

Mohammadian, A., Le Roux, D. Y., Tajrishi, M., 2007. A conservative extension of the method of characteristics for 1-D shallow flows. Applied Mathematical Modelling 31(2), 332–348.

Mohapatra, P. K., Chaudhry, M. H., 2004. Numerical solution of Boussinesq equations to simulate dam-break flows. Journal of Hydraulic Engineering, 156–159.

Monge, G., 1789. Graphical integration. Annal des Ing. Sortis des coles de Gand, Belgium.

Murty, K., 1976. Linear and combinatorial progamming. John Willey & Sons, New York.

Nasello, C., Tucciarelli, T., 2005. Dual multilevel urban drainage model. Journal of Hydraulic Engineering 131(9), 748–754.

Neelz, S. P., Pender, G., 2006. The influence of errors in digital terrain models on flood flow routes. River Flow 2006, September, 1955 1962ISBN 0 415 408148.

O'Loughlin, G., Reid, A., Seneviratne, I., 2006. Lessons from modelling piped urban drainage catchments. In: Urban Drainage Modelling and Water Sensitive Urban Design, Melbourne.

Ortloff, C. R., 2005. The water supply and distribution system of the Nabataean city of Petra (Jordan), 300 BC-AD 300. Cambridge Archaeological Journal 15(1), 93–109.

Oxford English Dictionary, 2008. http://dictionary.oed.com. Tech. rep., Oxford English.

Paquier, A., Tanguy, J. M., Haider, S., Zhang, B., 2003. Estimation des niveaux d'inondation pour une crue clair en milieu urbain : comparaison de deux modles hydrodynamiques sur la crue de nmes d'octobre 1988. Revue des Sciences de l'Eau 16(1), 79–102.

Pender, G., 2006. Introducing the Flood Risk Management Research Consortium. Proceedings of the Institution of Civil Engineers, Water Management 159(1), 3–8.

Pender, G., Wright, N. G., Bates, P. D., Mason, D., Hall, J., 2004. Next generation computer modelling for the prediction of flood level and inundation extent part 1: Technical specification of research needs. Tech. rep., available at http://www.floodrisk.org.uk.

Philips, B. C., Yu, S., Thompson, G. R., de Silva, N., 2005. 1D and 2D modelling of urban drainage systems using XP-SWMM and TUFLOW. In: 10th International conference on urban drainage, Copenhagen.

Pitt, M., 2008. Sir Michael Pitts final report: Learning lessons from the 2007 floods. The Pitt Review.

Ponce, V., Pikin, D. G., 1987. Kinematic, diffusion and dynamic catchement modelling. In: Proccedings, Engineering Hydrology Symposium. 3-5. Williamsburg, Virginia, 305-310.

Ponce, V., R.M., L., Simons, D. B., 1978. Applicability of kinematic and diffusion models. Journal of Hydraulics Divison 104(3), 353–360.

Ponce, V. M., 1991. The kinematic wave controversy. Journal of Hydraulic Engineering 117(4), 511–525.

Potter, M. C., Wiggert, D. C., 2001. Mechanics of Fluids. Brooks/Cole.

Preissmann, A., 1961. Propagation des intumescences dans les canaux et rivires. In: 1st Congress of the French Association for Computation. Grenoble, France, 433-442.

Quintela, A. C., 1996. Hidraulica geral. Fundacao Calouste Gulbenkian.

Rakha, K., Deigaard, R., Brprker, I., 1997. A phase-resolving cross shore sediment transport model for beach profile evolution. Coastal Engineering 31, 231–261.

Ramos, H., 1986. Modelos matematicos para simulacao de escoamentos variaveis em canais. modelos completos e de difusao. Master's thesis, IST/DECivil, UTL, Lisbon.

Ramos, H., 1995. Simulacao e controlo de transitorios hidraulicos em pequenos aproveitamentos hidroelectricos. modelacao e analise dos efeitos induzidos pela sobrevelocidade de turbogeradores. Ph.D. thesis, IST/DECivil, UTL, Lisbon.

Ramos, H., Almeida, A., 1987. Backwater effects with a diffusion type modeling. In: AIRH-Congress, Lausanne. p. 6pgs.

Roe, P., 1981. Approximate Riemann solvers, parameter vectors and difference schemes. Journal of Computational Physics 43, 357372.

Rossman, L. A., 2005. Storm water management model - user's manual Version 5.0. EPA - United States, EPA - United States, Cincinnati, http://www.epa.gov/ednnrmrl/models/swmm/epaswmm5-manual.pdf.

Samani, H. M. V., Mottaghi, A., 2006. Optimization of water distribution networks using integer linear programming. Journal of Hydraulic Engineering 132(5), 501–509.

Savic, D., 2002. Single-objective vs. multiobjective optimisation for integrated decision support. In: Integrated Assessment and Decision Support. Proceedings of the 1st Biennial Meeting of the iEMSs.

Schmitt, T. G., Thomas, M., Ettrich, N., 2004. Analysis and modeling of flooding in urban drainage systems. Journal of Hydrology 299(3-4), 300–311.

Simonovic, S., Nirupama, 2005. A spatial multi-objective decision-making under uncertainty for water resources management. Journal of Hydroinformatics 7(2), 117–133.

Spry, R. B., Zhang, S., 2006. Modelling of drainage systems and overland flowpaths at catchment scales. In: Urban Drainage Modelling and Water Sensitive Urban Design, Melbourne, (2), 267-274.

Stelling, G., Wiersma, A. K., Willemse, J., 1986. Practical aspects of accurate tidal computations. Journal of Hydraulic Engineering, ASCE 12, 802–817.

Stern, N., 2007. Stern Review: The economics of climate change. Cambridge University Press.

Thomas, L., 1949. Elliptic Problems in Linear Difference Equations over a Network. Watson Sci. Comput. Lab. Rept., Columbia University, New York.

Tsai, C. W.-S., Yen, B. C., 2001. Linear analysis of shallow water wave propagation in open channels. Journal of Engineering Mechanics 127(5), 459–471.

Tseng, M. H., Chu, C. R., 2000. The simulation of dam-break flows by an improved predictor-corrector TVD scheme. Advances in Water Resources 23(6), 637–643.

UK Government, 2006. Planning Policy Statement 25. Communities and Local Governement.

USACE, 2002. HEC manual, chapter 2.

Vaes, G., Bouteligier, R., Herbos, P., Berlamont, J., 2004. Modelling of floods caused by urban drainage systems. In: Int. Conference on Urban Drainage Modelling, Dresden 2004.

Vasconcelos, J. G., Wright, S. J., Roe, P. L., 2005. Current Issues on Modeling Extreme Inflow Conditions in Stormwater Sewers. In: Effective Modeling of Urban Water Systems, Monograph 13. James, Irvine, McBean & Pitt,. CHI, www.computationalhydraulics.com.

Vasconcelos, J. G., Wright, S. J., Roe, P. L., 2006. Improved simulation of flow regime transition in sewers: Two-component pressure approach. Journal of Hydraulic Engineering 132(6), 553–562.

Venutelli, M., 2004. Time-stepping Pade-Petrov-Galerkin models for hydraulic jump simulation. Mathematics and Computers in Simulation 66(6), 585–604.

Venutelli, M., 2006. A third-order explicit central scheme. Journal of Hydraulic Research 44(3), 402–411.

Verwey, A., 2007. Numerical modelling support to flood studies. In: 32nd congress of IAHR - Harmonizing the Demands of Art and Nature in Hydraulics, Venice.

Villanueva, I., Wright, N., 2006. Linking Riemann and storage cell models for flood prediction. Proceedings of the Institution of Civil Engineers, Water Management 159(1), 27–33.

Vojinovic, Z., Tutulic, D., 2008. On the use of 1D and coupled 1D-2D modelling approaches for assessment of floods in urban areas. Urban Water Journal, in press.

Wallingford-Software, 2000. Hydroworks, version.7, documentation.

Wallingford-Software, 2004. Does traditional calibration hide errors in your demand analysis?, news Articles, www.wallingfordsoftware.com/news/fullarticle.asp?ID=260.

Wallingford-Software, 2006. Infoworks CS. version.7.5, documentation.

Zhong, Z., 1998. General hydrodynamic model for sewer/channel network systems. Journal of Hydraulic Engineering 123(3), 30–315.

Zoppou, C., 2001. Review of urban storm water models. Environmental Modelling Software 16, 195–231.

* * *

List of papers in international scientific periodicals with referees where Jorge Leandro is the first author:

1. Leandro, J.,Chen, A. S., Djordjevic, S., and Savic, D. A. (2008, under review). "A comparison of 1D/1D and 1D/2D coupled hydraulic models for urban flood simulation." Journal of Hydraulic Engineering.

2. Leandro, J., Djordjevic, S., Chen, A. S and Savic, D. A. (2008, under review). "A dynamic objective function algorithm to calibrate a 1D/1D coupled hydraulic model." Journal of Hydroinformatics.

3. Leandro, J., Djordjevic, S., Chen, A. S., and Savic, D. A. (2008, under review). "Flood inundation maps using an improved 1D/1D Model" Proceedings of the Institution of Civil Engineers, Water Management.

4. Leandro, J., Chen, A. S., Djordjevic, S., and Savic, D. A.(will be submitted in October 2008). "A method for comparing and improving the flood-inundation-extent agreement between coupled hydraulic models in urban flooding" Journal of Hydrology.

List of papers in international scientific periodicals with referees where Jorge Leandro is a co-author:

1. Dawson, R. J., Speight, L., Hall, J. W., Djordjevic, S., Savic, D. and Leandro, J.(2008) "Attribution of flood risk in urban areas" Journal of Hydroinformatics, 10(4), 275-288.

2. Chen, A. S., Djordjevic, S., Leandro, J., Savic, D. A., Saul, A. and Blanksby, J.(will be submitted in October 2008) "The urban inundation model with bidirectional flow interaction between 2D overland surface and 1D sewer networks" Journal of Flood Risk Management.

List of papers in conference proceedings

1. Leandro, J. 2008. "A Dynamic Objective Function algorithm to calibrate a 1D/1D coupled hydraulic model versus a 1D/2D model" International Conference on Urban Drainage, Edinburgh, Scotland, UK. (shortlisted for the Poul Harremos Award for Best Urban Drainage Paper by a Young Author)

2. Chen A., Djordjevic S., Leandro, J., Evans B. and Savic D. 2008. "Simulation of the building blockage effect in urban flood modelling" International Conference on Urban Drainage, Edinburgh, Scotland, UK.

3. Leandro J, Djordjevic S, Chen A S and Savic D 2007 "The use of multiple-linking-element for connecting sewer and surface drainage networks" Proceedings of 32nd IAHR Congress, Venice.

4. Chen A S, Djordjevic S, Leandro J, and Savic D 2007 "The urban inundation model with bidirectional flow interaction between 2D overland surface and 1D sewer networks" Proceedings of NOVATECH, Lyon.

5. Djordjevic S., Chen A., Leandro J., Savic D., Boonya-aroonnet S., Maksimovic C., Prodanovic D., Blanksby J. and Saul A.2007 "Integrated subsurface/surface 1D/1D and 1D/2D modelling of urban flooding" Proceedings of Aquaterra World Forum on Delta and Coastal Development, Amsterdam.

6. Blanksby J, Saul A, Ashley R, Djordjevic S, Chen A, Leandro J, Savic D, Boonya-aroonnet, S, Maksimovic C and Prodanovic D 2007 "Integrated Urban Drainage: Setting the context for Integrated Urban Drainage Modelling in the United Kingdom" Proceedings of Aquaterra World Forum on Delta and Coastal Development, Amsterdam.

7. Hall, J., Dawson, R., Speight, L., Djordjevic, S., Savic, D. and Leandro, J. 2006 "Attribution of flood risk in urban areas" 7th Int. Conf. on Hydroinformatics, Vol. I, Nice, 280-287.

8. Leandro, J. 2006 "The Multiple-Linking-Element" Young Persons Papers Competition, Leeds, UK section IAHR2006 (2^{nd} prize award).